Fourth Pacific Area Meeting Papers

Symposium on

RECENT DEVELOPMENTS IN NONDESTRUCTIVE TESTING OF MISSILES AND ROCKETS

Published by the
AMERICAN SOCIETY FOR TESTING AND MATERIALS
1916 Race St., Philadelphia 3, Pa.

ASTM Special Technical Publication No. 350

DUKE
UNIVERSITY

LIBRARY

SYMPOSIUM ON RECENT DEVELOPMENTS IN NONDESTRUCTIVE TESTING OF MISSILES AND ROCKETS

Presented at the

FOURTH PACIFIC AREA NATIONAL MEETING

AMERICAN SOCIETY FOR TESTING AND MATERIALS

Los Angeles, Calif., October 2, 1962

Reg. U. S. Pat. Off.

ASTM Special Technical Publication No. 350

Price $5.25; to Members $3.70

Published by the

AMERICAN SOCIETY FOR TESTING AND MATERIALS

1916 Race St., Philadelphia 3, Pa.

© BY AMERICAN SOCIETY FOR TESTING AND MATERIALS 1963
Library of Congress Catalog Card Number: 63-21662

Printed in Baltimore, Md.
November, 1963

Eng'g
620.1127
S989SE

FOREWORD

ASTM Committee E-7 on Nondestructive Testing sponsored this Symposium on Recent Developments in Nondestructive Testing of Missiles and Rockets, held during the Fourth Pacific Area National Meeting of the Society in Los Angeles, Calif. The papers in this symposium, presented in two sessions on Tuesday, October 2, 1962, cover everything from the planning program through various techniques for actual nondestructive testing of the finished product and implementation of a quality control program.

Mr. E. L. Criscuolo, U. S. Naval Ordnance Laboratory, and Mr. S. A. Wenk, Varian Associates, served as symposium co-chairmen. Mr. Wenk presided over the morning session, with Commander R. W. Smiley, Bureau of Naval Weapons, acting as session chairman. Mr. D. Polansky, U. S. Naval Ordnance Laboratory, presided over the afternoon session, and Mr. L. P. Dolan, Space Technology Laboratories, served as session chairman.

NOTE.—The Society is not responsible, as a body, for the statements and opinions advanced in this publication.

CONTENTS

	PAGE
Introduction—E. L. Criscuolo and S. A. Wenk	1
Planning a Nondestructive Testing Program for Solid Propellant Rocket Motors—W. W. Mills, Jr.	3
Nondestructive Test Techniques for Filament-Wound Glass Fiber - Resin Rocket Motor Cases—E. Dane Harvey	9
Quality Control of High-Temperature Solid Rocket Control Components—Richard L. Ahearn	21
Numerical Film Reading Techniques for Interpretation of Liner-Propellant Interface of Solid Rocket Motors—Richard J. Mascis	36
Cinefluorography of Solid Fuel Rocket Motors—E. L. Criscuolo and D. Polansky	51
Discussion	59
Nondestructive Testing of Solid Propellant Missile Motors—Frank C. Hund	62
Gamma Scintillation Scanning for Inspecting Solid Rocket Motors—Paul E. Underhill	85
Nondestructive Testing of High-Strength Steel Rocket Motor Cases—J. A. Hendron	95
Infrared Nondestructive Testing of Glass Filament-Wound Rocket Motor Cases—Frederick E. Alzofon, Lester E. Florant, Richard K. Ronald, Marvin J. Vann, and Julian E. Fitzgerald	105

RELATED ASTM PUBLICATIONS

Radiography, STP 96 (1949).
Ultrasonic Testing, STP 101 (1949).
The Rôle of Non-Destructive Testing in the Economics of Production, STP 112 (1950).
Non-Destructive Testing, STP 145 (1952).
Nondestructive Testing, STP 213 (1956).
Nondestructive Testing in the Missile Industry, STP 278 (1959).

SYMPOSIUM ON RECENT DEVELOPMENTS IN NONDESTRUCTIVE TESTING OF MISSILES AND ROCKETS

INTRODUCTION

By E. L. Criscuolo[1] and S. A. Wenk[2]

In keeping with its mission, ASTM Committee E-7 on Nondestructive Testing has sponsored several symposia since its formation. The Symposium on Nondestructive Testing in the Missile Industry presented during the Third Pacific National Meeting, and published as *ASTM STP No. 278*, attracted an unusually large audience. As a sequel, the present symposium was organized to present the latest information in the missiles field.

Under the Department of Defense, a Polaris - Minuteman - Pershing Nondestructive Test Committee had been organized for the exchange of information on a classified basis. With the cooperation of this committee, the current symposium was organized on an unclassified level.

Committee E-7 gratefully acknowledges the cooperation and support of the members of the Polaris-Minuteman-Pershing Nondestructive Test Committee.

[1] U. S. Naval Ordnance Laboratory, White Oak, Silver Spring, Md.
[2] Varian Associates, Palo Alto, Calif.

PLANNING A NONDESTRUCTIVE TESTING PROGRAM FOR SOLID PROPELLANT ROCKET MOTORS

By W. W. Mills, Jr.[1]

Synopsis

Nondestructive testing is mandatory to assure the quality, reliability, and motor performance required by the solid propellant rocket motor industry. The motor performance desired demands minimum inert component weight and, therefore, precludes the luxury of wide material and design safety margins. Established techniques have been used where applicable, and new and advanced techniques have been evolved or modified for use. Extensive consideration and effort are being expended to develop automation and instrumentation for the readout and evaluation process so as to minimize subjective and qualitative interpretation of the test by providing objective and quantitative interpretation. Standards for evaluation of the test method used and the item produced are necessarily being upgraded. This correlation is found through direct measurement of specific properties, through experience based on past performance, or from destructive tests.

Nondestructive testing does not provide a specific method of solution for every problem; therefore multiple test methods are necessary to supply the information required to make an evaluation. This coupled with the current and anticipated problem areas emphasizes the need for a practical and sound nondestructive testing program for solid propellant rocket motors.

Today solid propellant rocket motors propel all types and sizes of missiles. Tomorrow some motors will be appreciably larger, others will be different in design and configuration, and many will be constructed from new materials. These and other considerations will dictate the direction that nondestructive testing must take in order that it can best serve the solid propellant rocket motor industry. A review of solid propellant rocket motor development and nondestructive testing as used therein will provide a foundation which, coupled with anticipated and predicted changes, will afford some insight into the need for and the role of nondestructive testing now and in the future.

Each motor design is the result of a trade-off between cost and time schedule to meet the over-all requirements of the missile system within the status of the technology at the time when the design must be frozen. Each design represents an attempt to integrate the best combination of propellants, materials, manufacturing techniques, performance, and reliability. These considerations define limits for nondestructive testing.

Motor Evolution

In the late 1940's, the Jet Propulsion Laboratory at California Institute of Technology made a major advance in

[1] Huntsville Plant, Thiokol Chemical Corp. Huntsville, Ala.

the design of solid propellant rocket motors by establishing that some elastomeric materials make excellent rocket motor fuel and demonstrating that composite propellant made with such material as binder could be bonded to the case wall. The first motors with case-bonded propellant were very simple, consisting of a pressure vessel loaded with the propellant, a nozzle, and an igniter. The propellant grain contained a central cavity which formed the initial burning surface, and the burning progressed outward toward the case wall with the propellant acting as a heat barrier to protect the case against the high temperature of the combustion products.

A design typical of this construction is shown in Fig. 1. The motor case is fabricated by deep drawing, necking down the nozzle end, and threading it for attachment of the nozzle assembly, which consists of a heavy forged adapter and a comparatively thin steel nozzle with a throat insert of carbon. Only a thin liner is needed to protect the case against local overheating where the propellant in the valley burns to the case wall first. The burning time is short, and the heat capacity of the exposed parts is sufficient to keep their temperature within safe limits. The igniter is a charge of pyrotechnic composition ignited by an electric squib.

Such motors as this, using the best materials and fabrication techniques available at that time, demonstrated the soundness of the design, which permitted both improved performance and high reliability, a combination never before achieved. As the evidence accumulated, application of the basic design was extended, and rapid strides were made in further development and improvement.

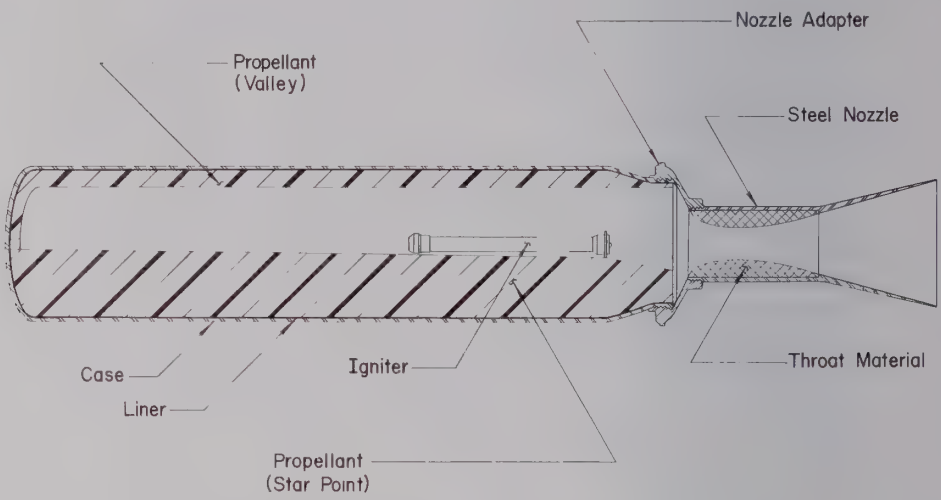

FIG. 1.—Rocket Motor with Case-Bonded Propellant.

These new applications created problems, however. For longer burning times, stressed parts had to be protected from prolonged heating, and more flexible control was needed. Normal burning times are determined by the propellant grain configuration and the burning rate characteristics of the propellant,

but there was a need for variation of the normal program by thrust termination or thrust reversal. Thrust modulation is more difficult to achieve, for there is no flow of unburned propellant to be controlled by throttling; but an on-off control can be effected by extinguishing and reigniting the propellant, and a limited degree of modulation can be attained by variation of the effective nozzle throat area during motor operation. A predetermined program of multiple-level thrust may be obtained by some variations of the propellant configuration or by loading the motor with propellants of two or more different burning rates.

Control of the direction and attitude of a missile is obtainable through thrust vector control, which can be provided by jet-vanes, jetavators, or movable nozzles; or if the motor operates within the denser atmosphere, aerodynamic controls can be used. In the latter case, it is necessary to provide attachment points on the motor case for the aerodynamic control surfaces.

Missile and motor envelope requirements may necessitate drastic departure from conventional design, and in propulsion systems of two or more stages, the interstage connections require attachment provisions on the pressure vessels. Also, since the solid propellant rocket motor case normally serves as a portion of the missile proper, thereby saving weight, the possibility of ignition from aerodynamic heating must be considered and protection provided, usually by exterior insulation.

Future improvements in performance can result only from an increase in the motor mass ratio of propellant to inert parts or from increased propellant specific impulse. Since the motor case accounts for the greatest percentage of the inert weight, that is the component where the greatest improvement in mass ratio can be effected. Therefore there is a demand for designs using materials of higher strength-to-density ratio, such as alloy steels, titanium, aluminum, fiber glass, and composites. The inert component of next highest weight is the nozzle, where similar improvement in strength-to-weight ratio can be effected.

EVOLUTION OF NONDESTRUCTIVE TESTING

During the development of the first case-bonded motors, little consideration was given to nondestructive testing, although X-ray inspection of cartridge-loaded grains of double-base propellant had been practiced for several years. This situation was due in part to the relative insensitivity of the elastic propellants to minor flaws and in part to the lack of adequate inspection methods. However, as the size of the motors increased, and as the demand for higher performance resulted in lower factors of safety in the design of cases and nozzles, the need for nondestructive testing was recognized.

X-ray radiography and fluoroscopy were the first methods applied. Then, as the need for evaluation of the case-propellant bond became evident, various means for detection of flaws in that bond were investigated. The first of these were ultrasonic methods; when their shortcomings were recognized, other methods were tried, including thermal and sonic tests as well as tangential radiography.

For inert parts, where applicable, magnetic field and penetrant inspection methods have been used. Filtered and electrified particle inspections have been conducted. All of these techniques have been for product evaluation and there has been little application of nondestructive testing for in-process evaluation or control.

In general, nondestructive testing has been used primarily for the detection of discontinuities and occasionally for the measurement of physical properties, and very few methods can be readily used with complex or composite constructed items.

Nondestructive testing has therefore been used wherever there was an opportunity to apply an already developed technique; but until the past few years, there has been no systematic and concerted effort to develop new techniques to fill the gaps.

In the development and application of nondestructive testing, acceptance standards for both the technique and the item evaluated have had to be generated. These have been predicated upon correlation with actual performance, destructive tests, and service life tests.

The techniques developed for evaluation of propellant integrity will be applicable tomorrow. With increased propellant specific impulse and with increased propellant loading density, the basic need for nondestructive testing in this area will be relatively unchanged. The same types of discontinuities will be detrimental, and there will be continued need for refinement and improvement of all applicable techniques.

The major changes will result from the materials and the advanced configurations used. As mass fractions increase, it is evident that advances in the application of nondestructive testing to the various inert components will be required. Fabrication techniques are now going through some major changes, and nondestructive testing must keep abreast of these developments. Two current developments are the use of fiber glass and titanium alloys for motor cases. In addition, some of today's motors are using composite construction for nozzles. These design changes are going to make nondestructive testing more difficult; however, the technology developed today will serve as the foundation for tomorrow. Some problems arise from the fact that no single nondestructive testing technique is capable of supplying the detailed information necessary for evaluation, and multiple tests must always be conducted.

Implementation of nondestructive testing should begin with the establishment of the original design and specification parameters. Reliability is a primary requirement with a rocket motor, and nondestructive testing is a potential aid in defining or establishing reliability. In many instances, the designer in consultation with a nondestructive testing engineer can specify the use of materials and manufacturing techniques that lend themselves to easier evaluation with available nondestructive testing techniques. As the production stage is reached, the nondestructive testing engineer should have available proper methods and techniques that have been automated and properly instrumented so that the human factor in product evaluation is minimized.

A mandatory concern in nondestructive testing is the obligation to develop acceptance standards which will define the quality level of the technique or method and provide standards of comparison for final product evaluation. These acceptance standards can be derived from the measurement of specific properties and phenomena, from service tests, and from destructive tests. Failure analysis and the participation in this analysis by nondestructive testing personnel is a "must." This participation will add to the nondestructive testing engineer's background, and will be especially useful in the classification of defects.

Nondestructive testing not only needs to be injected into the design and specification phase, but it must also be con-

tinuously applied and considered through all stages of development and into production. Management's direction and the customer's requirements are needed so that the role of nondestructive testing in any given motor program is adequately and properly defined. With the designer, the nondestructive testing engineer should be evaluating the various nondestructive testing methods currently available. Initially, methods should be stipulated, and tentative criteria for the test method and product acceptance established.

The development phase requires continuous surveillance to assure that the methods and techniques are adequate, and to refine both the methods and the acceptance criteria. This must be concurrent with production on a continuing basis, for it is at this time that confidence levels are developed. When the production phase is reached, standards and limits for each specific nondestructive test utilized will be defined and adequately proved if nondestructive testing has fulfilled its function.

During the course of our productive existence, we perform both as a consumer and as a producer. If we consider the producer aspect first, we realize that the direction we receive from management and the requirements of our customer sometimes place us in a difficult position. This occurs when the requirements are so stringent that we have no options and therefore have no latitude in planning the nondestructive testing program. For example, the cost of nondestructive testing is increased unnecessarily if high resolution is stipulated when a lower degree will suffice. Similarly, if the technique called for is not available, equipment must be procured, personnel must be trained, and experience must be gained before a confidence level is established, whereas both time and money can be saved by use of an acceptable alternative technique that is immediately available. If this is kept in mind, then our role as a customer will be more realistic. Quite properly, we should survey new vendors to establish their capabilities and limitations; then procurement specifications can be written to take advantage of any peculiarities that may exist. Experience has pointed out some obvious shortcomings: inadequate definition in specifications for both the method and the product acceptance criteria; too much reliance on military and organizational specifications and standards; lack of or inadequate comparison standards; too few technically oriented persons conducting tests; overtesting as well as inadequate testing; and lack of understanding of the cause and effect of discontinuities encountered.

Some specific examples will serve to emphasize the planning and consideration necessary for nondestructive testing in connection with solid propellant rocket motors. When titanium is used as a motor case material, the grain size in the solution-treated and aged parent metal is normally from 3 to 5. In heliarc welds, the grain size will run 00 to 000. High- or low-voltage electron-beam welding leaves a grain size of 2 or 3. The weld deposit solidification orients the grain at about 45 deg to the solid state material from the heat-affected zone inward, and the heliarc weld grains look like dendritic structures on the weld radiographs where fine or very fine grain film is used. This cause and effect must be taken into account in the interpretation of the radiographs, as the mottled images from the grain boundaries are readily evident on the film.

A partial list of flaws that can be encountered in a fiber glass motor case includes improper spacing or indexing of fibers, improperly joined ends, damaged threads or filaments, improper

tension on fibers, poor wetting of fibers, unbonded fibers, high-resin or low-resin areas, and inclusions. The exact effects of these conditions are not known, and in all probability some degree of nonconformance for any condition can be tolerated. This degree must be established by analysis of service life or destructive tests to define the acceptance criteria.

A solid propellant rocket motor program goes through three basic phases—design, development (including qualification), and production. Items to be considered in the planning of a nondestructive testing program for these phases include:

Design Phase:

Aid in selection of materials where an option exists, based on nondestructive testing available.
Establish tentative criteria for both the test method and product acceptance.
Indicate areas of testing where the technique or methods require refinement or development.
Enumerate new tests for consideration.
Enumerate reference standards required.
Review drawings and specifications for adequacy of nondestructive testing requirements.

Development Phase:

On a continuing basis, upgrade test methods along with technique and product acceptance criteria.
Review and revise reference standards.
Automate and instrument nondestructive testing.
Investigate and establish new methods and techniques.
Improve operator efficiency through education.
Review results for causes of discrepancies, and advise manufacturing personnel for corrective action.
Establish nondestructive testing confidence levels.
Define probability of critical discontinuity detection for various nondestructive testing methods.

Production Phase:

Have all possible nondestructive testing automated and instrumented.
Have firm, defined techniques and standards.
Have firm product acceptance standards and criteria.
Monitor type and frequency of discrepancies for processes requiring corrective action.
Redefine methods and standards.

SUMMARY

This discussion has pointed out that planning requires knowledge of the problems of both today and the future. Improvements in motor performance will result from increased propellant specific impulse and from increased mass ratio obtained by reduction of design safety margins and by material changes in the motor case, the nozzle, and the interstaging.

These changes will make the task of nondestructive testing more difficult because of the geometries and materials involved. Concurrently, with the establishment of the manufacturing techniques, nondestructive testing methods should be developed. Nondestructive testing is behind the technological level of design, fabrication, and production; intelligent, concentrated work is needed to close this gap.

Proper attitudes toward cost and reliability need to be cultivated. The fact that nondestructive testing is a valuable management tool needs to be emphasized. The use of nondestructive testing early in the manufacturing process is required through integration of nondestructive testing for automatic process control. Directed research and development of new and usable nondestructive testing must be accomplished. Since any natural chemical and physical phenomenon can serve as a possible basis for nondestructive testing, the field is broad and therefore requires careful, considered judgment based on specific needs to assure proper direction of the research effort.

NONDESTRUCTIVE TEST TECHNIQUES FOR FILAMENT-WOUND GLASS FIBER - RESIN ROCKET MOTOR CASES

By E. Dane Harvey[1]

With the advent of the filament-wound glass fiber - resin pressure vessel, a material unlike any encountered previously was brought into the field. Metals and plastics having anisotropic structures have been commonplace, to be sure, but a two-phase system consisting of fibers of high tensile strength embedded in a matrix of softer plastic was a new situation. The old testing problems, such as physical property testing, thickness gaging, defect detection, and so on, were still present, but a host of new structural parameters requiring nondestructive examination were found to exist. In many instances the "tried-and-proven" nondestructive test methods were ineffective for extracting needed structural information. A fortuitous exception to this was radiography, without which the entire glass fiber rocket motor case program would have been retarded.

It is the purpose of this paper, first, to discuss the filament-wound pressure vessel, then to delineate the various inspection points, describing the nondestructive test methods found to be most successful in providing the information desired in each instance.

The Filament-Wound Glass Fiber Rocket Motor Case

During the past decade a process was developed which has resulted in the ability to form dimensionally stable pressure vessels by winding a yarn of glass filaments impregnated with a resin around a mandrel, then curing to form a rigid vessel. This technique has been successful in providing a motor case having a strength-to-weight ratio much higher than that of steel. As the process was refined, it became apparent that other desirable features were inherent in this concept. The present glass fiber rocket case not only possesses high strength but also exhibits excellent resistance to corrosion, possesses good electrical and thermal properties, is easy and relatively quick to fabricate, and has low material cost. Table 1 clearly shows the superiority of the filament-wound - resin system with regard to strength versus weight.

At this time studies are being made to transform vessel winding, presently an art, into a science. Considerable effort in time and money is being expended by many companies and the Government to establish the significance of parameters affecting the glass fiber pressure vessel. To date the delivered glass strength of the filament-wound case has been extended from 100,000 to nearly 300,000 psi. Unconfirmed glass strength of 750,000 psi has been claimed.

Briefly, the motor case is fabricated as follows. First, a mandrel is formed to close tolerances. This mandrel could be made of metal, but since it must be removed from the finished vessel, it generally is formed of plaster (which is subsequently chipped out) or a water-soluble mixture, such as sand and salt, which

[1] Staff Physicist, Allegany Ballistics Laboratory, Cumberland, Md.

crumbles when exposed to water. These mandrels are formed over a mesh framework to the desired contour. Figure 1 shows a plaster mandrel being formed.

TABLE 1.—STRENGTH VERSUS WEIGHT OF ROCKET MOTOR CASE MATERIALS.

Material	Yield Strength to Density Ratio
Filament-wound composite.	2.90×10^6 in.
Titanium	1.10×10^6 in.
Steel	0.77×10^6 in.

The rubber is cured at a controlled elevated temperature; thickness gaging and integrity are checked. The insulator-mandrel combination is now ready for the actual winding of the pressure vessel (Fig. 2).

The type of glass used is designated as "E" glass by manufacturers such as Owens-Corning Fiberglas Corp. and Johns-Manville Corp., this nomenclature referring to its original purpose

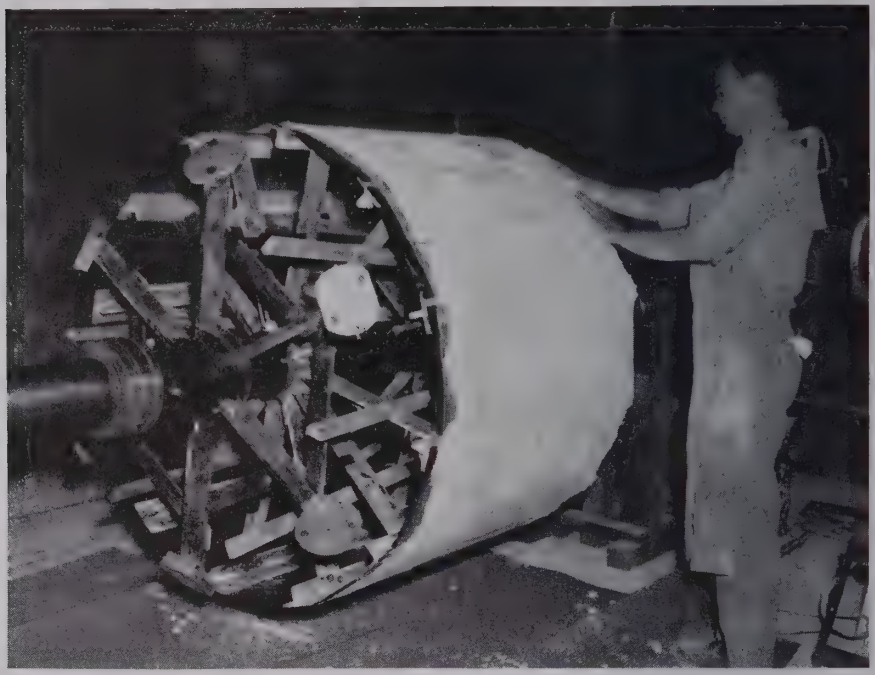

FIG. 1.—A Plaster Mandrel Being Formed.

The actual case assembly is started by laying the rubber heat insulator onto the mandrel. Special formulations of either SBR or NBR rubber filled with refractory materials are used for most applications, attention being focused on light weight and heat insulating properties. At this stage of fabrication, the phenolic or metallic nozzle bosses are positioned on the mandrel and the uncured rubber is mated to them.

of electrical insulation. The formulation is quite different from ordinary glass. A typical composition is shown in Table 2.

The glass industry has adopted a terminology which should be mentioned. The yarn used in winding comprises a group of 204 single filaments, each nominally 0.0004 in. in diameter; this grouping is called an "end." Twelve ends are grouped by twisting one or more turns per inch of length to form a

"roving." The case is wound with a band of these rovings, each band either 12 or 20 rovings wide, depending on the manufacture.

The first application of resin coating to the glass is made immediately upon drawing the filament, when using the most recently developed glass spinning techniques. Experience has shown that nascent filaments are coated as soon as possible with an epoxy resin or another finishing system to form a moisture barrier and improve handling.

The resin most used to date for chamber winding has been Shell 826 epoxy, which possesses characteristics considered desirable—namely, low viscosity at the winding temperature and good stability after curing and hardening. Many other compositions have been tried, but none has shown any significant advantage over the 826 system in general usage.

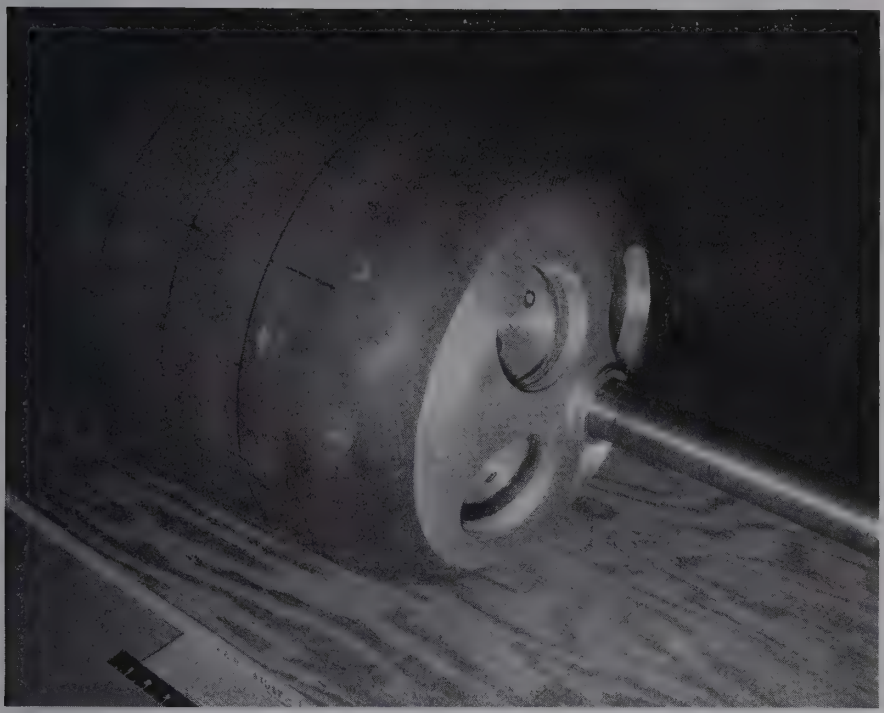

FIG. 2.—Insulator-Mandrel Combination Ready for Winding.

TABLE 2.—TYPICAL COMPOSITION OF E GLASS.

	Per Cent
SiO_2	55
CuO	17
Al_2O_3	15
B_2O_3	8.5
MgO	4.5

nascent (bare) fibers are quite sensitive to moisture, and the strength is seriously degraded by exposure to even a small amount of water vapor. For this reason, the resin, of course, is intended to hold the fibers in place and to provide a rigid pressure vessel as well as to provide environmental protection. It adds essentially nothing to the strength and, theoretically, it detracts from the strength a hypothetical "dry-wound"

case would have. Nominally, cases are wound containing 65 per cent fibers and 35 per cent resin (volumetric). With E glass and 826 resin this is about 80 per cent glass and 20 per cent resin by weight.

Returning to a typical winding process, the bobbins or packages of rovings are

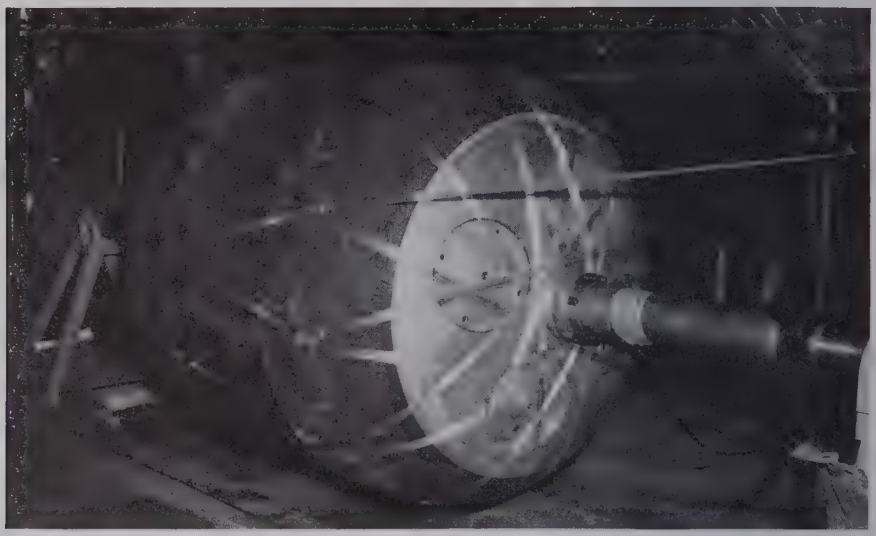

FIG. 3. –Initial Winding Process.

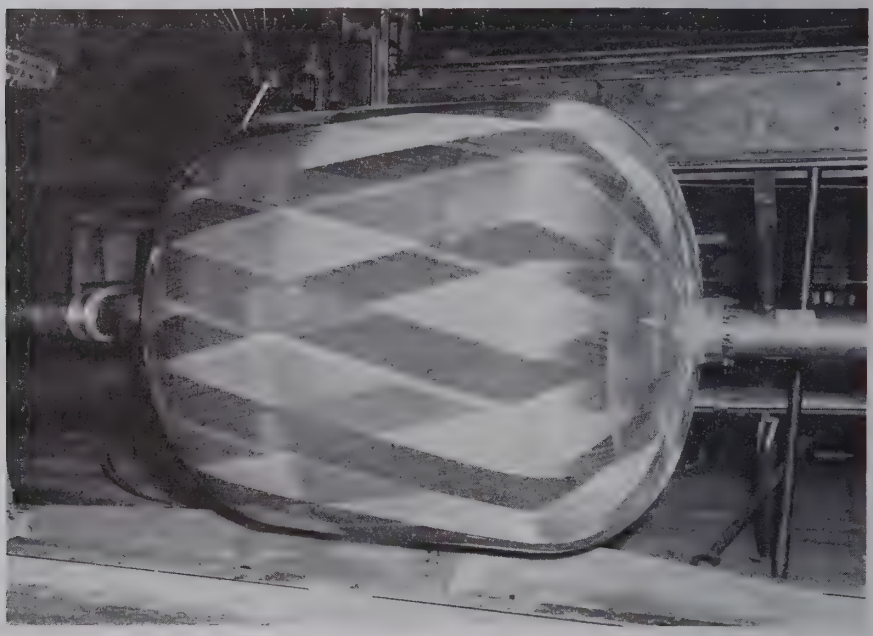

FIG. 4.—An Insulator on a Mandrel About Midway Through the Winding Process.

situated around the lathe on which the mandrel, covered with the cured insulator, is located. During winding, the rovings pass through guide eyes which form them into the band which is then integrally run through the resin bath and wound onto the insulator. Figure 3 shows the initial winding process. In order to ensure the ends being in tension and not becoming "catenary" or wavy, a reversed-clutch arrangement pulls on the band of rovings to provide the desired tension.

The winding pattern varies according to design and is achieved by programming both the rotation and point along the axis, at which the winding band is applied. Figure 4 shows an insulator on a mandrel about midway through the winding operation.

The only serious discontinuities deliberately introduced into the pressure vessel are the off-center nozzle bosses such as those used on the Polaris second-stage case. These require additional reinforcement around the port in order to transmit loads the cut filaments cannot carry about the opening.

Hoop winding is performed on the cylindrical portion of the chamber as the final winding step (Fig. 5). If metal "skirts" or adaptors are to be added, they are suitably mated, cemented in place, and final winding performed over them to provide a smooth contour.

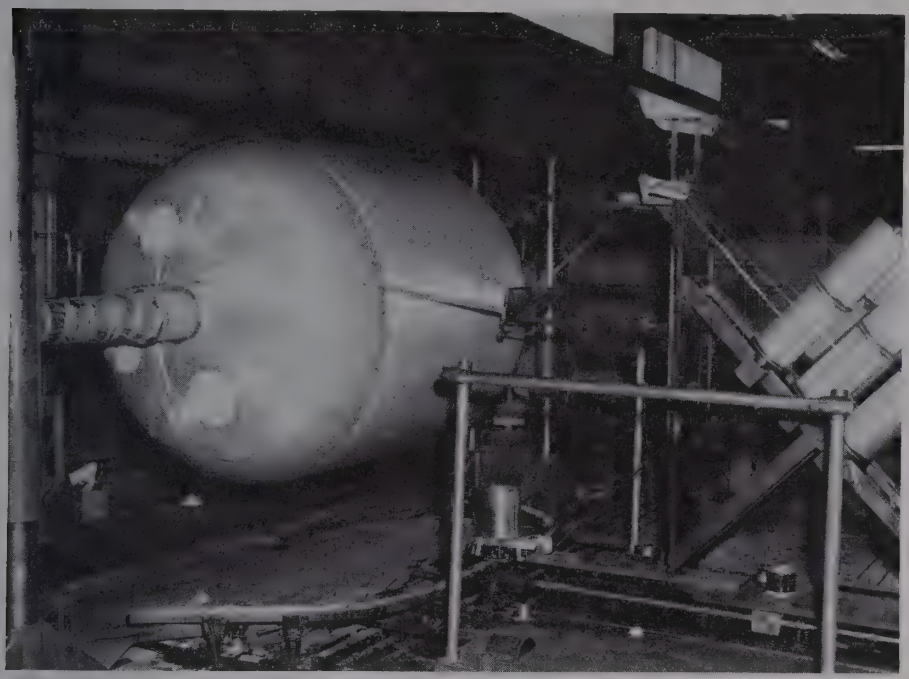

FIG. 5.—Final Winding.

The case is cured in a special oven having a controlled circulating atmosphere. Cure temperature and time vary according to design but are nominally 300 F and less than 1 day, respectively.

NONDESTRUCTIVE TESTING OF THE FILAMENT-WOUND CASE

One of the best questions one could ask is "What do you test for to assure optimum performance from a glass

filament-wound case?" Every operation performed on the glass during case manufacture reduces the physical strength of the glass. The high number of parameters affecting strength have not been separated or even categorized with any degree of success. Elaborate analyses are being performed by every company active in the filament-winding field. Progress is being made, but at this time the only successful method of testing is to perform every practicable test. (Destructive testing and hydrostatic testing are used and relied upon to a considerable degree, but are beyond the scope of this paper.)

Nondestructive Examination of the Rubber Insulator:

At least one facility known to the author is using a rubber material that is partly translucent to visible light in the raw stage, at which time it is in thin sheets. A candling technique employed by Aerojet-General (Sacramento) has been successful in detecting foreign material and internal cuts. Many discontinuities that subsequently disappear during the curing operation are also detected in this manner. Those that do not disappear are patched.

Once the insulator has been put on the mandrel and cured, it is necessary to gage the thickness as well as to inspect for tears and foreign material. The way this is accomplished varies widely with the type of mandrel used. If the insulator has been made on a metal mandrel (used for fabrication of the insulator above) it is necessary to cut it into two pieces in order to remove it. Thickness can be gaged while on the metal mandrel by use of eddy current techniques, which have been found to provide an accuracy of 5 per cent or better up to a thickness of about $\frac{3}{4}$ in. Capacitive and ultrasonic gaging have proved somewhat more accurate, ranging down to 2 per cent accuracy on insulators between 100 and 500 mils thick. Since the insulator is

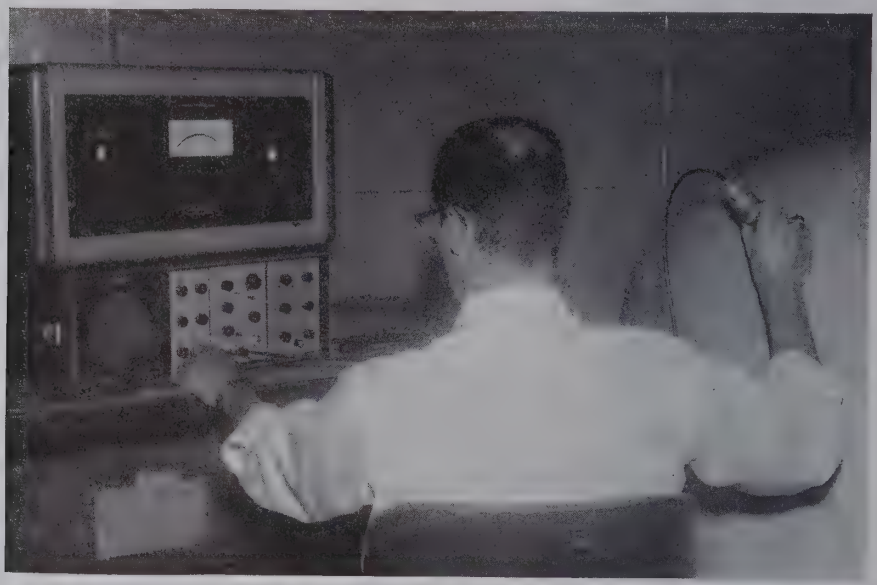

FIG. 6.—Ultrasonic Gaging of Area of Insulator.

removed from the metal mandrel, however, mechanical gaging is used to measure most of the desired area. Ultrasonic gaging is frequently employed for the "hard-to-reach" regions as well as for those positions where mechanical gage accuracy is difficult to obtain because of the geometry of the insulator (Fig. 6).

Whenever a plaster or sand-salt type mandrel is used, the situation is radically different. It will be recalled that this type of mandrel is not removed until after complete chamber fabrication. Rubber thickness must be known as soon as possible in order that corrective measures can be taken prior to the onset of winding.

Ultrasonic examination has not proved to be satisfactory because of coupling between insulator and the so-called "strippable liner," which is designed to facilitate removal from the mandrel. This interferes with a large number of the readings and makes interpretation impractical. In order to combat this, inserts of two thicknesses of aluminum foil (the type embossed with a mesh pattern) are situated between the insulator and the strippable liner. These readily reflect the ultrasonic wave and have extended the depth for which thickness can be accurately (2 per cent) determined to 0.75 in. The existence of this foil also permits capacitance gaging; it is of interest to note that in at least one instance at Allegany Ballistics Laboratory a higher accuracy was realized with the capacitance gage than with the ultrasonic instrument (1 to $1\frac{1}{2}$ per cent as compared with $1\frac{1}{2}$ to 2 per cent).

X-ray examination using low kilovoltage fine focal spot machines is performed on insulators that have been removed from the mandrel. It is possible to perform this inspection rapidly while demonstrating a 1 per cent sensitivity by using a rod-anode type X-ray generator and fine-grain film wrapped around the periphery of the insulator. An entire insulator can be inspected in less than 1 hr using this technique.

It is entirely feasible to gage thickness using radioactive sources and calibrated detectors, but the author is unaware of any attempts to employ this concept on rubber insulators used as part of glass-fiber rocket cases. Aerojet-General Corp.[2] has reported success using a corona or a "spark discharge" inspection on insulators to reveal internal paths and delaminations which can lead to pressure leaks.

Efforts are being made by several different ultrasonics companies to extend the thickness gaging range upward to cover the entire thickness range encountered. Methods being pursued generally employ lower frequencies, and some incorporate frequency sweeping to minimize standing wave effects.

Ultrasonic inspection is contemplated for second-stage A3/Polaris insulators with the transducer housed in a roller type device held against the insulator, moved along a spiral path in a lathe device. Readout would be twofold: a series of numbers would be printed out to represent thickness, while a "C" scan record would be produced to show discontinuities present in the insulator. The heart of the device would be the doughnut-shaped roller transducer which currently is being developed by Automation Industries at their Boulder, Colo., facility.

Nondestructive Examination of Bonds Between Glass Fiber Case and Metal or Phenolic Parts:

The bonds between the nozzle boss and the rubber insulator as well as those between boss and filament-wound case are examined thoroughly. Again, several

[2] *Report SRP:6000:1847:cs P-5647*, Aerojet General (Sacramento).

different methods may be used. Aerojet-General Corp. (Sacramento) has reported success using a special variation of the Sperry ultrasonic thickness gage as developed by D. C. Erdman.[3] This instrument is used wherever the rubber thickness does not exceed 0.400 in.; heavier sections are inspected tangentially using high-voltage radiography. This is attached to the case by means of an epoxy adhesive. The inspection for presence or absence of adhesive is performed immediately after the skirt has been attached, using a portable rod anode 150-kvcp machine. "Day pack" 70 mm wide fine-grain film is wound around the outer periphery of the case at the area of adhesion. If the film does not

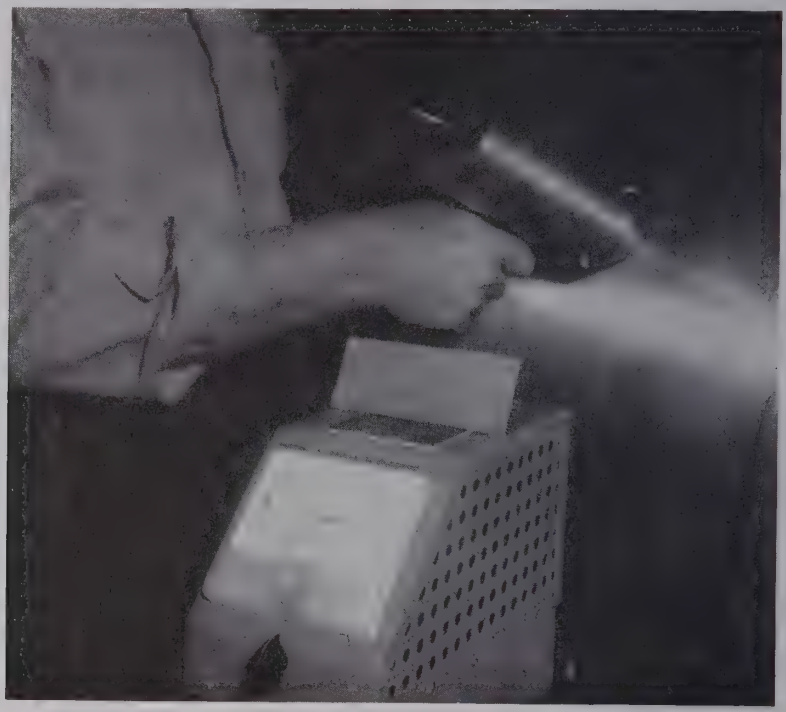

FIG. 7.—Moisture Detection Gage Being Used on Glass Fiber Case.

At Allegany Ballistics Laboratory this operation is performed by tangential radiography using the 24-Mev betatron exclusively. In either instance, detection of the bond condition is considered to be satisfactory.

The Polaris glass-fiber case is required to have an aluminum attachment skirt at the outside diameter where the cylindrical portion meets the domed ends. meet the defect standard, the skirt is removed and the operation is repeated.

After cure of the skirt bond adhesive, an ultrasonic check is made of the bond using a Branson Sonoray. This indicates the condition of the bond, not merely presence or absence of the adhesive, as told by the in-process X-ray examination.

Nondestructive Examination of the Finished Filament-Wound Case:

As mentioned above, it is believed widely that moisture adversely affects

[3] AGC Report to 17th Polaris-Minuteman-Pershing Nondestructive Testing Committee Meeting held at Martin-Orlando, Orlando, Fla., May 26, 1961.

the strength of a glass-fiber pressure vessel. Every case fabricated in the Allegany Ballistics Laboratory Polaris program has exhibited a surface phenomenon called "crazing." There is considerable speculation as to whether crazing is deleterious due to permitting moisture to penetrate through the resin onto the fibers.

Nondestructive tests for crazing are numerous. It is observed visually with visible and ultraviolet light. The indications can be amplified by using electrified particle techniques. It can be recorded directly by making a mold of putty pressed against the crazing.

Attempts to detect the moisture content of the glass fiber case have led to the development of a moisture detection gage by the U. S. Naval Research Laboratory.[4] This device operates on the principle that the electrical permittivity of epoxy is considerably less than that of water at radio frequencies. A capacitance probe is placed on the surface of the case. The effect of the dielectric on the capacitance of a high Q tuned circuit is indicated by a frequency shift which has been related to moisture content of the resin (Fig. 7). Unfortunately this concept integrates the moisture present over the field (humidity is added into the reading), and it is impossible at this time to tell how the moisture is distributed according to depth. This characteristic has been used in recent experiments to indicate unbondedness between case and liner. The success of these experiments has not yet been established; modification and development of such a tool will be seriously considered.

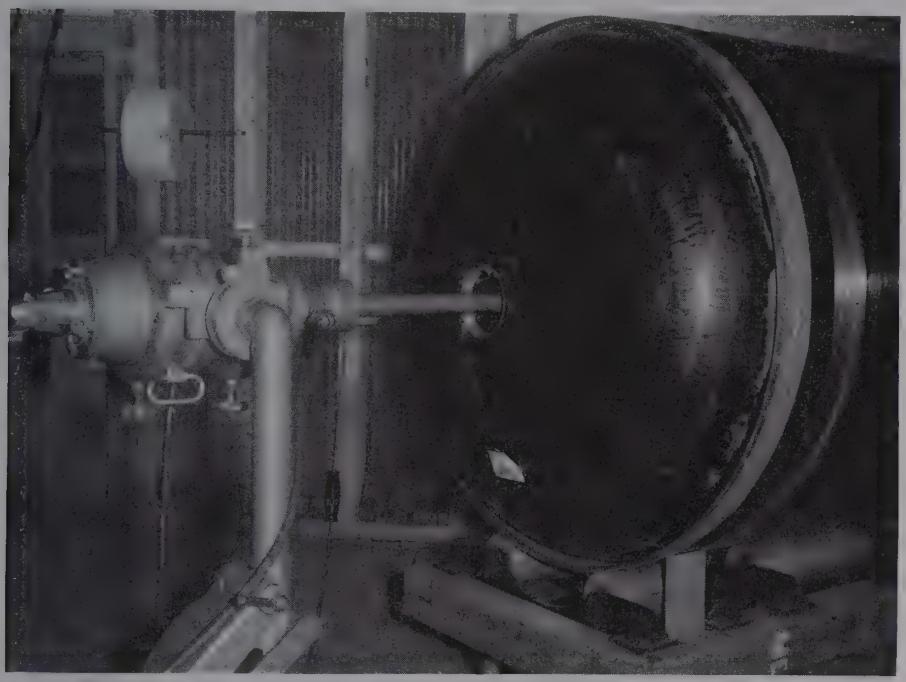

FIG. 8.—X-ray Examination of the Finished Case.

[4] J. O. Outwater and G. A. Gague, "On the Detection of Moisture in Rocket Case Materials," NRL Project 62RO5 19A, *Technical Memorandum 191*.

An interesting application of this gage is to trace the moisture path in a case which "wept" during hydrotest. Strong indications are obtained if the inspection is made soon after hydrotest. This enables repair to be made with a minimum of delay.

X-ray examination of the finished case is performed in a manner quite similar to that performed on skirt bond. A 150-kvcp rod anode X-ray generator is situated along the axis of the case and the finest grain film available is located right on the outer periphery of the case (Fig. 8). The sharpness and detail of film exposed in this manner is outstanding and the problem is that too much is detected. Discontinuities detected in this manner include resin-lean areas, broken fibers, knotted fibers, uneven winding, and relaxed or "catenary" fibers. It is questionable whether or not these are defects for which inspection should be performed. Each of these does degrade strength when present in a small specimen area, but there is a question as to the relative importance of the condition (or set of conditions) in a full-scale case. Unfortunately, at this writing no meaningful defect criteria exist.

FIG. 9.—Weaving Pattern of Fibers.

The U. S. Naval Ordnance Laboratory at White Oak, Md., has provided a technique which could be the key to the above problem. Into each band of rovings one end of leaded glass is incorporated. Under the type of X-ray examination described above, the leaded fiber stands out sharply, even when deep in the case. Evidence was recorded of

many of the above discontinuities. It is planned to wind several full-scale cases with a tracer in the band to establish the severity of these conditions by correlating firing results with the examination.

The leaded-filament tracer technique is valuable not only in production but also in research and development. As an example, destructive tests performed by different companies have revealed that it is desirable to program the tension to provide continuously less pull on the outer windings. Specimens cut out of hydroburst cases showed a weaving pattern of relaxed fibers; it was observed that the deeper in the layer, the greater was the tendency to weave (Fig. 9). This is almost certain to affect strength adversely because of nonuniform loading. The Naval Ordnance Laboratory tracer technique provides an excellent means of detecting any such condition.

Another nondestructive testing technique recently made available for chamber inspection is the infrared scanning of a case full of water which is heated to 120 to 150 F. The Palo Alto division of Lockheed Missiles and Space Co.[5] has developed an infrared detection system which has demonstrated high signal-to-noise ratios of liner-case and liner-nsulator unbonded conditions. This device is also extremely sensitive to delaminations in the glass-fiber case, but as yet no importance has been ascribed to this condition.

As was mentioned above, tangential radiography using the 24-Mev betatron is relied on heavily at Allegany Ballistics Laboratory. The extremely small focal spot size and penetrating power of this instrument enables it to reveal even minute discontinuities in the nozzle port area. Over the years a vast library of conditions in this area has been compiled and a realistic set of defect criteria has been generated. Other facilities have followed suit with various high-voltage generators and, while high-voltage radiography is primarily directed at loaded motors, the technique is being widely used in empty chamber inspection. In the domed ends of Polaris and Minuteman cases, the radii involved are such that chordal paths through the empty case frequently exceed 1 ft, and high-voltage equipment is needed for optimum exposures.

It should be mentioned that whenever pertinent, radiographic and ultrasonic inspections are required to be performed by the vendor on inert components. Close checks are maintained to ascertain quality of these inspections.

Areas in Which Nondestructive Testing Techniques Are Used for Research and Development

The lead roving tracer technique mentioned above is used as a research tool to detect patterns and locations of fibers in experimental winding research. A similar technique is employed wherein tiny lead grid wires are used to exhibit motion in various layers during stress tests. This can be used in conjunction with leaded fibers to show the relative motion of fiber and matrix during stress. Elongation of fibers can be measured by observing the motion of tracer dots indexed into rovings.

One of the most reliable means of determining filament modulus is accomplished by ultrasonic means. A filament is stretched between two crystal phonograph cartridges and is attached to the needle with red sealing wax. An audio oscillator drives one cartridge, while a sensitive a-c vacuum tube voltmeter is connected across the other crystal. The oscillator is tuned for a maximum indication on the vacuum tube voltmeter, at which point the filament is assumed

[5] F. Alzafon, Report to 22nd Polaris-Minuteman-Pershing Nondestructive Testing Committee Meeting held at AGC, Sacramento.

to be one-half wavelength long. It is easy to determine the modulus from the thin rod velocity relationship $v = \sqrt{Y/\rho}$, where Y is modulus and ρ is the density. This type of setup is used by Goodrich Research, Brecksville, Ohio.[6]

A method is being developed to monitor the degree of cure during the cure cycle using an infrared spectrum scan. At this writing, it is too early to predict the success of this test.

SUMMARY

In summary, it can be seen that without nondestructive testing of filament-wound cases severe penalties of time and money would have resulted.

It is further noted that filament-wound glass-fiber cases achieve but a fraction of the stress level they theoretically should withstand. Part of the blame for not having realized higher stress levels must be placed on insufficient testing of this new medium. Because of the dramatic successes and improvements in the Polaris and Minuteman missiles, further improvements in nondestructive testing systems will eventually be called for in even more advanced systems. As glass of higher strength is realized, thinner pressure vessels will evolve, each with a new host of structural test areas.

[6] Kenneth F. Gill, personal communication.

QUALITY CONTROL OF HIGH-TEMPERATURE SOLID ROCKET CONTROL COMPONENTS

By Richard L. Ahearn[1]

Some of the problems encountered in establishing quality requirements for jet vanes used in solid propellant rockets will be described as well as the processing techniques used to assure a reliable product. The development and testing of jet vanes was described in a previous paper.[2]

Quality control requirements for jet vanes are unique in that the usual concepts of material acceptance standards had to be revised to accommodate the unusual circumstances under which jet vanes operate. Material would ordinarily be considered unacceptable for use in a critical missile structure if it had the following characteristics: zero ductility, shattering like glass when dropped, large surface cracks and voids, and chemical analysis outside acceptable forge shop limits.

These characteristics, along with severe environmental conditions, would cause most missile designers to reject this material. However, rather than resort to a completely new thrust vector control system, since we did not know the material would not work, we used it, and it proved to be completely acceptable.

In dealing with a new material for a new application, the tendency is to go to extremes in setting tight acceptance standards to compensate for ignorance as to what the actual quality requirements should be. This attitude is very expensive. Our prime concern was to establish the true rejection standards for the part in relation to its function and then to control only those processing variables that affect the proper functioning of the part.

Quality Requirements Established by Material Performance

The purpose of the jet vane is to control the direction of the missile's flight by deflecting the jet blast at the exit of a stationary nozzle. Figure 1 shows the location of the jet vanes behind a rocket nozzle. The vanes must deflect, or actuate, from +25 deg to −25 deg from the center line of the missile within 1 sec. Figure 2 is a close-up view of a jet vane assembly after firing. The vane's leading edge must have minimum erosion so that an adequate lifting surface is maintained. The force of the supersonic exhaust produces a bending load of about 6000 psi, and the flame temperature is around 5500 F. The horizontal members, made from sintered and rolled molybdenum plate, serve to deflect the jet blast away from the vane actuating mechanism.

It is obvious that such a vital part of the missile's "steering system" must be extremely reliable. In fact, a major consideration in selecting a particular thrust vector control system is the reliability of the components. The jet vane control system is very simple in design, giving it an inherent reliability advantage over

[1] Design Specialist, Materials Laboratories, Research Division, Martin-Marietta Corp., Orlando, Fla.

[2] Richard L. Ahearn, "Development of Jet Vanes for Solid Propellant Missiles," *Journal*, Soc. Automotive Engrs., Aug., 1962, p. 53.

more complex systems such as movable nozzles or jetavators. However, the jet vane material is subjected to a more severe environment than in other systems since its leading edge is exposed to the total temperature and maximum velocity of the propellant gases.

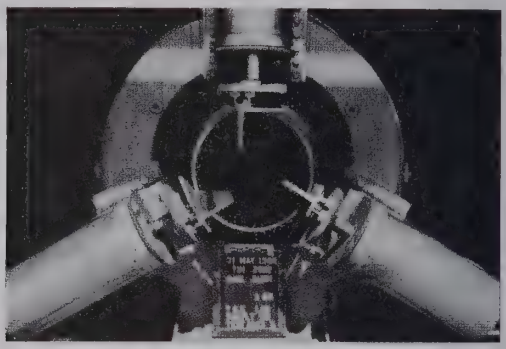

FIG. 1.—Jet Vane Assemblies Behind Motor.

FIG. 2.—15-85 Molybdenum-Tungsten Jet Vane Assembly After Firing.

After a static firing program which simulated actual flight environments, the jet vane material finally selected as meeting all the requirements for production was arc-cast 15-85 molybdenum-tungsten alloy. The vanes were machined from ingots supplied by Climax Molybdenum Co. and from centrifugal castings supplied by Oregon Metallurgical Corp. This material has zero ductility at room temperature; therefore the brittleness of the vanes must be considered in machining and handling. Upon analyzing the requirements of the jet vane in terms of its function, it is realized that room-temperature ductility is not a requirement. Neither is the absence of surface defects a requirement, because of the particular sequence of environmental conditions.

FIG. 3.—Bent Jet Vanes.

Figure 3 shows that jet vanes actually fail because of excessive ductility,

whereas a failure has never occurred because of brittleness or surface defects. Although the vane is completely brittle and notch-sensitive at room temperature, it is heated within several seconds after motor ignition to above the 500 F brittle-ductile transition temperature. On several occasions, vanes have left the test fixture during firing, traveled 150 ft through the air, and landed upon concrete without breaking. If it were required that the vane be ductile at room temperature, a 90-10 tantalum-tungsten vane would have to be used which would cost about six times as much as the 15-85 molybdenum-tungsten vane.

A similar situation existed several years ago with the Ford crankshaft. For years only forgings were used for crankshafts because the designer thought he needed a ductile, high impact-resistant part. Shipments of parts were accepted for use only after a 6 per cent minimum elongation was demonstrated. This requirement was established only because a crankshaft usually had more than 6 per cent elongation if it were forged and heat treated properly. Only after the actual part requirements were analyzed was it realized that a bent crankshaft would be just as useless as a broken one. After that, cast crankshafts with near-zero ductility were used satisfactorily.

The establishment of a high confidence level for jet vanes depends upon the control of the processing of the material from which the vanes are made. The determination of significant variables and the assurance of reproducibility of these variables is a difficult task with arc-cast ingots.

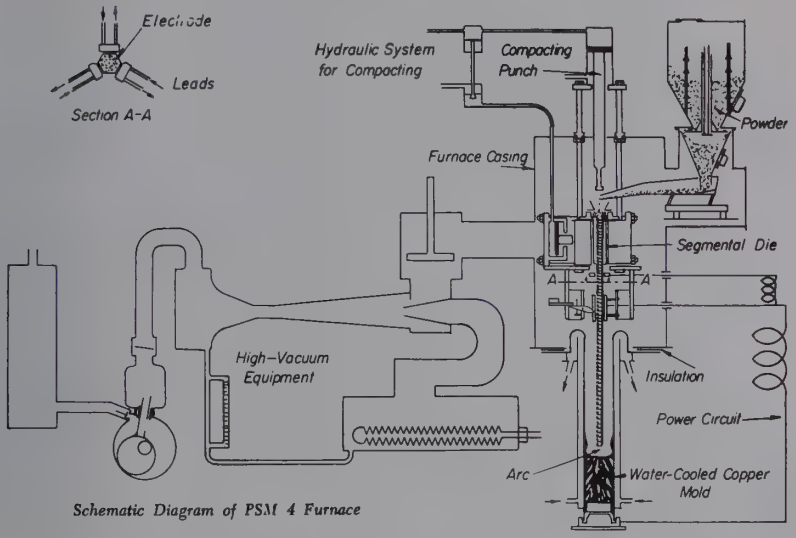

FIG. 4.—Automatic Press-Sinter-Melt Vacuum Furnace.

The methods used for quality control of arc-cast ingots, other than in the melting process itself, are chemical analysis, mechanical property tests, ultrasonic inspection, and dye penetrant inspection.

ARC-CASTING PROCESS CONTROL

A schematic diagram of Climax Molybdenum's continuous pressing, sintering, and melting furnace is shown in Fig. 4. The electrode is formed from molyb-

FIG. 5.—Arc-Cast 15-85 Molybdenum-Tungsten Ingot.

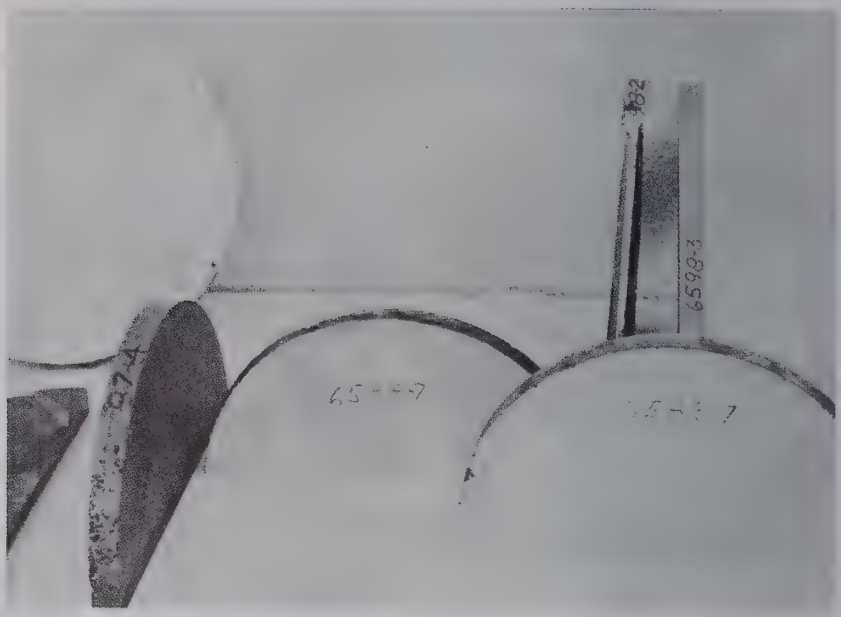

FIG. 6.—Slices of 15-85 Molybdenum-Tungsten Ingot.

denum and tungsten powder which has been blended with a small amount of carbon for a deoxidizer. Up to 30 per cent of chips, prepared by crushing arc-cast 15-85 molybdenum-tungsten turnings, can be included when available. This charge is fed from the hopper above the furnace by a vibrating plate to the hydraulically operated compacting dies. The pressure must be such that the compact will have sufficient green strength so that it will not crumble. The electrode must then be sintered so it can support its own weight when it reaches the bottom of the mold. One contact of the sintering circuit is the die; the other is a pair of water-cooled copper shoes approximately 10 in below. The sintered electrode must be straight and centered to avoid contact with the side of the mold.

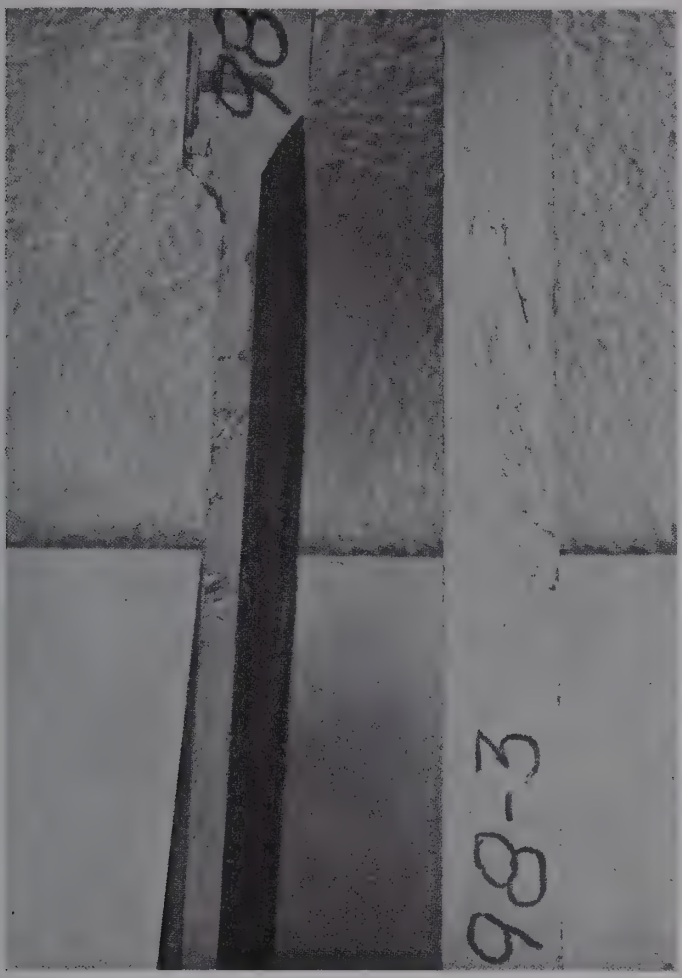

FIG. 7.—Grain Pull-out During Machining.

Alternating current flows from the water-cooled copper shoes through the electrode to the arc gap (where melting occurs), then to the bath and solidified ingot, and finally to a water-cooled copper plate forming the bottom of the mold. The mold is also water-cooled copper. The entire operation of pressing, sintering, and melting is performed in a vacuum of 2 μ.

Close process control is required to maintain a satisfactory vacuum, make a suitable electrode, and coordinate electrode feed with melting rate. Each lot of powder is examined microscopically for particle size and structure. The powder must also meet a maximum weight loss requirement on heating and a minimum compressive strength when compacted under a specified load.

Figure 5 shows a 30-in. long $9\frac{3}{8}$-in. diameter ingot stripped from the mold.

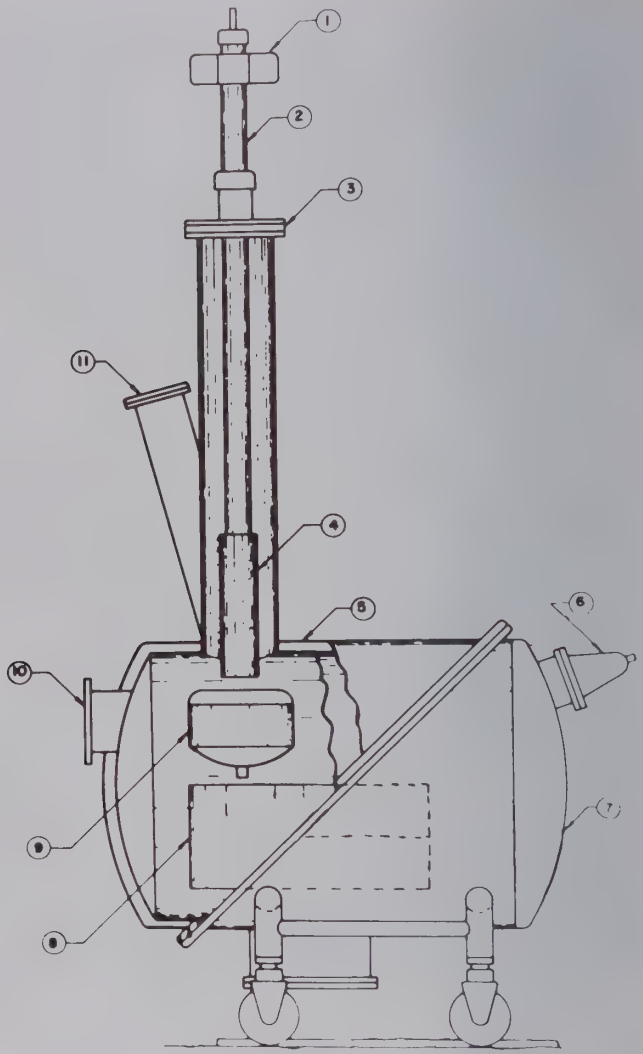

1, Power lead clamping plate,
2, Water-cooled electrode ram,
3, Micarta insulator,
4, Electrode,
5, Water-cooled vacuum chamber,
6, Light port,
7, Mobile vacuum chamber,
8, Mold spin tub,
9, Water-cooled crucible,
10, Vacuum port, and
11, View port.

FIG. 8.—Arc Melting and Centrifugal Casting Equipment.

About $\frac{1}{4}$ to $\frac{1}{2}$ in. is machined from the surface in a lathe, using a carbide tipped tool. Figure 6 shows some of the defects encountered in some slices sawed from an 11-in. diameter ingot of arc-melted material. A circular crack is barely visible in the center piece. This linear type of crack is unacceptable in jet vane material. The slices are shown with dye penetrant developer on them. Note the rings of porosity near the surface and the deep porosity on the exterior surface. The surface porosity is of no consequence because this area is cut away when the vane is machined out of the slab. The slab on the right of the picture shows the partially machined vane leading edge portion. This is shown in a closer view in Fig. 7. Notice the severe chipping, or grain pull-out, and apparent cracking. This is only a surface grain condition and is not significant for jet vane application. It is caused by the large grain size of the arc casting, as will be shown later. This ingot was particularly difficult to machine because of grain pull-out at sharp edges.

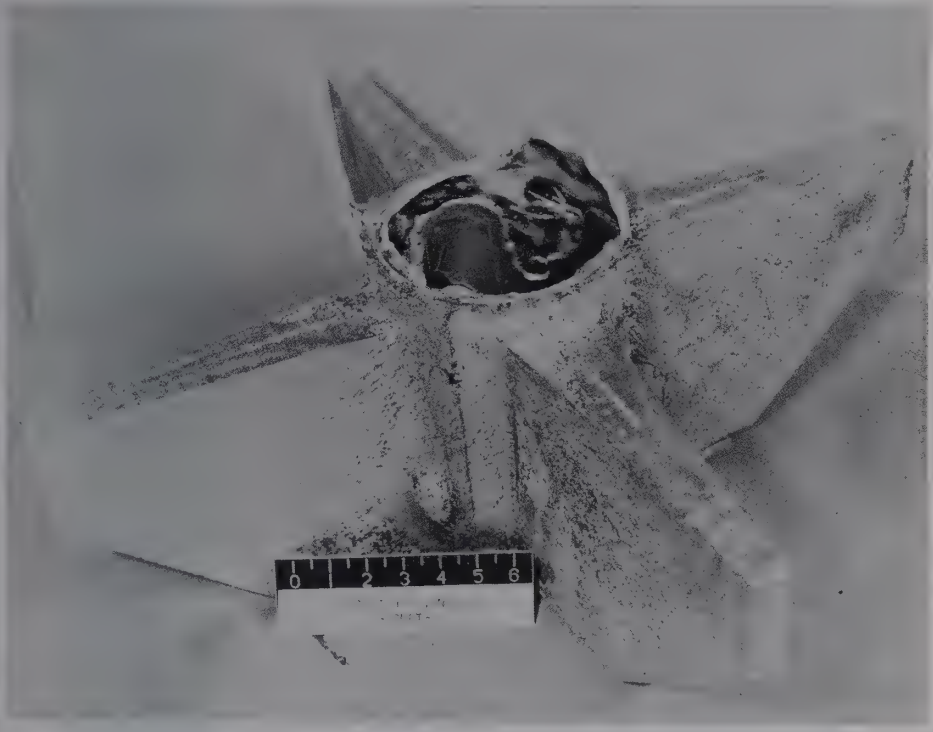

FIG. 9.—Four Jet Vanes Connected with Gating and Riser Metal After Removal from the Graphite Mold.

Linear or circumferential cracking may be detected by visual, dye penetrant, and ultrasonic inspection, although its cause is difficult to determine. This type of cracking was attributed to an increased ratio of ingot to electrode diameter in going from a $9\frac{3}{8}$-in. to an 11-in. diameter ingot. Cracking had also been reported in ingots when going to a smaller diameter than the normal production run. This was attributed to a faster cooling rate. Arc instability is another cause of ingot

cracking. The high melting point of tungsten requires high power input, thus increasing the chance of arcing through the crucible and rough ingot surfaces. Once cracking is eliminated, all the variables in the arc melting process must be rigidly controlled.

An attempt was made to relate the cracking and grain pull-out tendency of the 11-in. diameter ingot to the room-temperature flexural strength of the material. The flexural strength of this ingot was compared to that of $9\frac{3}{8}$-in. diameter ingots since the latter material had never given trouble with cracking. However, no correlation existed. It was surprising to discover that flexure specimens polished to 16 rms finish and tested at room temperature did not fracture in areas of grain pull-out, even though near-maximum stress occurred in these areas.

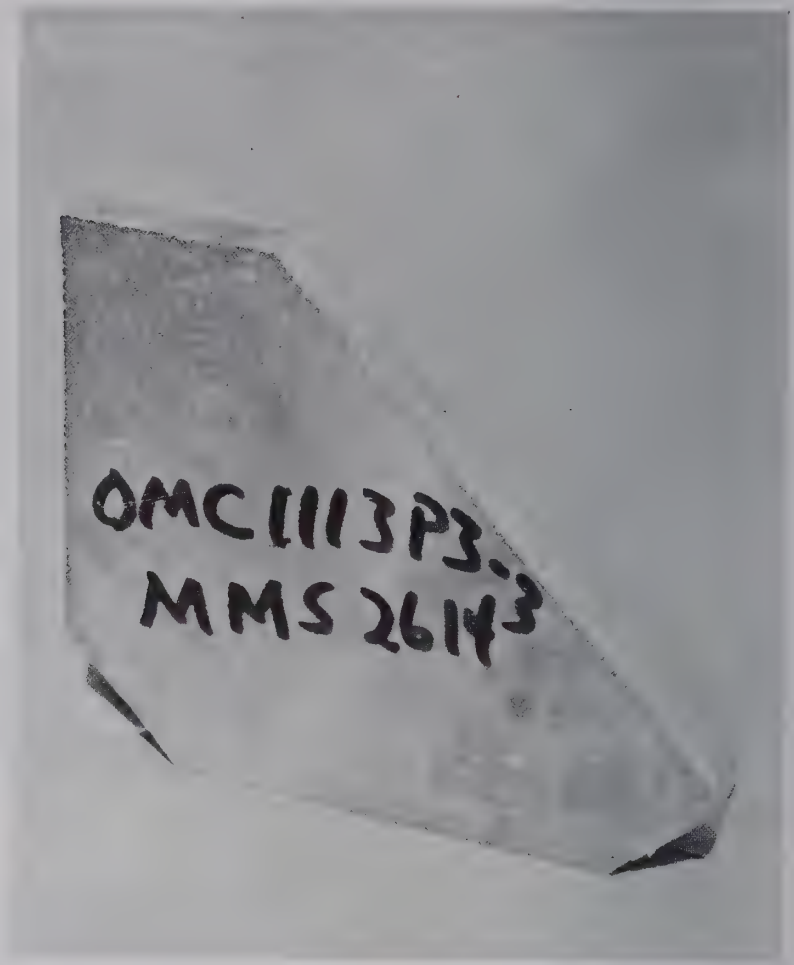

FIG. 10.—Rough Trimmed Jet Vane Casting.

CENTRIFUGAL (HIGH-PRESSURE) CASTING PROCESS CONTROL

The centrifugally cast product from Oregon Metallurgical Corp. employs a

vacuum arc melting furnace (Fig. 8) similar to that previously described except that the presintered electrode is manually fed into the molten metal and the proper arc gap is maintained by observation of the arc through a view port. After the electrode is melted, the water-cooled copper crucible is tilted and the molten metal poured within 4 sec into the center of a graphite mold which is rotating at 400 rpm. The electrode, crucible, and mold are enclosed in a water-cooled vacuum chamber. The chamber is evacuated in $\frac{1}{2}$ to $\frac{3}{4}$ hr; the melting and pouring requires only 5 min. Then the casting is allowed to cool in the spinning mold for about $1\frac{1}{2}$ hr. The chamber vacuum is about 15 μ just before the chamber is opened.

Figure 9 shows four jet vanes connected with gating and riser metal, after removal from the graphite mold. Initial pourings were made with 3-piece castings which weighed 345 lb plus about 25 lb of funnel "skull" or metal solidified on the pouring surface of the crucible. In order to melt this quantity of metal in 5 min, a 34,000-amp at 42 v, d-c power supply is required. This power requirement is greater than that of the standard arc-cast

FIG. 11.—Finish Machined Jet Vanes.

PURE MO HIGH-PRESSURE CAST

1.5X R_B 83 1.5 GRAINS / MM

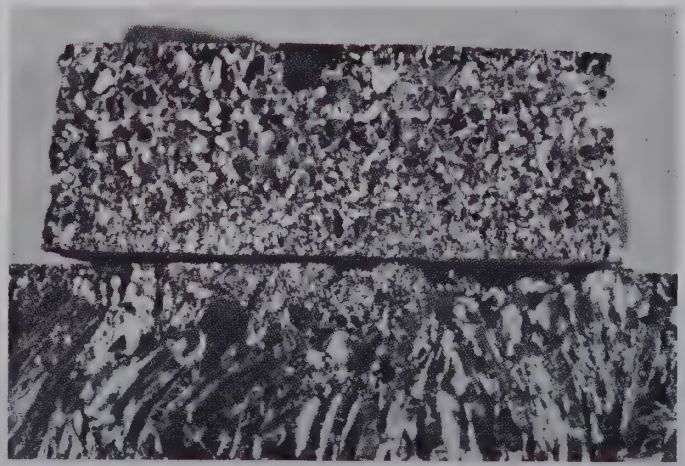

1.5X R_B 80 0.5 GRAINS / MM

PURE MO ARC-CAST INGOT

PURE W HIGH-PRESSURE CAST

1.5X R_C 32 1.0 GRAINS / MM

1.5X R_C 34 0.2 GRAINS/MM

PURE W ARC-CAST INGOT

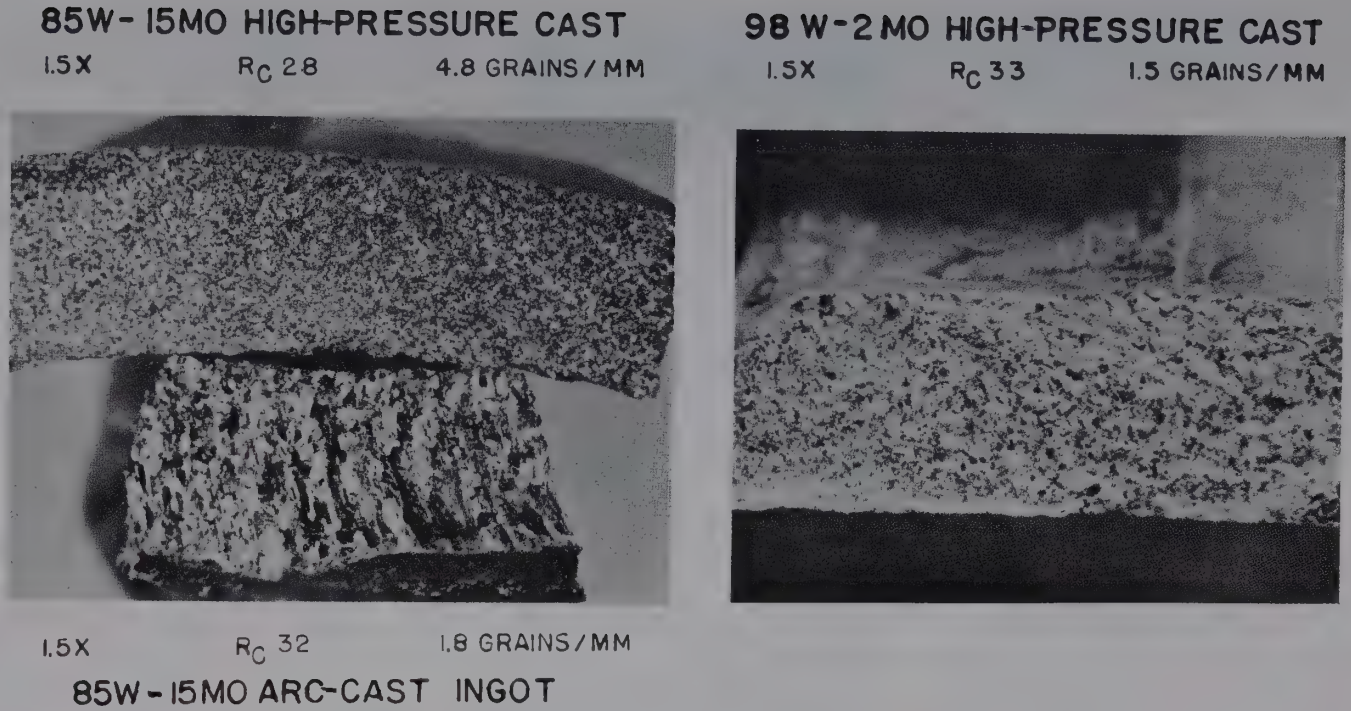

FIG. 12.—Grain Size Comparison of Arc-Cast and Centrifugal (High-Pressure) Cast Ingots.

ingot furnace in order to melt quickly and keep a large volume of metal molten within the crucible. In the previously described continuous pressing, sintering, and melting furnace, only a small amount of metal remains molten as the ingot solidifies within the copper crucible.

The jet vane walls are tapered with a 6 deg included angle in order to prevent shrinkage porosity. The tip of the as-cast vane is about 1 in. thick and the riser section is about $1\frac{1}{2}$ in. thick. The individual vanes are broken away from the central riser and stress relieved at 1000 F in a gas-fired furnace. The vanes are packed in graphite to prevent excessive oxidation during heating. The surface carbon picked up during casting in the graphite mold and during stress relieving is removed by machining. The riser area is cut off to remove piping and shrinkage porosity, and the edges are trimmed as pictured in Fig. 10. This rough trimmed casting is about 0.9 in. thick at the base and 0.6 in. at the tip.

Comparison of Arc and Centrifugally Cast Product

The finish machined jet vane is shown in Fig. 11, as viewed from the leading edge. The vane on the left shows the smooth surface typical of the fine-grained centrifugal casting. The other vane's leading edge contains numerous surface defects and cracks produced in the machining of the columnar-grained arc-cast ingot slab. A surface finish of 16 rms can be produced by special machining techniques. The centrifugal casting process causes an acceleration of the molten metal solidification rate. This produces the fine-grained structure in contrast to the columnar grain of the standard arc-cast ingot.

A comparison of grain size between the arc-cast ingot and the centrifugal or high-pressure casting is shown in Fig. 12. The macrographs of the fractured surfaces are at 1.5×. The 85-15 tungsten-molybdenum material is shown in the bottom left-hand corner. The centrifugally cast specimen has an average grain size of 4.8 grains per mm, whereas the ingot grains are almost three times as large. The pure molybdenum and pure tungsten specimens, shown in the upper half of the photograph, have much larger grain size in both the centrifugally cast and ingot material. The addition of only 2 per cent molybdenum to pure tungsten decreases

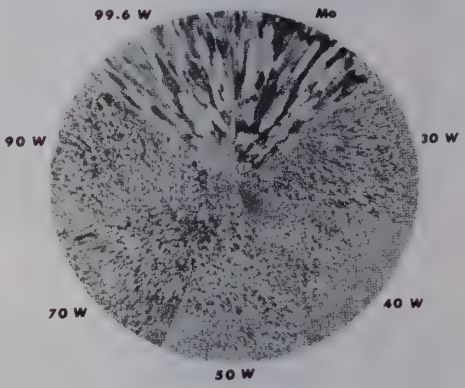

FIG. 13.—Effect of Alloying on Grain Size of Molybdenum and Tungsten-Molybdenum Arc-Cast Ingots 7 to 9 in. in Diameter.

the centrifugally cast grain size by 50 per cent, as shown in the lower right-hand photograph. The effect of alloying on the grain size of 7- to 9-in. diameter arc-cast ingots is again shown in Fig. 13. Notice that the grain size of the molybdenum-tungsten alloys is smaller than that of either pure tungsten or pure molybdenum. This smaller as-cast grain size contributes to the higher elevated-temperature strength of the alloys and to better machinability of 15-85 molybdenum-tungsten than pure tungsten.

The uniformity of grain size is also greatly improved in the centrifugal casting because of the equiaxed nature of the grain and the more uniform cooling rate.

Figure 14 shows photomacrographs of the thick and thin sections of a jet vane centrifugal casting at 150×. Also shown is a macrograph at 2.2× of the riser section of a vane casting broken across a shrinkage cavity stringer.

(*a*) Thick end, 0.890 in.; 6.1 grains per mm (×750). (*b*) Thin end, 0.610 in.; 7.7 grains per mm (×150).

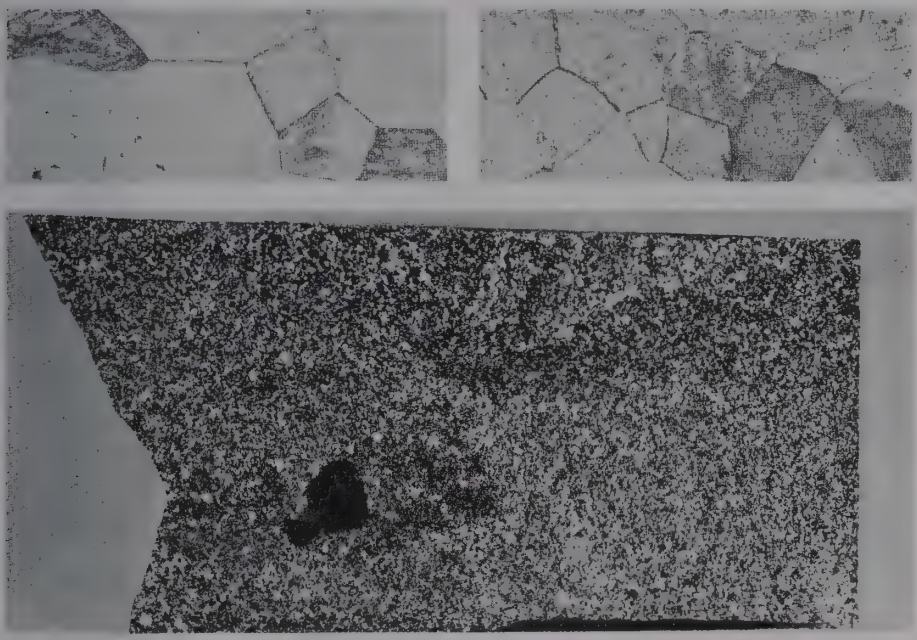

(*c*) Riser section (×2.2).

FIG. 14.—Grain Size of a 15-85 Molybdenum-Tungsten Jet Vane Centrifugal Casting.

NONDESTRUCTIVE TESTING

The depth of shrinkage defects and porosity within the casting is determined by submerged ultrasonic inspection. A recorded trace of a jet vane casting is shown in Fig. 15. The vane surface was scanned and defects recorded automatically using Automation Industries equipment. The heavy dark area at the base of the vane is internal piping or shrinkage voids. The small indications in the center of the vane are slight shrinkage porosity. The unsound metal at the base of the vane is removed in rough machining. The dark areas outlining the vane are edge reflections. Untrasonic inspection is quite effective in detecting internal defects in the centrifugal cast material having small nondirectional grains. However, the large grain size and grain directionality of arc-cast ingots limit the effectiveness of ultrasonic testing.

The sensitivity in the detecting of subsurface defects depends on the sonic frequency of the transducer. Sensitivity increases with increasing frequency and decreasing wavelength. However, as the frequency is increased, the sonic wavelength approaches the dimensions of the grain size of the material and absorption and dispersion of the wave occurs, resulting in a loss of backface reflection. Because of this, the effectiveness of ultra-

sonic inspection is diminished when testing the arc-cast ingot material shown in Fig. 13. Also, the highly oriented grains complicate interpretation of defects.

Another unfavorable characteristic of the high-frequency sonic wave is that it is impossible to resolve subsurface defects near the surface. Very often it is necessary to distinguish between surface grain boundary etching due to electrolytic machining and actual intergranular cracks. Eddy current testing has been used to advantage in detecting surface cracks which have been obscured to dye penetrant testing by grit blasting of the surface. If surface cracks are found, they may be ground out provided minimum part dimensions are held.

Ultrasonic reflections are greatly influenced by material composition, fabrication history, grain size, grain orientation, surface condition, and surface contour. Therefore it is essential that a standard test block of the same material as the production part be used. An actual jet vane, rejected for dimensions, with

FIG. 15.—Ultrasonic Trace of Jet Vane Casting.

$\frac{1}{16}$-in. flat bottom holes at varying depths was used in this program to set up the equipment. The sensitivity is reduced to the point where the $\frac{1}{16}$-in. flat bottom hole indication is clearly seen but where the majority of the "noise" is eliminated. Critical attention is given the second and third back reflections. Any reduction in back reflection amplitude is considered suspect. The test pattern is cross checked. The crystal is moved in one di-

rection until the entire area is covered. Then the surface is retested at 90 deg to the original direction. The crystal path is overlapped approximately $\frac{1}{3}$ the crystal width. When both scans are completed, disposition of the vane is made.

Dye-penetrant and ultrasonic inspection is required on jet vane material after the rough machining operation. After the final machining, dye-penetrant inspection is again required. Fluorescent penetrants may be used in lieu of dye penetrants. However, the fluorescent technique has shown surface indications that are not indicative of true surface cracks. Because of the difficulty in defect interpretation due to increased indication sensitivity, the fluorescent method is not required. Close visual inspection is required after the jet vane is assembled with the molybdenum deflectors and shaft.

High-energy X-ray inspection has been used to verify gross ultrasonic indications. However, this is not a reliable method for delineation of fine multidirectional cracks.

Chemistry Effects

Tungsten and its alloys are extremely sensitive to trace impurities, both interstitials and metallics, in the parts per million range. Oxygen is analyzed by both the vacuum fusion and Leco conductimetric methods. Although producers report fairly good reproducibility within their own laboratory, accuracy and reproducibility between laboratories using different analysis methods are poor. Nitrogen determination is made by the vacuum fusion and Kjeldahl techniques. The same accuracy and reproducibility situation exists with nitrogen as with oxygen. Another common quality control measure for critical amounts of oxygen in molybdenum and alloys of low tungsten content is the appearance of oxide inclusions in the grain boundaries under the metallograph, and the occurrence of transgranular fractures. However, in the higher tungsten alloys such as 15-85 molybdenum-tungsten, the fractures are always partly transgranular and partly intergranular.

Carbon is added to the electrode to reduce oxygen. However, carbon in the parts per million range has a pronounced effect on ductility at elevated temperatures. Tension tests made at Oregon Metallurgical Corp. showed that at 1000 F the elongation drops from 30 per cent to 5 per cent in going from a 20-ppm carbon content to one of 200 to 300 ppm.

The present spectrographic standards are not adequate for trace metallic impurities in amounts which may affect forgeability.

An important advantage in using 15-85 molybdenum-tungsten in the as-cast condition is that these micro contents of trace elements are not as critical for successful performance in jet vanes as they are for adequate forgeability. This permits the use of material that would be rejected by the mill or forge shop. However, as with the example of an unrealistic elongation requirement mentioned before, restrictive chemical requirements should not be imposed on a material just because they are necessary for forgeability.

Since the measure of the quality of a part is in its performance, the quality of cast 15-85 molybdenum-tungsten jet vanes has been established by over 50 motor firings using 147 vanes, without a single failure.

NUMERICAL FILM READING TECHNIQUES FOR INTERPRETATION OF LINER-PROPELLANT INTERFACE OF SOLID ROCKET MOTORS

By Richard J. Mascis[1]

Synopsis

Numerical standards have been established for the interpretation of radiographs of large solid propellant propulsion units. One numerical method, commonly referred to as the density ratio, is obtained from a comparison of two film density readings taken with a densitometer in the area of the radiograph containing the suspected defect. The resulting ratio may be used successfully as a standard to differentiate between a normal and a defective area.

Density scans taken normal to the area of the radiograph to be interpreted provide even more possibilities for quantitative analysis of radiographs. Automatic scanning densitometers have been developed which produce highly reliable density scans with relatively good speed. In addition to accuracy, density scans make possible the establishment of several numerical standards including the density ratio.

Numerical standards provide a vital tool for the evaluation of radiographs; relatively inexperienced radiographers can perform the production evaluation of radiographs (or gammagraphs) by using the density ratio or density scan system. Quantitative techniques will find wide application in the solid rocket field for the detection of internal flaws. Numerical inspection data will provide a system for the establishment of firm acceptance-rejection criteria.

Quantitative knowledge of separations, voids, and other defects obtained from radiographic inspections of solid propellant rocket motors and other related hardware will greatly accelerate the establishment of firm acceptance-rejection criteria. The interpretation technique presented in this study makes this quantitative reporting method possible, and, furthermore, the method may be used effectively by technicians, thereby releasing the more experienced radiographers from the everyday routine of film interpretation.

A relatively simple numerical system is presented that is used effectively in the interpretation of cobalt-60, 1000-c gammagraphs of solid propellant motors. Experiments showed that by taking two film density readings, one in the area of suspected separation and the other $\frac{3}{4}$ in. below that location, a significant density ratio could be established from the readings. The ratio is a numerical value that represents either a normal or a separated condition, and the determination is independent of visual interpretation.

Separations cause the darkest areas on a gammagraph, and these areas provide the highest density readings when

[1] Special Projects Office, Quality Assurance and Reliability, Washington, D. C.

checked with a densitometer. This fact would provide a satisfactory method for detecting separations and other defects if all gammagraphs consistently had the same density level, but many variables are involved in film exposure and film processing that affect the density of a gammagraph. The effect of these variables can be minimized but not eliminated. As a result, two gammagraphs of equivalent areas will provide different density readings and comparison is impossible. The actual film densities of equivalent areas have ranged from 2.3 to 3.95 on some gammagraphs, but the ratio derived by comparing the film density for propellant and liner in equivalent areas remains almost constant regardless of the actual values of the film densities. It is thus possible to compare gammagraphs of different motors without regard to film exposure by comparing the density ratios of equivalent areas or zones.

A theoretical technique for determining the film density ratios for a particular motor configuration was established as a first step. Most of the theoretical density ratios have been substantiated by experimental density ratios for normal and separated areas of specific motors. Initial experimental data were obtained by constructing representative sections of the motors and determining experimental film density ratios for normal and defective areas. The theoretical data were further verified by constructing full-scale motors with built-in liner-propellant separations and other defects.

The density ratio is simply the comparison of two film density readings that are related to specific locations on a density scan. A density scan may be obtained by taking film density readings across the area of the film to be interpreted. The construction of a density scan before the advent of automatic scanning densitometers was a tedious operation and could not be adapted to the production evaluation of gammagraphs. Consequently, since the density ratio represented a quick method for establishing a numerical standard it was developed first on a crash basis. The successful demonstration of the density ratio technique led to the development of an automatic scanning densitometric system. At the time of this writing, several nondestructive testing facilities associated with the solid propellant industry are employing quantitative methods of film interpretation through use of automatic scanning densitometers or microphotometers.

Although the density ratio method presented here was developed by the author while associated with the Aerojet-General Corp., Bujes previously presented a method for the evaluation of radiographs indicating interface separation (1).[2] His subsequent trips to Aerojet in November 1959 led to a meeting with this writer which resulted in initiating the density ratio technique now used at Aerojet (2). Meanwhile, the problem of differentiating between bonded and separated conditions on a radiograph was also under extensive study at the U. S. Naval Ammunition Depot, Concord, Calif. (3). This study also proposed a reliable method of quantitatively differentiating between bonded and separated conditions.

INTERNAL CONFIGURATION OF CASE-BONDED MOTORS

If a cross-section of the cylindrical portion of a case-bonded solid propellant rocket motor were examined, it would reveal layers of steel, liner, and propellant, and in some areas, steel, insulation, liner, and propellant. It is essential to know the condition of the

[2] The boldface numbers in parentheses refer to the list of references appended to this paper.

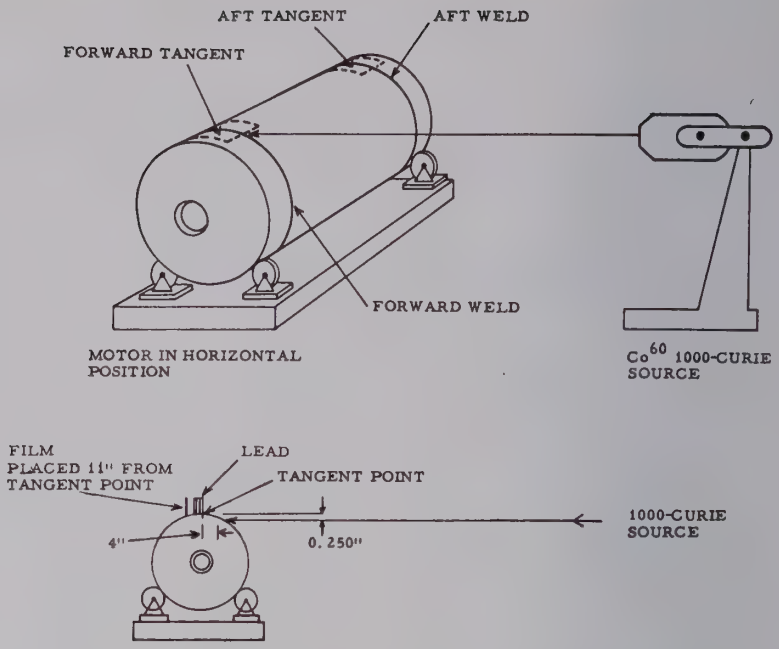

FIG. 1.—Cobalt-60, 1000-c Gammagraphic Plan for Forward and Aft Cylindrical Sections.

NOTE.—The camera is aimed approximately 4 in. in front of the tangent point or uppermost section of the motor; therefore the center of the beam will penetrate the motor about 0.250 in. below the tangent point.

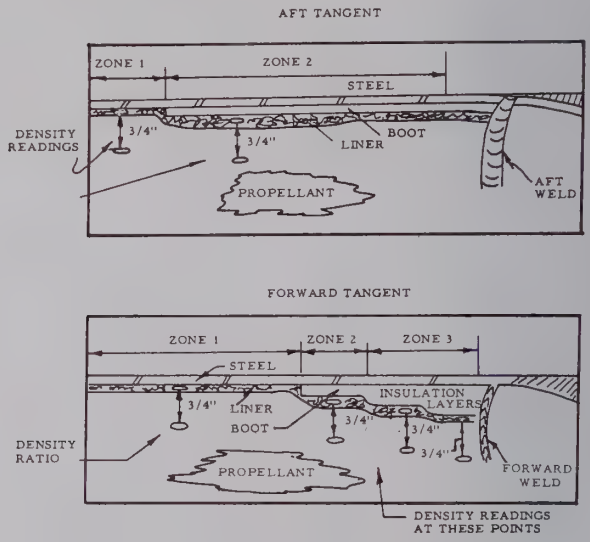

Zone 1, steel and liner.
Zone 2, steel, boot, and liner.
Zone 3, steel, insulation, boot, and liner.
NOTE.—The boot and insulation layers are made of the same material.

FIG. 2.—Zones of the Forward and Aft Cylindrical Sections.

Each gammagraph is divided into zones containing equivalent cross-sectional layers.

liner-propellant bond after a motor is cast and during subsequent environmental tests. Furthermore, the condition of this bond will determine the disposition of a motor scheduled for delivery to the testing sites, and radiographic and gammagraphic inspection techniques have been developed to assist in making this vital decision. Figure 1 illustrates a method of obtaining tangential gammagraphs of the cylindrical section of large rocket motors by using a 1000-c cobalt-60 source. The gammagraphs of the forward and aft central body tangents reveal the portion of the motor extending from approximately the girth weld to the edge of the insulation in the cylindrical section. The approximate coverage of the gammagraphs and the zones containing equivalent cross-sectional areas are shown in Fig. 2.

The liner material in this case has a relatively low mass density compared with that of the insulation or propellant, and it will cause a darker area to appear on a gammagraph. Frequently the higher film density for that darker area is mistaken for a liner-propellant separation. This situation is further complicated because many other variables in film exposure and film processing affect the over-all film density of a gammagraph. As a result, corresponding areas on different gammagraphs will have different values of film density, and comparison of these densities cannot be considered a reliable means of differentiating between a normal liner condition and a separated area. In addition, the thickness of the liner material for many case-bonded motors cannot be rigidly controlled and consequently a normal liner-propellant bond may appear suspicious when viewed from a radiograph.

FIG. 3.—Equipment Used to Obtain a Film Density Ratio.

FILM DENSITY RATIOS VERSUS FILM DENSITIES

Densitometric determinations of film density in the liner area have ranged from 2.3 to 3.95 when equivalent zones on a gammagraph were compared, but the ratio between film density for propellant and film density for liner remained almost constant regardless of the actual values of film density. Varia-

bles such as source distance, exposure time, and film processing procedures have a great effect on the density of a film but have a negligible effect on the density ratio. The density ratio is herein defined as the ratio between film density readings taken in the liner area and in an area $\frac{3}{4}$ in. below in the propellant, as illustrated in Fig. 2. The $\frac{3}{4}$-in. distance is not critical, and it was found to be convenient for this particular application; however, once a distance is decided upon, it should not, of course, be changed if the ratios are to be compared. Figures 3 and 4 illustrate the equipment and technique used in obtaining an experimental density ratio. The equipment in Fig. 3 from right to left is shown as follows: densitometer, gammagraph, special template with slits spaced at $\frac{3}{4}$ in., marking pencil, slide rule, and viewer. To obtain a density ratio, the template is placed over the gammagraph at the desired location and the markings are made; the ratio is then determined by dividing the higher density reading (liner) by the lower reading (propellant). Density ratios differ from one area of the motor to another. These areas are separated into zones, each having its own density ratio and requiring a separate analysis.

Before the calculation of the theoretical density ratio may be attempted, the equivalent areas or zones must be defined as shown on the forward and aft gammagraphs. Sample zone locations are shown in Fig. 2 which represent typical internal configurations of solid propellant rocket motors.

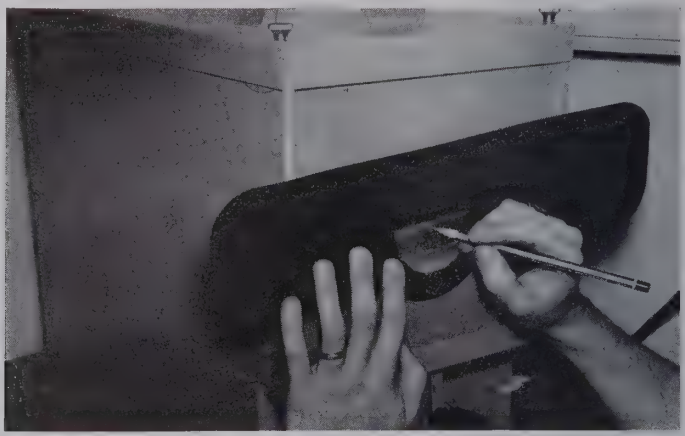

FIG. 4.—Preparation of Gammagraph for Density Readings.

Template with $\frac{3}{4}$-in. spacing between slits is placed on gammagraph and the required markings are made.

Here zone 1 includes the cylindrical section of the chamber between the edges of the fore and aft insulators; a cross-section in this zone would reveal layers of steel, liner, and propellant. Zone 2 refers to the portion of the gammagraph that covers the insulation extension or boot end, and a cross-section here would reveal layers of steel, boot, liner, and propellant. Zone 3 encompasses the remaining portion of the gammagraph of the weld, and a cross-section of this area would reveal two or more layers of insulation material. Cross-sections of a typical solid propellant motor are shown in Fig. 5.

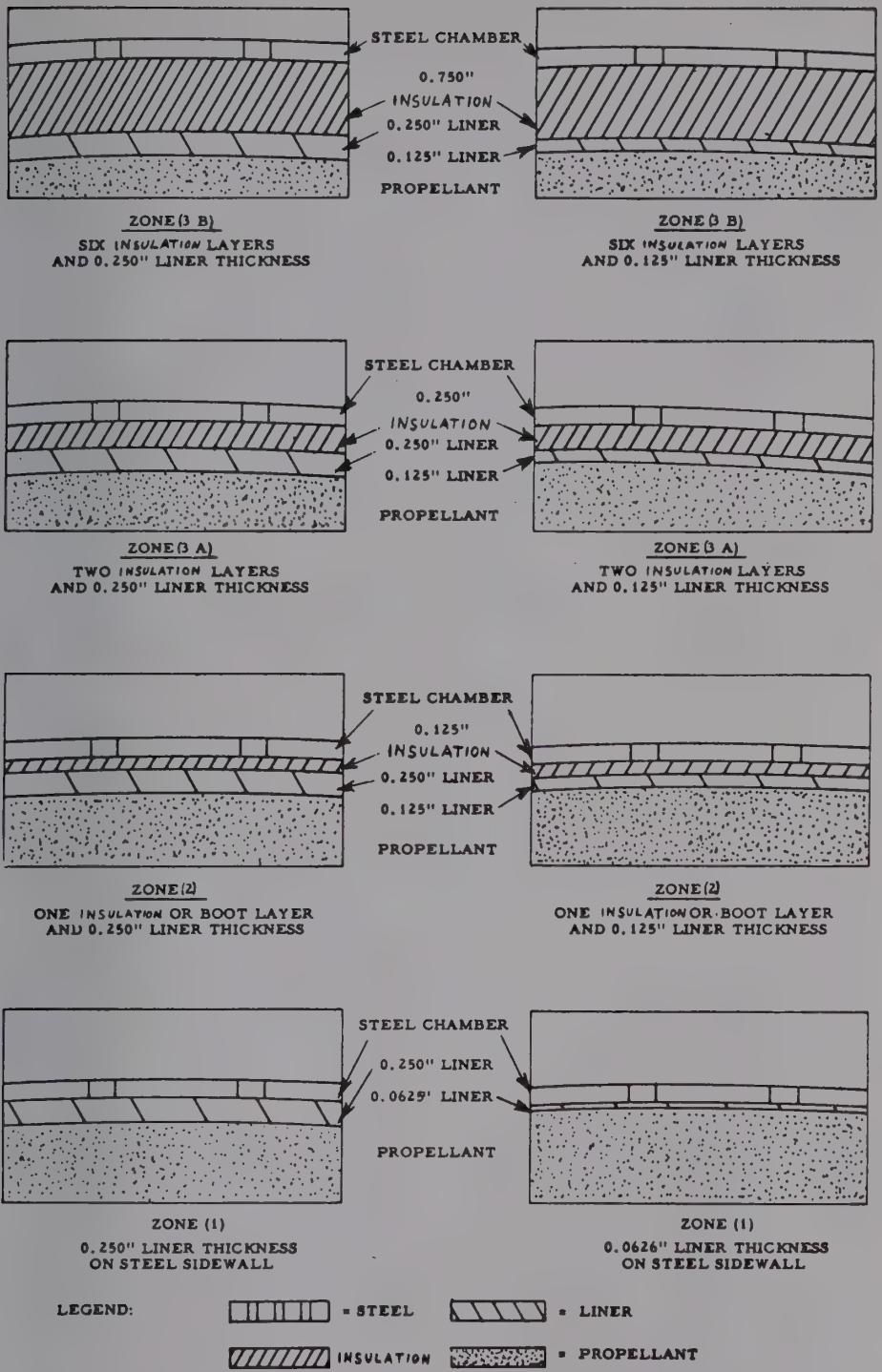

FIG. 5.—Typical Internal Configurations of a Solid Propellant Motor with a Thick Steel Chamber.

The above are conditions that exist in typical large-scale solid propellant rocket motors. The theoretical density ratios were calculated for each zone by using the technique illustrated in Fig. 6.

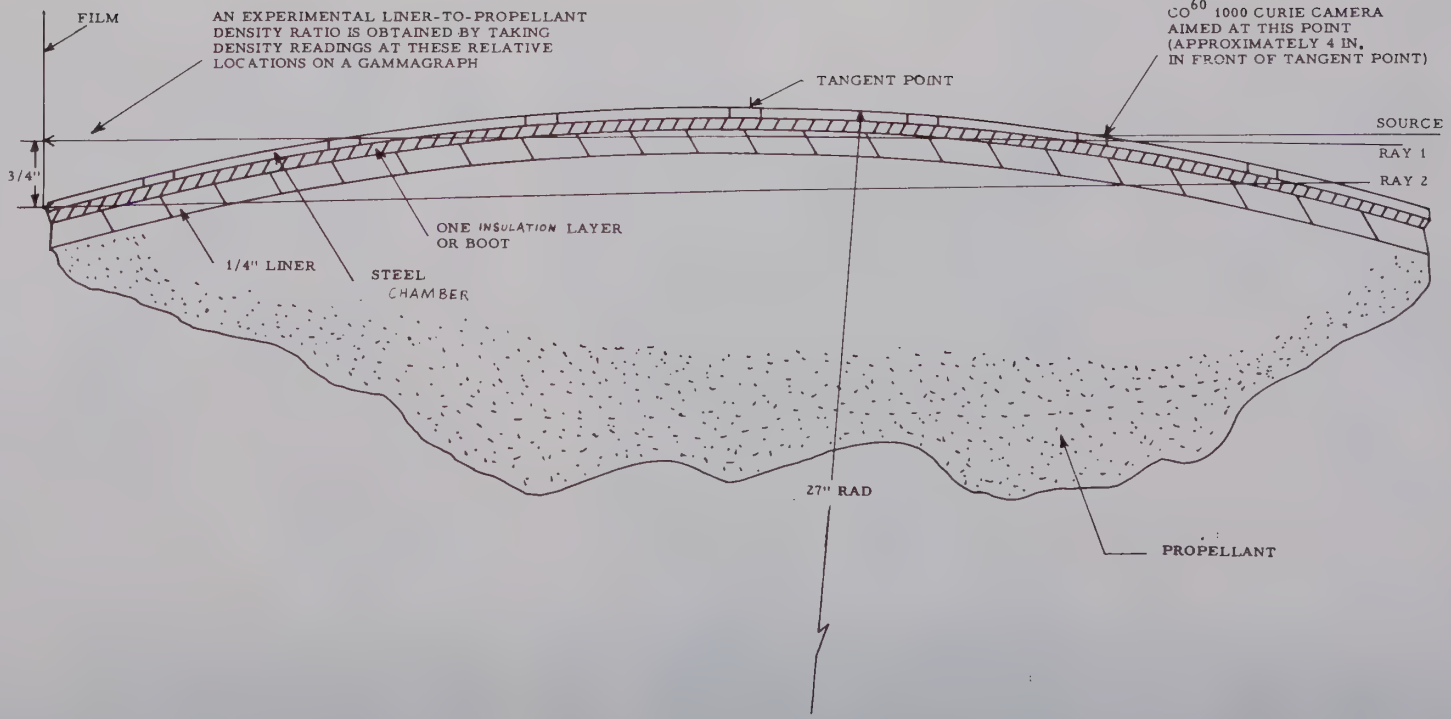
FILM
AN EXPERIMENTAL LINER-TO-PROPELLANT DENSITY RATIO IS OBTAINED BY TAKING DENSITY READINGS AT THESE RELATIVE LOCATIONS ON A GAMMAGRAPH
CO^{60} 1000 CURIE CAMERA AIMED AT THIS POINT (APPROXIMATELY 4 IN. IN FRONT OF TANGENT POINT)
TANGENT POINT
SOURCE
RAY 1
RAY 2
3/4"
ONE INSULATION LAYER OR BOOT
1/4" LINER
STEEL CHAMBER
27" RAD
PROPELLANT

	Steel	Insulation	Liner	Propellant	$\Sigma\mu x$
Gamma ray 1	1.41 in.	2.13 in.	5.4 in.	0 in.	2.729
Gamma ray 2	0.795 in.	1.125 in.	2.563 in.	9.637 in.	3.902
Liner absorption coefficient	0.95 per in.	0.256 per in.	0.157 per in.	0.256 per in.	...

Theoretical density ratio: 2.11.

FIG. 6.—Cylindrical Section of a Thin Steel Chamber with 0.250-in. Liner on Boot End (Zone 2).

LINEAR ATTENUATION COEFFICIENTS

Gammagraphs or radiographs reveal areas of different density levels, which in turn indicate the number or intensity of X-rays that have penetrated the specimen. The number of X-rays impinging on the film determines the film density, and a densitometer is used to take the density reading.[3] Dark areas (high film densities) are obtained when rays of relatively high intensity have impinged on the film surface. The dark areas may be attributed to the low mass density of materials through which the rays have passed, to the configuration of the specimen, or to separations and voids.

X-rays or gamma rays are absorbed or attenuated in accordance with the usual exponential equation:

$$I = I_0 e^{-\mu x}$$

where:

I = intensity after passage through the specimen,
I_0 = initial intensity,
e = base of natural logarithms, 2.718,
μ = linear attenuation coefficient, and
x = thickness of the specimen.

This equation is extremely useful in calculating the attenuation properties of different materials. Generally the attenuation of gamma rays is proportional to the mass density of the material through which they must pass; for example, steel will absorb more rays than propellant and propellant will absorb more than liner.

When the attenuation coefficient is known, the intensity, I, or X-rays impinging on a film can be calculated if thickness, x, of the material is known. The thicknesses of steel, liner, asbestos, and propellant penetrated by the gamma rays during gammagraphic inspection were obtained from a series of full-scale drawings. It is strongly recommended that μ values be determined experimentally under the actual exposure conditions.

CALCULATION OF THEORETICAL DENSITY RATIOS

The cobalt-60 1000-c source is aimed at a point approximately 0.250 in. below the tangent point at the uppermost section of the chamber while the motor is in a horizontal position, as shown in Fig. 1. A theoretical analysis is then made by assuming that two gamma rays pass through the chamber, one through the middle of the liner and one through the propellant at a point 0.750 in. below the middle of the liner, as measured at the film (Fig. 6). In this example, the film is approximately 8.5 in. from the tangent point; and the two gamma rays are shown to be slightly divergent to simulate an expansion of approximately 25 per cent. The object-to-film distance is 11 in., and the object expansion is approximately 30 per cent.

The next step is to measure the thickness of each material passed through by each gamma ray. This technique was applied in all the cases shown in Fig. 5. The over-all attenuation coefficient, $\Sigma\mu x$, for each gamma ray was obtained by taking the sum of the individual products of thickness and attenuation coefficient determined for each material passed through by the ray, as follows:

$$\sum \mu x = \mu_s x_s + \mu_l x_l + \mu_a x_a + \mu_p x_p$$

where the subscripts s, l, a, and p denote steel, liner, asbestos, and propellant, respectively. The chord length of each material passed through was determined from drawings representing cross-sections of all zones; an example is shown in Fig. 6. The chord lengths may also be determined mathematically for a particular motor configuration.

Calculation of absolute value of intensity, I, is difficult because of

[3] Density refers to film density determined with a densitometer unless otherwise specified.

unpredictable scattering, characteristic absorption effects, and other factors influencing the intensity of radiation. For this reason, a log relative-intensity ratio is extremely useful and is obtained as shown in the following example:

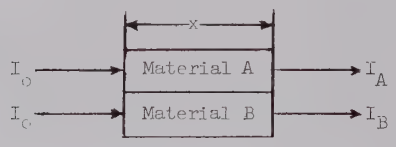

$$I_A = I_0 e^{-(\mu_A x_A)}$$

$$I_B = I_0 e^{-(\mu_B x_B)}$$

$$\log \frac{I_A}{I_B} = \log e^{-(\mu_A x_A - \mu_B x_B)}$$

The log relative intensity is calculated without knowing the initial intensity, I_0, by solving the right-hand side of the last of the above equations. Characteristic curves are then used to determine the density ratio.

Characteristic curves show the relationship between film density and log relative intensity (or exposure). The theoretical density ratio can be determined by using the characteristic curve, the calculated log relative intensity, and an assumed film density value for the liner or propellant.[4] A sample calculation for a gammagraph of a motor (Fig. 6) is as follows:

$$I_1 = I_0 e^{-\Sigma \mu_1 x_1}$$

$$I_2 = I_0 e^{-\Sigma \mu_2 x_2}$$

where:

I_1 = intensity incident on film from gamma ray No. 1,

I_2 = intensity incident on film from gamma ray No. 2, and

$$\frac{I_1}{I_2} = \frac{I_0 \exp\left(-\mu_{s(1)} x_{s(1)} + \mu_{a(1)} x_{a(1)} + \mu_{l(1)} x_{l(1)}\right)}{I_0 \exp\left(-\mu_{s(2)} x_{s(2)} + \mu_{a(2)} x_{a(2)} + \mu_{l(2)} x_{l(2)} + \mu_{p(2)} x_{p(2)}\right)}$$

When the actual values from Fig. 6 are substituted, the equation reduces to:

$$\frac{I_1}{I_2} = \frac{e^{-2.729}}{e^{-3.902}}$$

from which the log relative exposure is obtained as

$$\log \frac{I_1}{I_2} = (3.902 - 2.729) \log e = 0.508$$

By assuming the film density for the liner material (gamma ray No. 1) as 3.0 and entering the appropriate characteristic curve, the density value for the propellant (gamma ray No. 2) may be obtained and the density ratio is established:

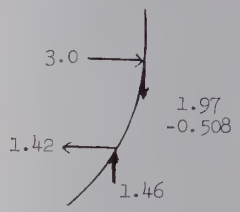

$$\text{Density ratio} = \frac{3.0}{1.42} = 2.11$$

The assumption of a density value of 3.0 is not critical, as the effect of using a different film density value would be negligible. (Experimental results of a calibration sample described below will illustrate the negligible effect of film density on the density ratio.) A density ratio higher than 2.11 would indicate a separation in the case bond area.[5]

It should also be mentioned that this technique depends upon being a straight-line relationship between exposure and photographic density. This is not strictly true in the high-density range, even for

[4] The use of an assumed density value has a negligible effect on the density ratio. This will be emphasized by experimental results from a calibration sample with a chamber steel thickness of 0.200 in.

[5] For a complete discussion on the calculation of theoretical density ratios, the reader is referred to the original work by Mascis (**2**).

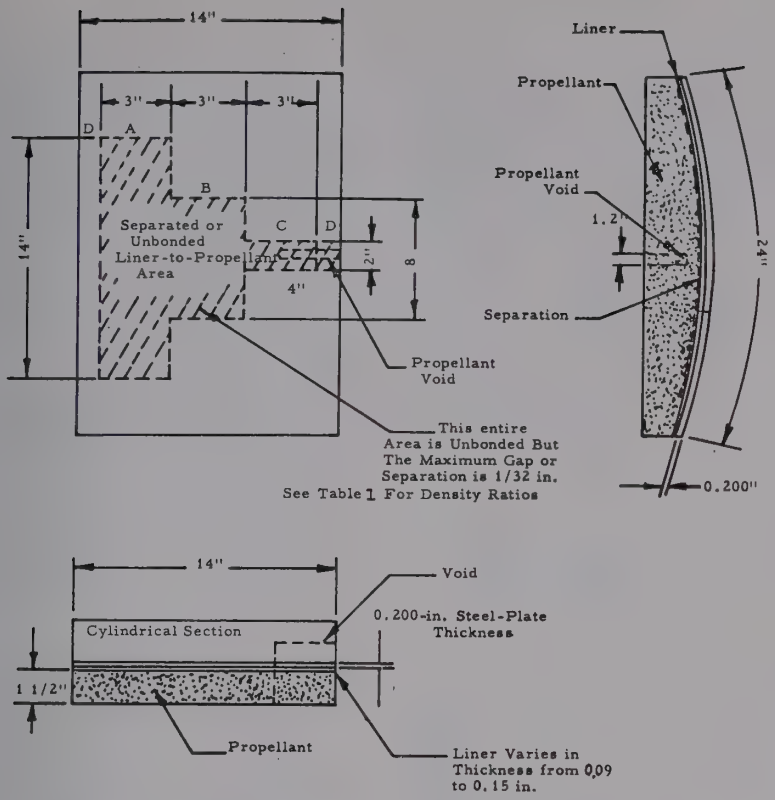

FIG. 7.—Calibration Sample Representing Zone 1 of a Motor with a 0.200-in. Wall Chamber.

TABLE 1.—EXPERIMENTAL DENSITY RATIOS FOR CALIBRATION SAMPLE.

It is obvious from the values given that the film density has little or no effect on the density ratio.

Section of Sample (see Fig. 7)	9-ft Source-to-Film Distance at 12-min Exposure Time[a]			10-ft Source-to-Film Distance at 8-min Exposure Time			
	Density Reading		Density Ratio	Density Reading		Density Ratio	Theoretical Density Ratio
	Liner or Separation	Propellant		Liner or Propellant	Propellant		
A (unbonded for 14 in.)	2.26	1.48	1.53	1.33	0.88	1.51	1.64
	2.25	1.46	1.54	1.36	0.89	1.53	...
	2.14	1.41	1.52	1.32	0.89	1.49	...
B (unbonded for 8 in.)	1.93	1.44	1.34	1.26	0.96	1.31	...
	1.83	1.41	1.30	1.24	0.93	1.33	...
	1.96	1.42	1.38	1.28	0.99	1.29	...
C (unbonded for 2 in.)	1.59	1.27	1.25	1.17	0.97	1.21	...
	1.59	1.27	1.25	1.18	0.98	1.20	...
	1.60	1.28	1.25	1.13	0.92	1.23	...
D (bonded)	1.44	1.27	1.13	0.79	0.72	1.10	1.14
	1.41	1.31	1.08	0.67	0.62	1.09	...
	1.42	1.18	1.20	0.70	0.63	1.11	...

[a] Normal procedures for taking cylindrical section gammagraphs.

the fine-grain, high-contrast X-ray films considered in this study. However, the experimental results indicate that deviations from linearity are not great enough to be significant. Nevertheless, it is recommended that other users of this technique verify, under their own operating conditions, that density ratios are sufficiently independent of exposure conditions.

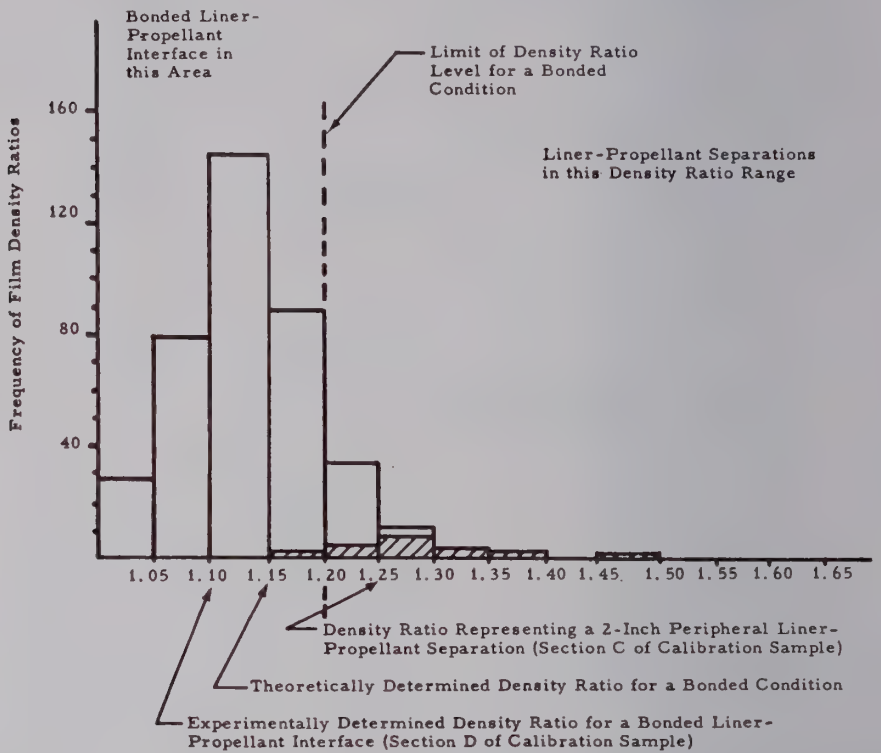
Bonded Liner-Propellant Interface in this Area
Limit of Density Ratio Level for a Bonded Condition
Liner-Propellant Separations in this Density Ratio Range
Frequency of Film Density Ratios
160
120
80
40
1.05 1.10 1.15 1.20 1.25 1.30 1.35 1.40 1.45 1.50 1.55 1.60 1.65
Density Ratio Representing a 2-Inch Peripheral Liner-Propellant Separation (Section C of Calibration Sample)
Theoretically Determined Density Ratio for a Bonded Condition
Experimentally Determined Density Ratio for a Bonded Liner-Propellant Interface (Section D of Calibration Sample)

FIG. 8.—Film Density Ratio Distribution of the Cylindrical Section of a Large Solid Propellant Motor with 0.200-in. Chamber Thickness.

NOTE.—Densities in the liner and propellant areas were collected from the gammagraphs of 15 motors. The shaded areas were interpreted by experienced radiographers to be liner-propellant separations. The experimental ratios were obtained from calibration samples representing the cylindrical section of the motor.

EXPERIMENTAL DENSITY RATIOS OF NORMAL AND SEPARATED AREAS

By constructing a calibration sample representing an actual section of a rocket chamber, the theoretical results were fully substantiated. The sample (Fig. 7) was constructed with a minimum separation gap at three different circumferential lengths. One gammagraph of the sample was taken at a 9-ft source-to-film distance and at 12 min exposure time; another gammagraph was taken at a 10-ft source-to-film distance and at 8 min exposure time. The ratios obtained under the two different sets of conditions were remarkably constant, indicating the validity of the ratio technique.

The results shown in Table 1 indicate that the density ratios of gammagraphs

of different motors may be compared regardless of exposure time and other variables that affect film density; the closeness of experimental and theoretical ratios is also shown. It is reasonable to assume that the theoretical ratios for other zones would also indicate close correlation with the experimental values. This assumption is supported by the experimental results obtained with many motors of similar configurations inspected under various conditions. Figure 8 illustrates the density ratio distribution of the cylindrical section of large solid propellant motors with 0.200-in. chamber steel thickness. The frequency chart was constructed from more than 400 density ratio values of 15 motors. Statistical evaluation of the data, together with the experimental results of the aforementioned calibration sample, indicated that a density ratio level of 1.20 was the limit for a normal liner-propellant bond. Density ratios greater than this value would indicate a liner-propellant separation. Obviously separated liner-propellant areas would give density ratios well to the right of the limiting value, but only those ratios

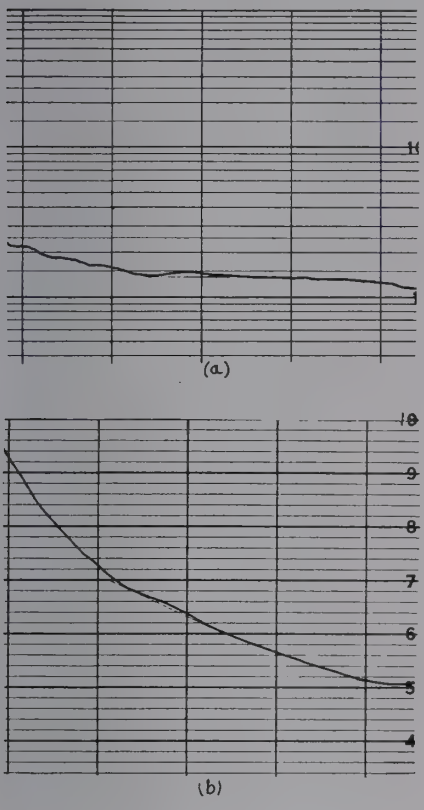

(*a*) Differential density trace.
(*b*) Density trace.

FIG. 9.—Density Traces of a Bonded Region; No Front Screen, a 10-mil Lead Rear Screen.

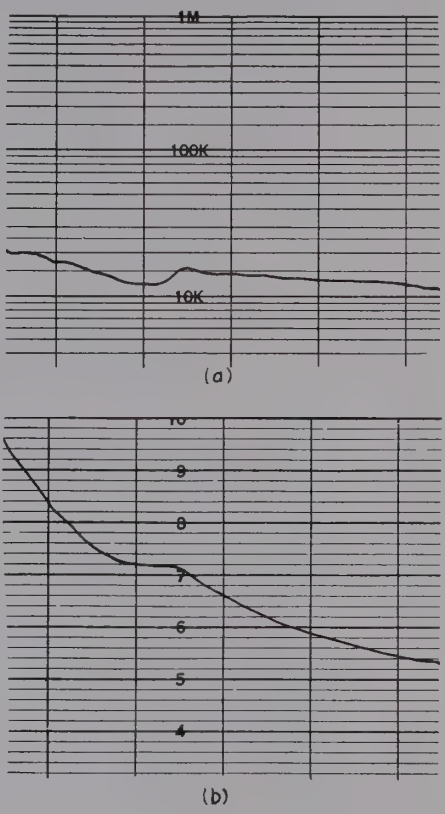

(*a*) Differential density trace.
(*b*) Density trace.

FIG. 10.—Density Traces of a 10-mil Propellant-Insulator Separation; No Front Screen, a 10-mil Lead Rear Screen.

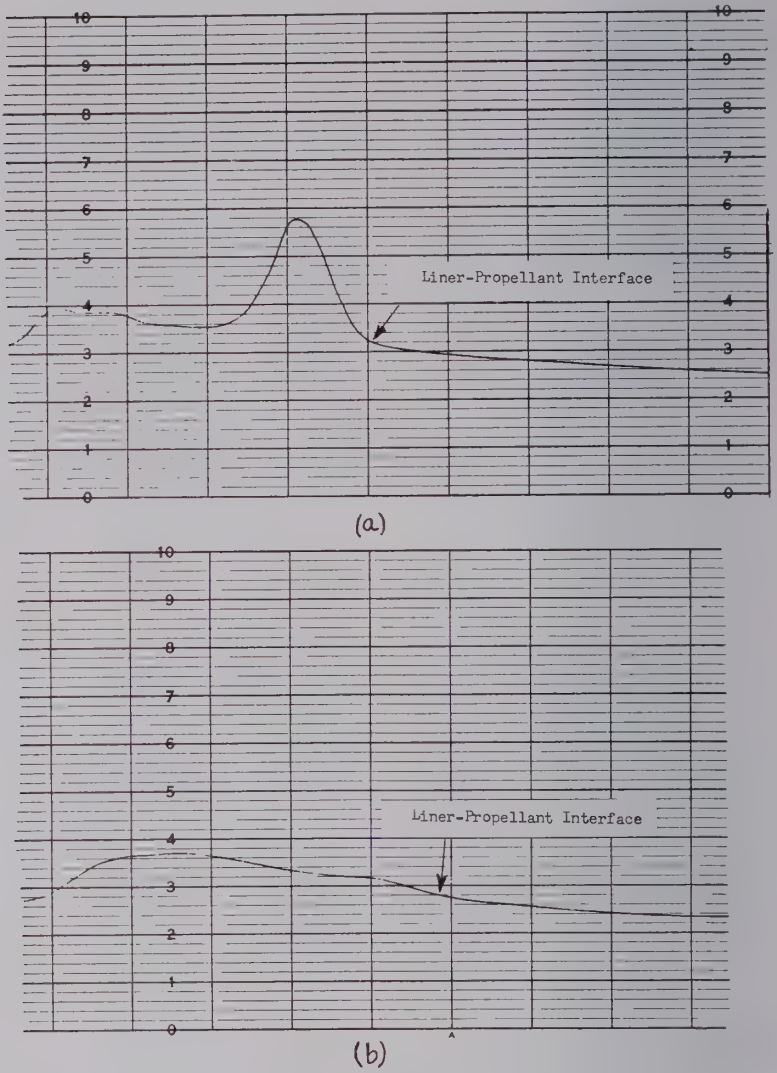

(*a*) Scan of motor with liner-propellant separation.
(*b*) Scan of motor with normal liner-propellant bond.

FIG. 11. —Comparison of Traces Representing an Actual Separated Condition in a Full-Scale Motor with a Normal Case Bond Condition.

constituting borderline conditions were used in the tabulation.

AUTOMATIC SCANNING DENSITOMETER

Although the density ratio technique has become a valuable procedure for interpretation of cobalt-60 gammagraphs, density scans taken normal to the area of the film to be interpreted provide even more possibilities for quantitative analysis. Automatic scanning densitometers have been developed

which produce highly reliable density scans with relatively good speed.[6] It should be emphasized that the density ratio technique examines only two points on a radiograph and more information is obtained by taking a density scan across the area to be interpreted. The scan technique enables one to examine many more points on a radiograph. In addition, the scan technique makes possible other quantitative methods of evaluation which include rate of change of density, density difference, and the shape of the scan. A calibration sample similar to Fig. 7 was used to obtain information about the density and differential density scans for areas of separations and for a normal case bond condition (4). This motor sample contained gap sizes ranging from 10 to 115 mils between the propellant and the case. The trace obtained from the scanning system for the 10-mil separation is compared with a bonded condition in Figs. 9 and 10. Note the differentiation which can be made between the 10-mil separation and the bonded condition. The density differences are even greater when comparing traces from separations with larger gap sizes. Also, it can be concluded from Figs. 9 and 10 that a density ratio taken from the trace with the separation would be somewhat higher than a ratio from the normal trace, thereby also providing differentiation by means of a density ratio.

The significance of the density scanning system is further emphasized by a comparison of traces representing an actual separated condition in a full-scale motor with a normal case bond condition (Fig. 11).

[6] An automatic scanning densitometer system was developed by A. D. Lucian, Aerojet-General Corp., Sacramento, Calif., and is in use at the time of this writing.

MICROPHOTOMETERS

Recent studies on betatron radiographs indicate that these radiographs do not lend themselves to accurate quantitative interpretation with either the density ratio technique or density scanning using conventional densitometers. This may be explained by the relatively low contrast of 25-Mev radiographs in comparison to the 1000-c cobalt-60 gammagraphs. In addition, the increased definition of the higher Mev radiographs could only prove advantageous if the density scanning system aperture is sufficiently small to permit analysis of extremely small areas on the radiographs. However, it was found that the minimum detectable separation or density change by conventional densitometric equipment was the equipment limitation dictated by the physical size of the aperture. Consequently, in order to interpret quantitatively low-contrast, high-definition radiographs, microphotometers containing very small aperture sizes were explored. A Jarrell-Ash 23050 recording microphotometer has been used to detect small changes in relative exposure on Eastman Kodak Type AA film (5). The Jarrell-Ash scanning photometer has successfully detected interface separations of 0.005 in. and smaller on 25-Mev radiographs. At least four nondestructive testing facilities concerned with the manufacture or inspection of solid propellant propulsion units are actively developing microphotometer scanning systems for the quantitative evaluation of radiographs.[7] Some scanning systems are being provided with automatic readout systems using computer type equipment.

[7] Allegany Ballistics Laboratory, Rocket Center, W. Va.; Naval Ammunition Depot, Concord, Calif.; Naval Ordnance Test Station, China Lake, Calif.; and Thiokol Chemical Corp., Redstone Division, Huntsville, Ala.

MICROPHOTOMETERS VERSUS MICRODENSITOMETERS

The response of a photometer is a linear function of the film transmission, T, while a densitometer is an instrument whose response is a linear function of film density, D. Density and transmission are related by the expression $D = -\log T$. A theoretical discussion on the application of scanning photometers and densitometers is presented in reference (5). According to this analysis, the optimum sensitivity for the scanning photometer is obtained by a low film density (0.7 to 1.0). Conversely, the optimum sensitivity of the densitometer scanning system is at the region of high film density (approximately 3.0). Additional studies may indicate that the optimum sensitivity of scanning systems employing densitometers may be in the extremely high density ranges. Consequently, the performance difference of the two scanning systems gives the preference to the photometer when one considers the development of very large solid propellant propulsion units which require relatively high exposure times during radiographic inspection.

It should be emphasized that the development of a microphotometer scanning system may be pursued concurrently during normal radiographic inspection of a unit. For example, radiographic exposures of AA film and M film may be performed simultaneously. Such a technique will provide a proper density range on the AA film for visual interpretation and at the same time make available an M film in the low-density range for microphotometer scanning evaluation.

SUMMARY AND CONCLUSIONS

Quantitative techniques presented in this study should find extensive application in the radiographic interpretation of solid propellant propulsion units. As mentioned earlier, several numerical methods are currently in use by rocket motor manufacturers and associated nondestructive testing laboratories. The significance of the density ratio and density scanning techniques may be emphasized by the following advantages or applications:

1. The techniques are effective in the correlation analysis of inspection and firing results, and will greatly accelerate the establishment of firm acceptance/rejection criteria.

2. Quantitative methods of reporting inspection results ensure comparable and uniform inspection data regardless of the background of the interpreter.

3. Quantitative techniques may be used successfully to interpret radiographs of moderate sized motors with relatively low-cost gamma source equipment, eliminating the need for expensive X-ray units or elaborate installations.

REFERENCES

(1) J. I. Bujes, "Evaluation of Radiographs Indicating Interface Separations," presented at the Ninth Polaris Nondestructive Testing Committee Meeting.

(2) R. J. Mascis, "Application of the Density Ratio Method for the Interpreptation of Radiographic Film of Large Solid Propellant Rockets," *Proceedings*, Fifth AFBMD-STL-Aerospace Symposium, Vol. 11, 1960, pp. 3–54.

(3) "Nondestructive Testing of Polaris Missile Motors," *Report QE/CO 59-23*, Naval Ammunition Depot, Concord, Calif.

(4) M. J. Johnson, "Development Program for the Automatic Scanning Densitometer," Aerojet-General Corp., presented at the 20th Polaris/Minuteman/Pershing Nondestructive Testing Committee Meeting.

(5) J. I. Bujes and R. H. Knipe, "The Effect of Exposure of Photographic Detection of Small Differences in Relative Exposure," 21st Nondestructive Testing Polaris/Minuteman/Pershing Committee Meeting.

CINEFLUOROGRAPHY OF SOLID FUEL ROCKET MOTORS

By E. L. Criscuolo[1] and D. Polansky[1]

Synopsis

A cinefluorographic system developed for the study of internal burning of rocket motors during static tests is described. This system uses a 9-in. image intensifier tube with a light intensification of approximately 2000 coupled to a 35-mm movie camera. A 250-kvp, 5-ma X-ray machine is used to penetrate a 5-in. diameter test motor containing voids and cracks. Performance data of the cinefluorographic system at X-ray energies of 250, 1000, and 2000 kvp and 10 Mev are presented.

Radiography is used to inspect solid propellant rocket motors before firing to locate defects and ascertain the general condition. Before an evaluation of the defect can be made, it is necessary to have a correlation of defect versus performance. One method of achieving this is to fire motors with various defects and record performance data. While this is the most direct approach, it is costly and may not yield satisfactory information because of the variables that might influence motor performance. Another way to obtain correlation data is with a test motor with a defect where most of the variables not under study have been eliminated. Both methods have been used in various missile programs.

This report describes the development of a cinefluorographic method that can be applied during motor firing to observe the effect of voids and other irregularities on the flame front.

One method of obtaining a sequence of radiographs is by making a series of separate X-ray exposures. Because the burning rate of the propellant is about 0.3 in. per sec, an exposure of 0.1 sec or less is required to minimize blurring due to motion of the flame front. This approach requires a very high intensity X-ray source and a satisfactory film indexing system to move large sheets of X-ray film in and out of the X-ray beam. The medical field has developed several systems, one of which uses a mechanical film indexing where 6 exposures per sec can be made. Another method, developed by Westinghouse, uses a large roll of film which is continuously moving, and an X-ray source pulsed at 10 μsec with a repetition rate of 50 to 150 frames per sec. This system is limited by the relatively low output of the X-ray source and consequently by the small thicknesses of motors that can be penetrated. Cinefluorography using an image intensifying tube and a motion picture camera is used extensively in the medical field.[2, 3, 4] In industry the

[1] U. S. Naval Ordnance Laboratory, White Oak, Silver Spring, Md.

[2] R. H. Morgan, "The Performance of Screen Intensification and Cinefluorographic Systems," *Journal of Roentgenology, Radium Therapy and Nuclear Medicine*, Vol. 86, No. 6, Dec., 1961.

[3] L. B. Lusted, "Current Technical Problems in Cinefluorography," *Radiology*, Vol. 73, No. 4, Oct., 1959.

[4] P. C. Hodges and R. D. Moseley, Jr., "Cinefluorography Employing Split-Image Television Type Image Amplifiers," *Radiology*, Vol. 73, No. 4, Oct., 1959.

application of this system is more difficult because of the heavy masses involved.

Test Motors with Defects:

Before a cinefluorographic system can be designed it is necessary to know the nature of the object to be studied and the characteristics to be measured. The Allegany Ballistics Laboratory has developed a 5-in. diameter end-burner test motor made of 5-in. diameter disks from 1 to 3 in. thick which have been cemented together (Fig. 1). Disks of propellant containing natural or artificial defects can be made part of the motor. The propellant is then inserted into a steel motor tube with $\frac{1}{4}$-in. thick walls.

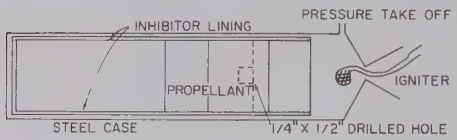

FIG. 1.—Diagram of Test Motor.

This motor is well suited to a preliminary study of cinefluorography of motors during static firing because: (1) experiments can be performed on a small scale; (2) the end-burner type produces a simple burning front geometry; (3) defects can be inserted at any desired position; and (4) motor tubes can be reused.

Radiographic Parameters:

The motor to be penetrated contains 5 in. of propellant and has a total steel thickness of $\frac{1}{2}$ in. The X-ray attenuation in the propellant can be calculated from the half-value layer which is 1.5 in. for 250-kvp X-ray radiation. This motor contains 3.3 half-value layers of propellant or an attenuation of $(2)^{3.3} \cong 9$. The steel absorber results in an additional attenuation of 10 resulting in a total attenuation of 90. The X-ray machine used in this experiment is a 250-kvp, 5-ma unit which has an output of 8 r per min or 133 mr per sec at 1 m. At a frame rate of 8 per sec where $\frac{1}{16}$ sec is used to move the film and the other $\frac{1}{16}$ sec is the exposure, the X-ray dose is 90 μr per frame.

In considering the possible use of X-ray film directly, one quickly notes that the most sensitive X-ray film technique requires about 5 mr for film blackening, therefore another approach must be used. The use of image intensifier tubes as brightness amplifiers is well documented. The evaluation needed here is whether a gain in an intensifying tube

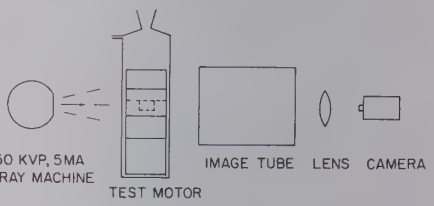

FIG. 2.—Diagram of Cinefluorographic System.

having an incident radiation intensity of 90 μr per frame is sufficient to produce film of value. Figure 2 is a diagram of a system using the image tube with a movie camera.

RELATIVE BRIGHTNESS MEASUREMENTS WITH IMAGE TUBE

A comparison of the light output of the image tube, a zinc sulfide screen (Type PFG), and a sodium iodide crystal was obtained as a function of X-ray intensity. The brightness was measured with a 1P21 phototube having an S2 spectral response. A circular area of $\frac{1}{2}$-in. diameter was selected for the comparison. Since the phototube peaks in the blue region, the sodium iodide crystal will be favored; no attempt was made to normalize the results. A reasonable

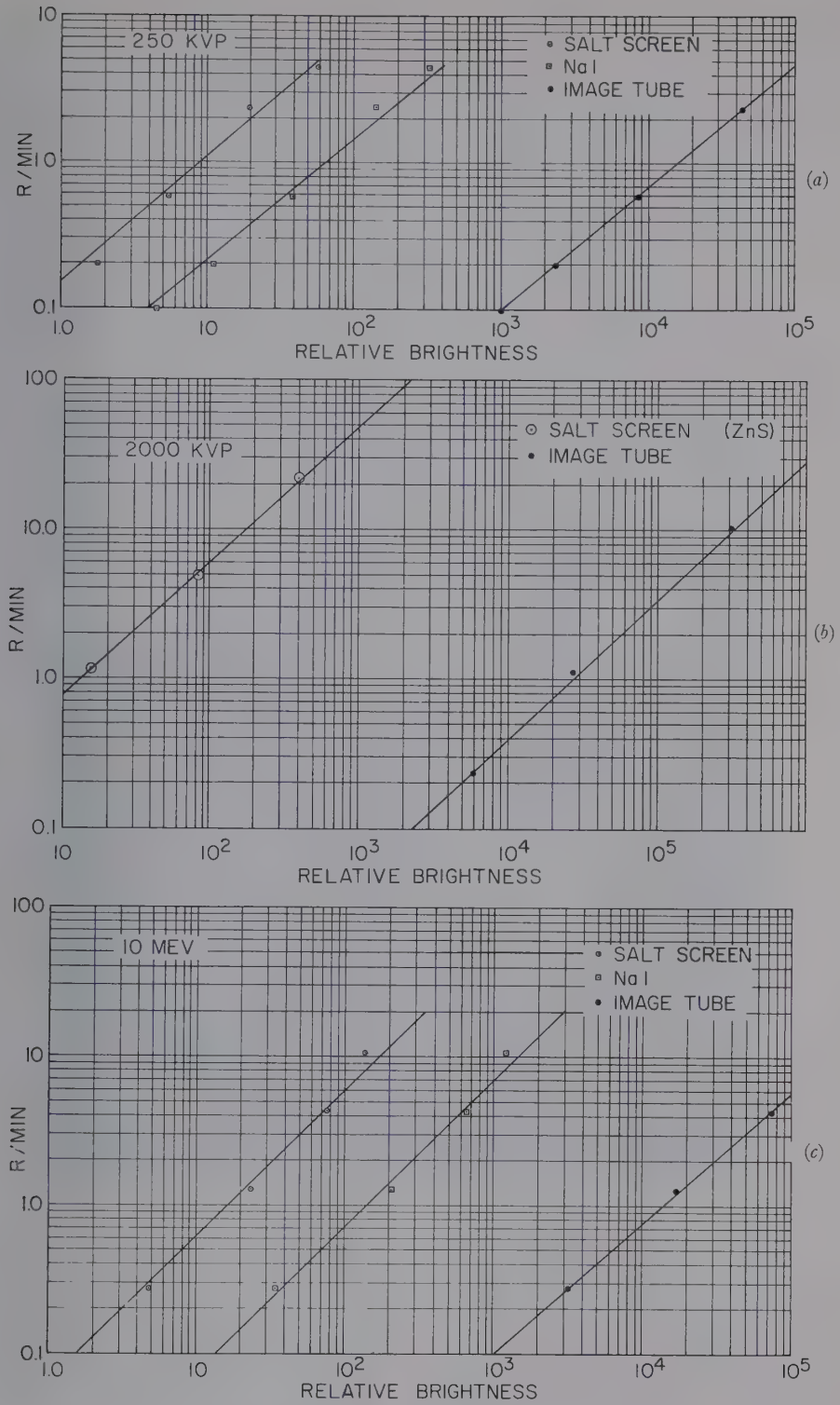

(*a*) At 250 kvp. (*b*) At 2000 kvp. (*c*) At 10 Mev.

FIG. 3.—Relative Brightness Versus Roentgens per Minute.

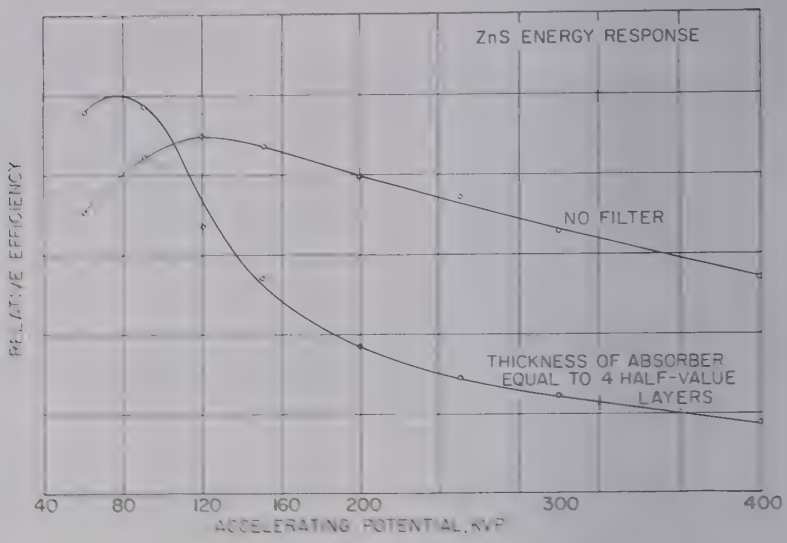

FIG. 4.—Zinc Sulfide Energy Response.

FIG. 5.—Camera Setup for Cinefluorography.

comparison can be made between the PFG screen and the image tube since they generate approximately the same wavelength light.

The results at 250 kvp, 2000 kvp, and 10 Mev are shown in Figs. 8 at, b, and c, respectively. The effect of dark current and direct excitation of the phototube has been subtracted from the results. The gain of the image tube over a PFG screen is approximately 2000. This gain appears as a constant

over the X-ray energy range even though the total light generated is less with the high-energy sources.

A typical energy response for a zinc sulfide fluoroscopic screen is shown in Fig. 4 where the peak occurs at about 100 kvp. The energy response for an image tube is similar; therefore when using an image tube or zinc sulfide screen above 100 kvp it is very important to minimize scatter since the tube or screen is more sensitive to the low-energy scatter. One method of reducing the effect of scatter is to shield the tube with lead.

Image Tube-Camera System:

The screen of the image tube was photographed with a 35-mm movie camera in which an f/0.75 110-mm focal length lens was mounted with about a 1.5:1 reduction. Although this optical system was not optimum, it served to demonstrate the experimental technique. The camera used was an Automax manufactured by Traid Corp. The shutter was modified from a 25 to a 50 per cent open shutter time. The frame rate was varied by reducing the voltage applied to the drive motor. Figure 5 illustrates the camera setup.

Image Resolution:

A common means of measuring image quality in radiography is through the use of a penetrameter. In the test setup, a plastic penetrameter of the same density as the propellant and containing a 1T hole[5] was used. The propellant was about 5 in. thick with a $\frac{1}{4}$-in. thick steel case. Measurements were made with a 250-kv source at 3 ft using a 35-mm movie camera operating at about 8 to 12 frames per sec. The images were recorded on Ansco Hypan film. A 4.2 per cent penetrameter was detected.

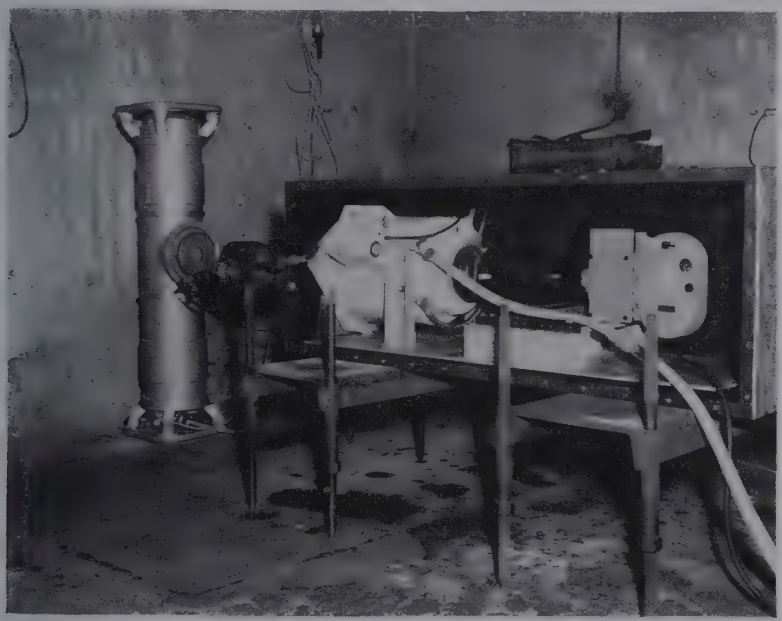

FIG. 6.—Cinefluorographic Equipment and Motor.

[5] Method for Controlling Quality of Radiographic Testing (E 142), 1961 Book of ASTM Standards, Part 3.

FIG. 7.—Films Showing Effect of Void on Burning Front.

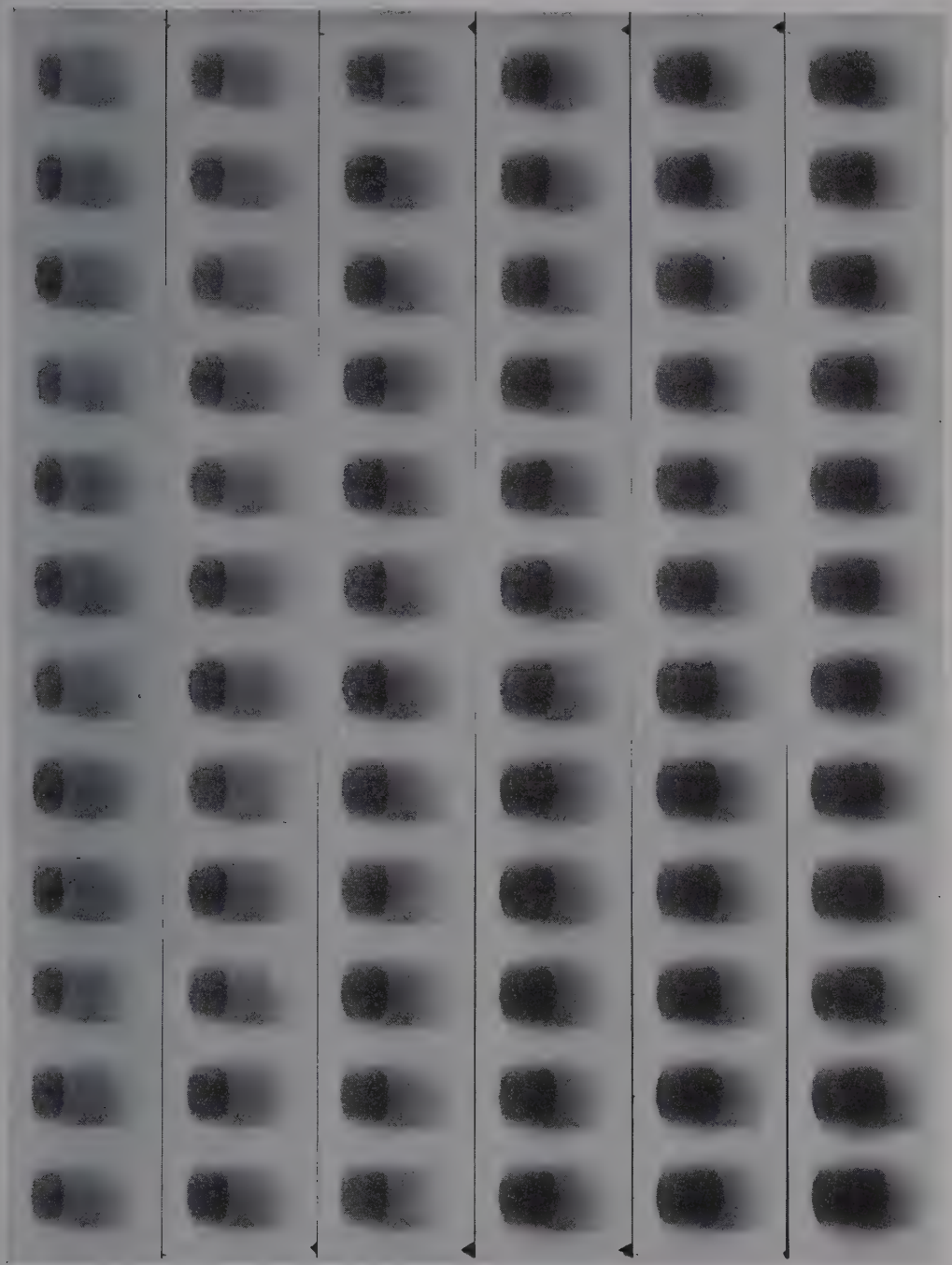

FIG. 8.—Films Showing Effect of Slit on Burning Front.

Although this sensitivity does not compare with that obtainable with radiography, the resolution was sufficient to extract useful information.

Static Firing of Motors:

The cinefluorographic equipment previously described was assembled and mounted in a light-tight box. It was then moved to the firing bay at the Allegany Ballistics Laboratory, Rocket Center, W. Va., in order to perform a series of static firings. The equipment and motor are shown in Fig. 6.

The series of test motors prepared contained different types of discontinuities, such as drilled holes and slits. The section of the motor containing the defect was aligned with the face of the image tube. A 9-in. length of the motor was observed with this system. Figure 7 shows the effect of a $\frac{1}{4}$-in. diameter by $\frac{1}{2}$-in. deep void on the burning front. A small distortion of the front is first seen, increasing until it spreads over the entire burning front. Figure 8 shows the effect of a slit upon the front; this effect is similar to that of the void but of greater severity. These films may be viewed through a motion picture projector and studied frame by frame.

SUMMARY

The feasibility of cinefluorography of small-diameter propellant has been demonstrated using a 250-kvp X-ray source, an image intensifier with a 9-in. face, an f/0.75 Fluoro-Ektar lens, and a 35-mm movie camera. This system can be improved with a lens system specifically designed for 1 to 1 work and higher X-ray intensities, which would permit the use of finer grained film. Using higher energy X-ray equipment (with its associated higher X-ray intensities) and a cinefluorographic system, one should be able to observe the burning in selected areas of large-diameter motors.

Acknowledgment:

Staff members D. P. Case and C. H. Dyer contributed materially to this task in assembly of the system and taking the films of the test motors. The cooperation of the Allegany Ballistics Laboratory in furnishing the test motors and conducting the static firing tests is appreciated.

This work was sponsored by the Special Projects Office of the Bureau of Naval Weapons, U. S. Navy Department.

DISCUSSION

MR. G. M. CORNEY (*by letter*).[1]—This paper represents a very interesting extension to industrial radiography of cinefluorography with image amplifiers, which up to now has been considered largely, if not entirely, a medical technique.

In medical cinefluorography, users are constantly faced with decisions as to the optimum "gain" or speed of their amplifying-recording systems. High gains minimize patient dosage but increase the deleterious effects of quantum scintillation in the input phosphor of the image amplifier. Lower speeds increase patient dosage, but at the same time give a superior image because the increased number of X-ray quanta per frame decreases the quantum fluctuation.

Users of industrial cinefluorography may often be faced with a similar choice. Fortunately, however, the physical effects of radiation absorption within the specimen are rarely a consideration in this field. It is my opinion, based on admittedly insufficient evidence, that the trend in industrial cinefluorography will be to use the maximum possible tube loadings, and then to decrease the speed (or gain) of the amplifying-recording system as much as possible and still achieve a satisfactory exposure at the minimum useful frame rate. There will also be many applications, no doubt, in which tube load, amplifier gain, lens speed, and film speed will all have to be pushed to the limit to get an acceptable image.

I am sure we will all watch developments in this field with great interest.

MR. D. T. O'CONNOR (*by letter*).[2]—The paper by Criscuolo and Polansky brought to mind the early work on radiography of double-base propellants which concerned itself with the phase that the authors describe as the inspection of solid propellant before firing to locate defects. In 1943 double-base propellant powder grains, particularly the Mark I used in the old mousetrap, were static fired in two 1000-unit lots, and for the first time a definite correlation was found between frequency and size of transverse fissures and the maximum pressures developed. Subsequently, through the cooperation of Captain Clark at the Aberdeen Ballistics Laboratory, an attempt was made to determine the burning pattern of the cruciform double-base grain by flash radiography. Captain Clark's courtesies to his visitors were repaid by the bursting of one rocket motor and the consequent destruction of this precious flash tube.

The present paper graphically demonstrates the progress made since those days. The technical skill of the authors and their co-workers is reflected in the quality of the results obtained by the more modern techniques of image tube motion picture photography. Although the equipment hazards apparently have not changed much, the results are infinitely more informative.

[1] Research Laboratories, Eastman Kodak Co., Rochester, N. Y.

[2] Magnaflux Corp., Chicago, Ill.

Was consideration given to an experimental motor case having more favorable characteristics than the ¼-in. wall steel case chosen? Specifically, would not a filament-wound case of approximately the same dimensions provide adequate protection and make more imaging radiation available? Do the authors feel that additional useful radiation would improve the quality of image? Do they think that the image might be impaired by the superimposed windings?

MESSRS. E. L. CRISCUOLO AND D. POLANSKY (*authors*).—The ¼-in. steel wall was originally chosen so as to withstand any overpressure that might develop during the test. It is felt that additional useful radiation would definitely improve the quality of the image. The superimposed windings on a filament-wound case would not impair the image formed in this system.

MR. S. BRANMAN[3] (*by letter*).—Most X-ray inspection systems in which an image is produced are "light limited." That is, they require many more X-ray photons than information theory shows are necessary just to raise the light level high enough for operator observation. It may be possible that this system, which obtains information for each frame on relatively few photons, is "statistics limited." A statistics limited system occurs when the statistical variation in the number of photons hitting a point is comparable to, say, the intensity variation caused by a defect. If this is the case, the mentioned improvements in the lens system may produce more light, but no new information.

Experiments and theoretical developments by Larson and Nitka of Ansco indicate that even in X-ray film inspection systems (which are generally considered light limited) detection statistics limit the resolution of very small detail. Have the inherent limitations of statistics on resolving power been calculated or considered for this system?

A fiber optics detection system may offer an advantage over the one described in the report if the one described has reached the maximum resolving power consistent with statistics. First, the fiber optics system would detect more of the available photons. This more efficient detector will increase the information detected. Second, practically all of the light generated by the scintillant can be channeled by the fibers to the face of the image tube. This provides more efficient use of the light than any lens system. Have the authors considered the use of fiber optics for this application?

Aerojet has used a different approach to the problem of following the flame front in a burning motor. Minute quantities of radioactive material (or radioactive seeds) are placed at key points in the grain. A radiation detector is placed adjacent to the motor during firing. A step-type decrease in radiation during the firing means that a seed has been vaporized and ejected. The time at which the flame front reached these points is thus determined very accurately.

If the number of points of interest in the motor is small, say two edges of a crack, less extensive equipment would be required for the radioactive seed than for cinefluorography. If the number of points of interest is large, say determining the burning pattern of a large number of small voids, cinefluorography may offer some advantage. It would be an advantage if it could indeed resolve the small voids.

In the paper the authors stated that larger motors could be X-rayed with a more powerful X-ray generator. The effect of say a chamber burn through use of a larger motor could destroy both

[3] Aerojet General Corp., Azusa, Calif.

the X-ray generator and detector. If protection is provided, either by shielding or distance, the X-ray intensity may be reduced to the point where the system may not work. Thus the risk of destroying valuable equipment may limit the size of motors that can be used in these experiments.

MESSRS. CRISCUOLO AND POLANSKY.—The limitation on resolution due to statistical fluctuations of the number of photons has not been calculated. Work by Morgan and Sturm[4] gives a fairly detailed analysis.

Fiber optics were not considered for this application since they were not in a suitable state of development at this time.

---

[4] R. E. Sturm and R. H. Morgan, "Screen Intensification Systems and Their Limitations," *American Journal of Roentgenology and Radium Therapy*, Vol. 62, No. 5, Nov., 1949, p. 617.

NONDESTRUCTIVE TESTING OF SOLID PROPELLANT MISSILE MOTORS*

By Frank C. Hund[1]

Synopsis

Requirements, techniques, and procedures for nondestructive testing of large solid propellant motors for the Polaris, Minuteman, Skybolt, and other missiles are discussed. Among the applications of nondestructive testing covered are: radiography, magnetic particle, and ultrasonic examinations of welded steel cases; radiography, penetrant, eddy current, and ultrasonic examinations of refractory metal nozzles; ultrasonic testing of the case-liner bond; and radiography of the completely assembled solid propellant motor for integrity of the grain, insulation, and bonded surfaces. Filmless radiation techniques are outlined, and the current state of vibration, low-frequency ultrasonic, infrared, and other testing methods are discussed, with the trends these tests are taking.

A missile must be absolutely dependable. It performs one time only and it must be known with assurance that it will perform satisfactorily. In addition to proper design, a successful performance depends on adequate quality assurance and control of the production of the components. Any judgment about the serviceability of a new missile motor, one that has been in storage, and one involved in test programs requires knowledge about all of the pertinent factors. Destructive firings give necessary information but cannot be used with adequate sampling because such firings are too costly and delay the production. Nondestructive testing must provide the necessary quality evaluation. As one of its task assignments, the Naval Weapons Station at Concord has investigated and developed nondestructive tests for motor cases, nozzles, and other hardware, and has examined a considerable number of complete motors.

Description of Solid Propellant Motors

Essentially, a solid propellant motor consists of a case, thermal insulation, the solid propellant, and one or more nozzles. Figure 1 shows typical configurations of motors.

Case:

The case must withstand the high internal pressures generated by the burning propellant and must be relatively thin to save weight. Cases have been made of steel, titanium, and fiber glass. The metal cases are usually welded; the fiber glass cases are continuous filament-wound with a resin binder.

Thermal Insulation:

The thermal insulation consists of layers of impregnated asbestos or rubber

* See also "Nondestructive Testing of High-Strength Steel Rocket Motor Cases" by J. A. Hendron, p. 95.

[1] Technical Director, Quality Evaluation Laboratory, U.S. Naval Weapons Station, Concord, Calif.

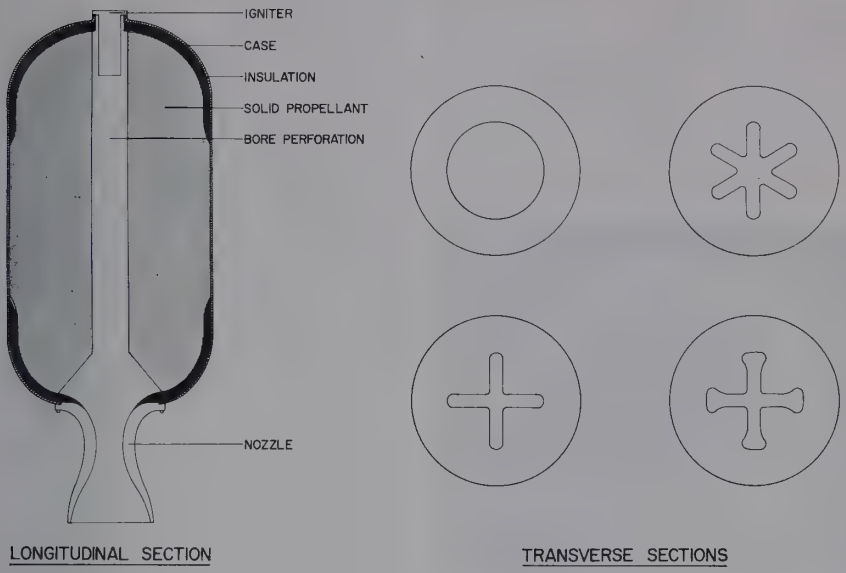

FIG. 1.—Configurations of Typical Solid Propellant Missile Motors.

TABLE 1.—APPLICATIONS OF NONDESTRUCTIVE TESTING TO SOLID PROPELLANT MISSILE MOTOR COMPONENTS.[a]

Component	Nondestructive Testing Application
Metal case, heads, and closure	MPI and R-UT of rough and machined steel forgings; MPI, R-UT, and XRT of welded steel case after welding, heat treatment and hydrostatic test
Insulated fiber glass case	X-RT and UT of formed and insulated case
Refractory metal nozzle inserts	UT, PT, and EC of sintered and infiltrated billets and machined inserts
Nozzle plastic liners	PT, LD, and UT of molded and machined liners
Nozzle outer shell	MPI of rough and machined forging
Graphite nozzle inserts	EC of rough and machined blocks
Nozzle assembly	PT, UT, EC, and LD of assembled and sealed assembly
Igniter assembly	LD of sealed assembly
Insulated chamber	LD, R-UT of insulation, and UT of insulation, case and insert bonds

[a] Test Code:

MPI = Magnetic particle inspection,
R-UT = Resonance ultrasonic thickness measurement,
UT = Pulse-echo ultrasonic testing,
EC = Eddy current testing,
XRT = X-ray radiography,
LD = Leak detection, halogen and other techniques, and
PT = Fluid penetrant testing.

that line the inside of the case and protect it from the hot gases. Protection depends on the presence of sufficient insulation to retard the flame for the time of burning and the absence of gaps in the layers that might permit the hot gases to reach the case.

Solid Propellant:

Polaris and other missile motors have a vacuum-cast propellant made of polyurethane, oxidizer, and powdered metal. Other cast solids have essentially similar compositions but may differ in specific fuel and oxidizer compositions. A second

large class of motors are the so-called "double-base" propellant motors, which are composed of colloidal mixtures of nitrocellulose and nitroglycerin. A motor is loaded with this type of propellant by packing small grains into the case and

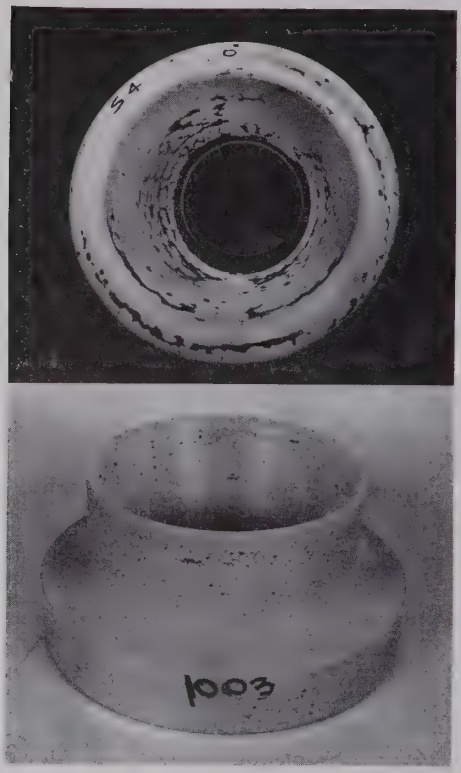

Upper, Uninfiltrated areas on infiltrated tungsten insert.
Lower, Surface porosity on sintered tungsten insert.
FIG. 2.—Penetrant Tests of Nozzle Liner Inserts.

then filling the spaces with additional plasticized nitroglycerin.

The propellant grain in large-diameter motors is designed for internal burning. For this purpose, a central perforation is present in the grain running end-to-end. This perforation may be circular, or shaped as illustrated in Fig. 1.

NONDESTRUCTIVE TESTING OF MISSILE MOTOR COMPONENTS

The need for assurance of quality is such that every phase of processing and fabrication must be covered. It is normal for a motor manufacturer to establish a "master plan" of quality assurance that traces the forming and assembly of every component in the motor. Table 1 lists some of the examinations and tests that appear on master plans.

Welded Steel Cases:

Quality assurance and nondestructive testing of welded steel solid propellant motor cases are similar to the practices used in other fields in which critical components are welded. The plate material is submitted to stringent chemical and physical tests, examined by ultrasonic techniques for thickness and flaws, and tested by some radiation techniques.

After joining, magnetic particle and fluid penetrant tests are used to inspect the welds. These are sensitive tests, but they detect only those defects that come to the surface. Also, they depend for reliability not so much on the equipment and materials as on the way the inspector performs the test and on his alertness in spotting indications. Radiography is a valuable method for determining internal soundness, and all welds are radiographed after completion and after the surfaces have been ground smooth. The thin welds of a rocket motor case are radiographed best with low kilovoltage X-rays from a beryllium window X-ray tube. Fine-grained film and good scatter reduction procedures are used because high radiographic sensitivity is necessary. The most serious defect in a weld is a crack. Radiographs do reveal the presence of cracks in case welds, and the ability to detect cracks must be the basis for establishing the radiographic procedure. Fluoroscopy has not been sufficiently sensitive for use in

inspecting case welds. Pulse-echo ultrasonic testing with the shear wave and surface techniques is applied to some case welds. Unfortunately, problems arise from the graininess of the weld metal, the sonic mismatch between the weld and base metal, and irregular weld surfaces which necessitate very carefully controlled testing and evaluation procedures.

Finished cases must pass the hydrostatic test; it should be noted that the hydrostatic pressures in these tests approach the ultimate strength of the material.

Nozzles:

Exhaust nozzles for solid propellant missile motors are made in a variety of designs. A nozzle for a large-diameter motor, in which the burning lasts longer than a few seconds, is usually made in sections. One critical section is the venturi, and only graphite, some ceramic materials, and the high melting point refractory metals may be used. Tungsten, with a melting point of 6170 F, has excellent properties for nozzle use.

A nozzle insert must be uniform throughout the section, and it must be free of cracks. In pressed-and-sintered tungsten made with less than 100 per cent density, the porosity must be uniform, and the subsequent infiltration must fill all of the pores. Dye penetrant tests have been made on most of the tungsten inserts tested at the Naval Weapons Station, Concord. This method readily shows cracks, holes, and surface discontinuities as well as areas of inadequate or incomplete infiltration which extend to the surface, and the penetrant test is recommended for a nozzle insert after infiltration. Figure 2 shows the results of penetrant tests on two inserts. The upper photograph shows penetrant indications on an infiltrated insert; the lower shows indications of surface porosity on a high-density pressed and sintered tungsten insert which was not infiltrated.

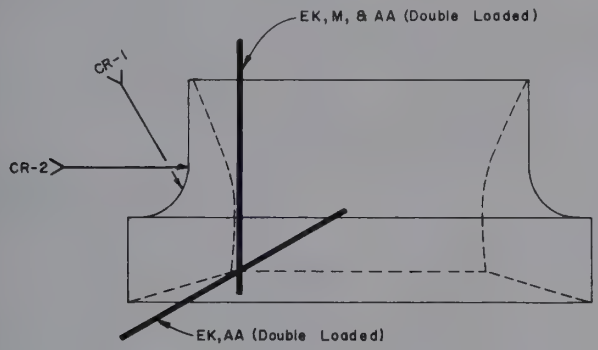

FIG. 3.—Radiographic Exposure Plan for Tungsten Nozzle Insert; *CR-1* and *CR-2*, Twelve Exposures at 30-deg Intervals.

Eddy current tests have been attempted on several inserts and billets with the Magnaflux Model FM-110 conductivity meter, the Model ED-500 eddy current test unit, and the DuMont cyclograph. They were sensitive to changes of infiltration on the surface as well as to cracks. It was difficult, however, to distinguish between surface cracks and linear porosity by the eddy current test alone.

Radiographic examinations are made of all inserts. The 2-Mev X-ray unit is

used for thicknesses up to about $2\frac{1}{2}$ in., and the 10-Mev linear accelerator for greater thicknesses. Maximum thicknesses radiographed have been about $4\frac{1}{2}$ in., and standard 1 per cent penetrameters are regularly displayed. When an insert has moderate differences in section thicknesses, film of two different speeds must be used in each cassette. Figure 3 shows the exposure plan for an insert. For this design, two regions are exposed. A minimum of twelve exposures around the insert are required for adequate coverage in each position, a total of 24 shots. The complex shape of the cross-section frequently requires considerable blocking with lead shot, bricks, and sheet. A small cone is used on the 2-Mev source to reduce scatter, and sometimes a $\frac{1}{4}$ in. thick lead filter is used to harden the beam for further scatter reduction.

FIG. 4.—Water-Coupled Ultrasonic Testing of Nozzle Insert with Sperry Type UR Reflectoscope.

Radiographs have shown clearly the regions of low density and lack of infiltration. Cracks have also been demonstrated, and radiography is a recommended test for tungsten nozzle inserts.

Immersed and contact pulse-echo ultrasonic tests were investigated. Several inserts tested contained cracks; others had areas of incomplete infiltration that were revealed by radiography and penetrant inspections. In all cases the cracks and porosity were indicated by the ultrasonic examinations. In most cases, the indications were greater than from an $\frac{1}{8}$-in. diameter flat bottom hole when tested at 1.0 and 2.25 mc per sec test frequency. Cracks in one insert were

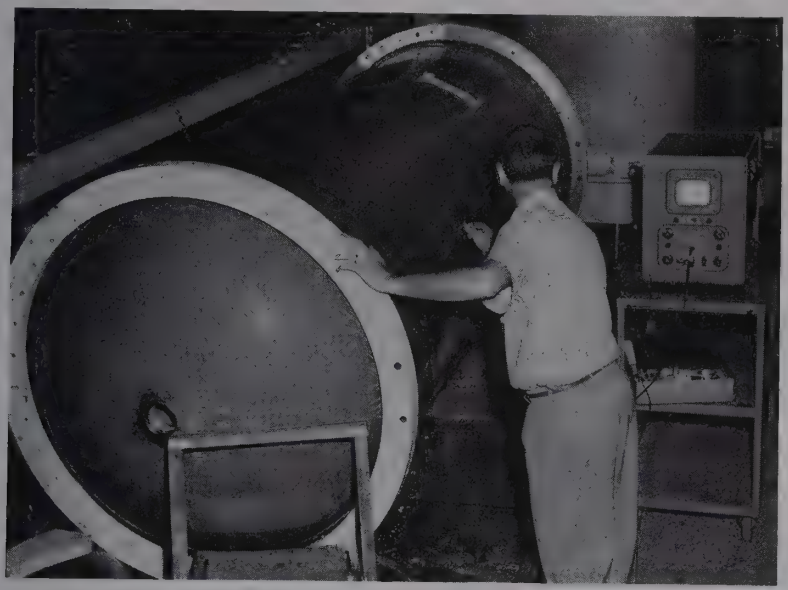

FIG. 5.—Ultrasonic Testing for Case to Liner Bond Separation on a Solid Propellant Missile Motor.

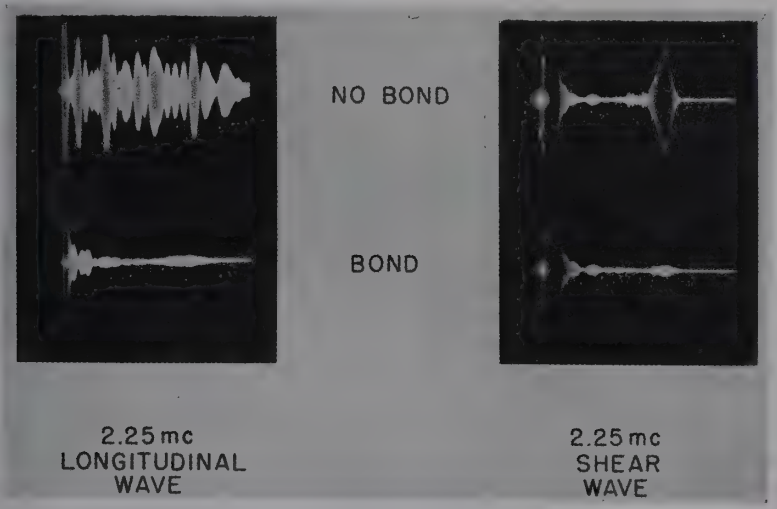

FIG. 6.—Oscillographs of Reflectoscope Patterns of Separated and Bonded Case-Liner Interfaces with Longitudinal and Shear Waves at 2.25 mc per sec Frequency.

readily distinguished from internal uninfiltrated areas which were also present. Figure 4 shows a water-coupled ultrasonic test of a nozzle insert with the Sperry reflectoscope. Radial and axial scans with both longitudinal and shear waves are recommended, and 1 mc per sec is the preferred frequency.

NONDESTRUCTIVE TESTING OF ASSEMBLED SOLID PROPELLANT MOTORS

In spite of the extensive tests and examinations made of most of the components that go into a solid propellant motor, the integrity of some parts can be determined only after the motor is assembled and the solid propellant is installed. Also, it is often necessary to reexamine installed components for the effects of testing. It has been necessary, therefore, that inspection procedures be developed that are capable of detecting substandard and defective missile motors in the fully assembled condition. For this, radiography solves several inspection problems, and an ultrasonic test is used to detect case-insulation separations.

Ultrasonic Testing of Case-Liner Bond:

For structural rigidity and other reasons, it is necessary that the propellant in the larger diameter motors be solidly bonded to the case. The plastic insulating liner accomplishes this by adhering firmly to the interfaces of the case, insulation, and the grain. Assurance of a sufficient and continuously adherent layer of insulation is best determined immediately after application and is usually done at this time. Often, however, an adequate examination is not possible until after the propellant has been installed.

Investigations have shown that a practical and very sensitive method for detecting case-insulation separations is the contact longitudinal-mode ultrasonic technique. A long pulse and exact tuning of the instrument to match the case thickness are required in this technique. Several commercial ultrasonic flaw detectors with standard crystal transducers have been found adequate for this application. As Fig. 5 shows, in this technique the operator scans the surface of the motor with the ultrasonic transducer and notes the response on the screen. When liner material is separated from the back case surface, little sonic energy is lost and the oscilloscope shows numerous resonance envelopes due to feedback into the circuitry. The damping effect of adherent liner material results in resonance patterns of much less amplitude. Figure 6 shows typical oscillographs of the reflectoscope patterns for bonded and separated conditions and also shows a similar effect in the shear wave technique.

Radiography of Assembled Solid Propellant Motors:

At the Naval Weapons Station in Concord and in many other testing facilities, radiography is used to reveal the following conditions in an assembled solid propellant motor: cracks, voids, and other defects in the propellant; liner-propellant separations; irregularities in the case and insulation; and improper assembly of closures and igniters. Although the techniques are recognizable to one with experience in the field of metals radiography, the application of radiography to solid propellant motors is more complicated because of the large thicknesses and masses involved, the low atomic number and low density of the solid propellant, insulation, and in some motors, the fiber glass case, the shape and makeup of the peripheral areas, and because of the routine necessity for the best attainable radiographic sensitivity.

Radiographic Procedures.—Basically, only two radiographic procedures are used to examine a motor. In one plan, the propellant grain and other internal components are examined, while in the second plan the insulation and liner-propellant bond are covered. In both plans, numerous exposures are needed to (1) cover the length and section of a large motor, and (2) provide sufficient angular coverage to improve the probability of finding both cracks in the grain exposures and separations in the tangential exposures.

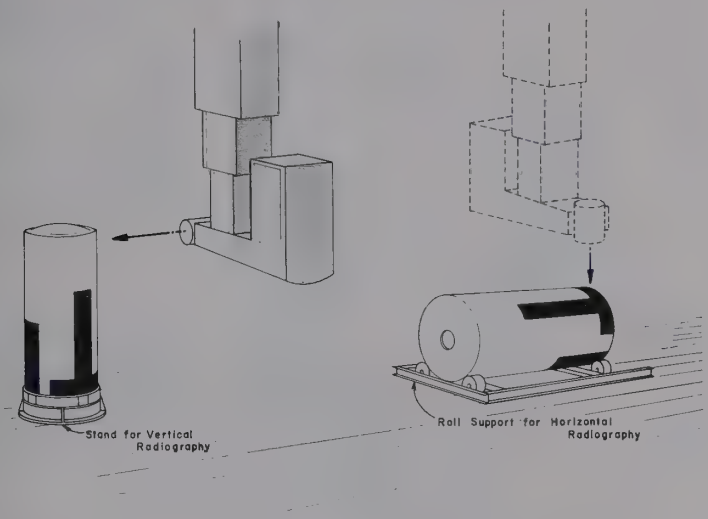

FIG. 7.—Arrangement of Solid Propellant Missile Motors for Radiography in Vertical and Horizontal Attitudes.

Motor Attitudes During Radiography.—The development of radiographic procedures for examining motors is dependent upon the attitude of the motor during the testing. Vertical attitude radiography may be required by the design of large-diameter solid propellant motors. For production inspection where only one motor size and design are examined, vertical attitude is preferred. In practice, this is done in one of two ways: in the first, the motor is placed on an elevating turntable and the source is placed in a fixed position. Coverage is then provided by lifting and rotating the motor. In the second, the motor is placed on a turntable and the source is made to elevate and angulate. Figure 7 illustrates the second arrangement, which is used at Naval Weapons Station, Concord. Shown are the arrangements for both vertical and horizontal radiography with the Varian 10-Mev linear accelerator.

The design of many large case-bonded motors is such that handling and radiography of these units may be done in the horizontal position. Figure 7 shows a motor on the roll stand with the linear accelerator in position above the section of the motor being exposed in horizontal attitude radiography. The use of such a roll stand requires the installation of rolling rings at the ends of the motor. If the design of the motor prevents the use of end rings, a continuous belt can

be used to support the motor. Horizontal radiography is most practical in a facility that examines a variety of sizes and types of solid motors.

Motor Handling.—Transferring and positioning motors within the radiographic facility is accomplished with an overhead crane and the use of several lifting and inverting devices. Figure 8 illustrates four methods in use with large diameter motors. This figure shows the use of the Pneuma-Grip, made by the Presray Corp. In this device, inflatable tires surround and grip the motor. The yoke permits inverting, and release is accomplished by deflating the tires and slipping the device off. Figure 9 shows the arrangement of handling and radiographic equipment at the Naval Weapons Station, Concord. This facility contains in one large exposure room, the Varian 10-Mev linear accelerator and the General Electric 2-Mev Resotron. All handling is performed with the overhead crane. Temperature is controlled in the facility and maintained around 75 F.

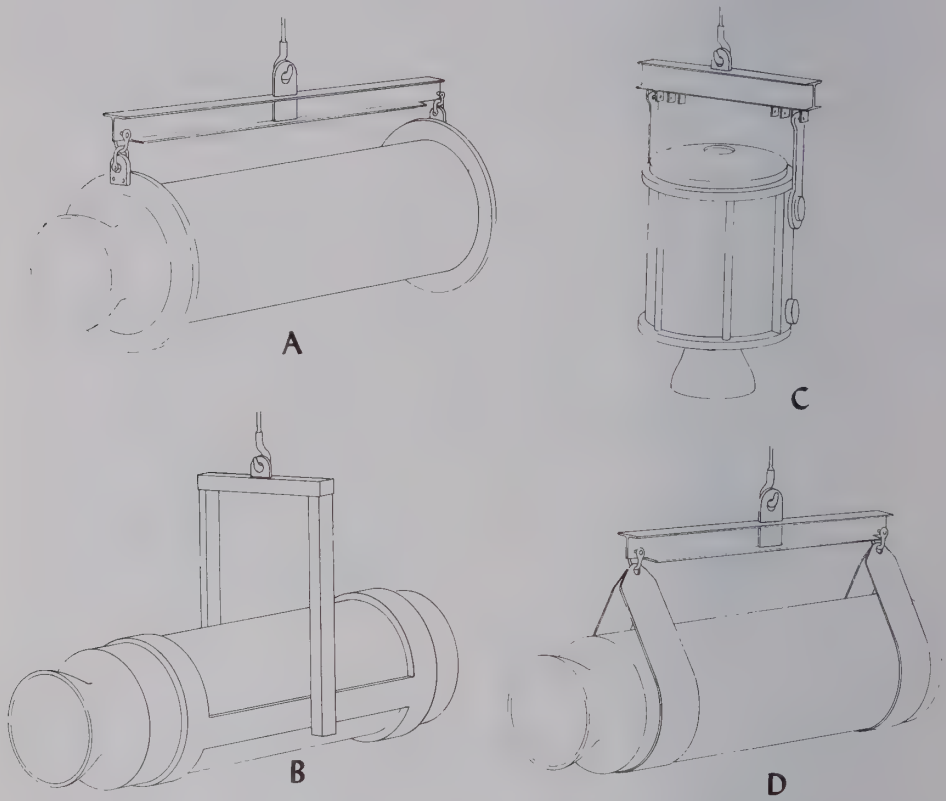

A, Spanner beam and end rolling rings.
B, Pneuma-Grip (inflatable tubes).
C, Lifting yoke and shipping harness for inverting motors.
D, Spanner beam and wire-reinforced rubber-covered slings.

FIG. 8.—Motor Handling Methods.

Selection of the Source.—The selection of the source involves many factors and must be given very careful consideration.

FIG. 9.—Radiographic Facility at U. S. Naval Weapons Station, Concord, Calif., Containing 2-Mev X-ray Unit and 10-Mev Radiographic Linear Accelerator.

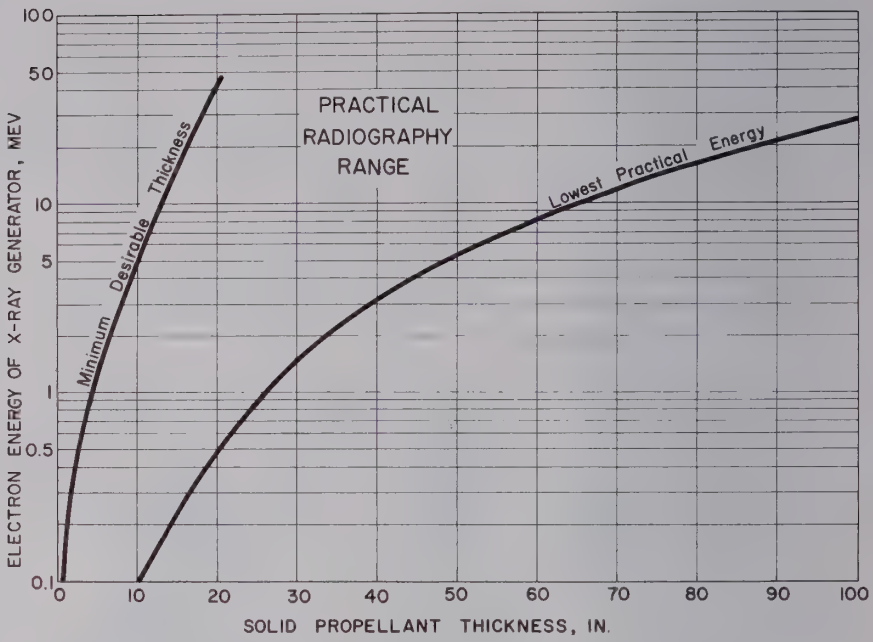

FIG. 10.—X-ray Energy for Practical Radiography of Solid Propellant.

TABLE 2.—COMPARISON OF HIGH-ENERGY X-RAY GENERATORS.
Aerojet-General Corp., Sacramento, Calif., Chart No. TP3892, Aug. 25, 1961.

Generator Type	Linear Accelerator				Betatron
Maximum Energy	8 to 10 Mev	13 to 16 Mev	25 Mev	40 Mev	25 Mev
Focal spot, mm	1 to 3	1 to 3	1 to 3	5	0.1 × 0.2
Intensity, r per min at 1m	500 to 2000	up to 3000	up to 40,000	70,000	50[a]
Cone angle, ½ intensity, deg	30	26	14	8	14
Focal-film distance, 14 by 17 in. coverage, in.	60	80	156	180	156
Exposure for 50 in. propellant at 10 ft focal-film distance, min	10	0.9	0.11	0.015	17
Half-value layer of steel	1.25	1.3	1.3	1.3	1.3
Half-value layer of propellant	6.5	7.25	8	8.1	8

[a] Compensated.

The optimum X-ray energy for radiography is a function of propellant thickness, and for great thicknesses, sources with higher energy and intensity must be used. The upper thickness limit of a source, regardless of output intensity, however, is often restricted by resulting image quality and scattered radiation factors to a definite number of half-value thicknesses. Bly and Burrill[2] place the

[2] J. H. Bly and E. A. Burrill, "High-Energy Radiography in the 6- to 30-Mev Range," Symposium on Nondestructive Testing in the Missile Industry, *ASTM STP No. 278*, Am. Soc. Testing Mats., 1959, p. 20.

limit for solid propellant at between 10 and 14 half-value thicknesses. This limit may be realized in the future when radiographic sources with optimum efficiency and maximum output are produced. With equipment available today, however, the practical limit for radiographic linear accelerators appears to be about 10 half-value thicknesses, and for betatrons about 9. Thus, as Fig. 10 indicates, it is not practical to use less than 1 Mev to radiograph 26 in. of propellant, or less than 10 Mev for 66 in. The lower thickness limit plotted at the left in Fig. 10 is based on the general rule that it is desirable to avoid radiography of less than 2 half-value thicknesses.

Other important features of a source for solid propellant motor radiography and upon which procedures are based include the radiation output intensity, field size and radiation intensity across the field, and source diameter. Table 2 shows a comparison of high-energy X-ray units. Higher energy sources are desirable because of the increased penetration and the greater radiation intensity. Unfortunately, higher energy sources also have a greater forward beaming effect, and may require the use of a compensator to produce a beam with a uniform intensity across a useful angle. A second advantage of the higher energy sources is the improved scattering conditions. At 1 and 2 Mev, considerable shielding is needed in tangential exposures, for example, to protect the film from scattered radiation, whereas no shielding is needed in the 10- to 25-Mev procedures. A disadvantage of the higher energies appears to be the loss in resolution that results from the proportional increase of film-screen unsharpness with energy.

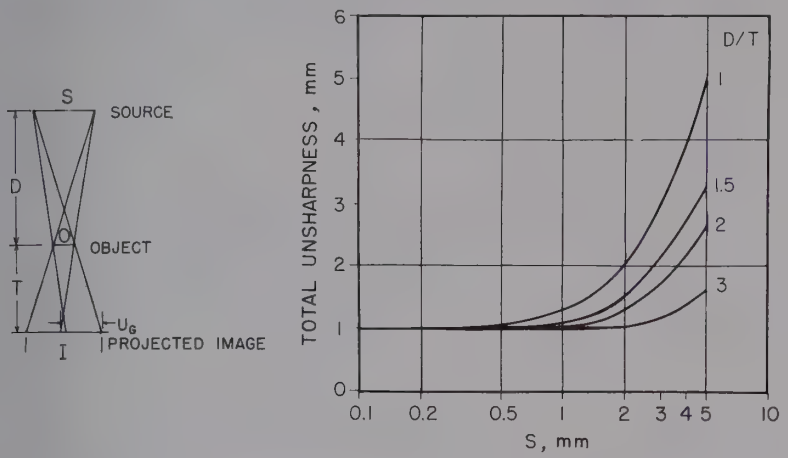

Courtesy of Cusick and Haimson

FIG. 11.—Image Unsharpness in Radiography of Large Rocket Motors.
Type M film, 0.60-in. lead screens, 10 Mev, U_F = 1.0 mm.

Image magnification, $i = O + \frac{O}{D/T}$

Geometric unsharpness, $U_G = \frac{S}{D/T}$

Film-screen unsharpness, U_F

Total unsharpness, $U_{TOT} = (U_F^3 + U_G^3)^{1/3}$

[3] E. L. Criscuolo, J. A. Holloway, D. Polansky, and C. H. Dyer, "Radiography of Large Solid Propellant Rocket Motors," Symposium on Nondestructive Testing in the Missile Industry, *ASTM STP No. 278*, Am. Soc. Testing Mats., 1959, p. 3.

Inherent unsharpnesses of 0.5 to 1.0 mm have been reported by Bly[2] and Criscuolo[3] for energies up to 10 Mev. From these data, it is expected that film-screen unsharpness for higher energies would be somewhat greater than at 10 Mev. As a consequence of the ways that geometric and film-screen unsharpnesses combine, no improvement in the total unsharpness is expected from extremely small focal spots around 10 Mev. In the radiography of large missile motors, where source-object-film ($D:T$) ratios are small, the practical upper limit to source sizes is about 1 mm. Figure 11 from Cusick[4] shows the rapid increase in total unsharpness at $D:T$ ratios of 1 to 3 as source size increases beyond 1 mm. The figure also shows that there is

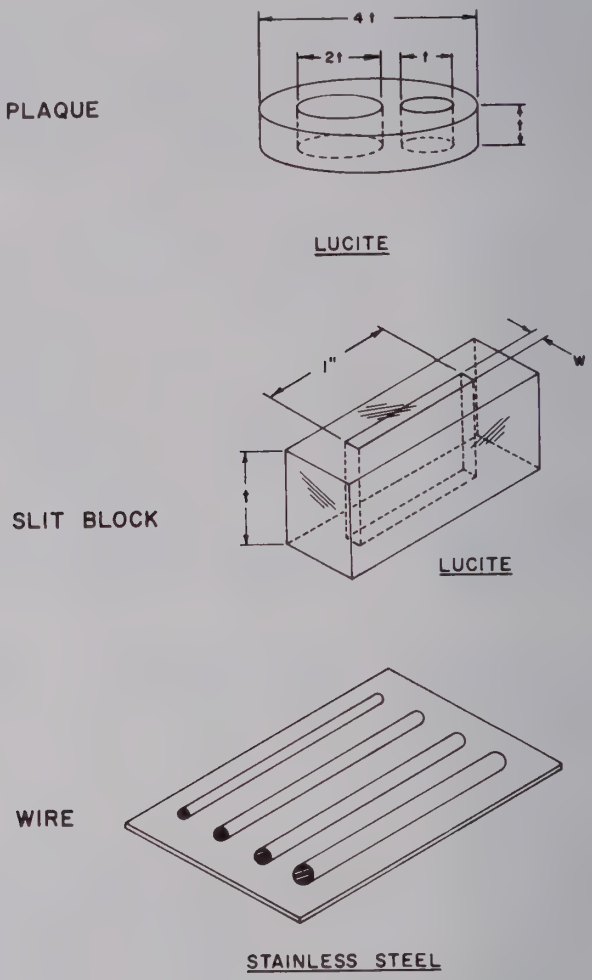

FIG. 12.—Penetrameters for Grain and Tangential Radiography of Solid Propellant Motors.

[4] J. H. Cusick and J. A. Haimson, "10-Mev Rotating Target Linear Accelerator for Radiography of Large Rocket Motors," *Proceedings*, Bureau of Naval Weapons Missiles and Rockets Symposium, April, 1961.

no advantage in using sources smaller than 1 mm at energies in which the film-screen unsharpness is close to 1.0 mm.

Penetrameters.—Recently great emphasis has been placed on the assurance of good radiographic quality by including in the specifications the requirements that penetrameters be used to demonstrate adequate sensitivity. Figure 12 shows three types of penetrameters used in solid propellant motor radiography. The drilled plaque type used in the grain exposures should ideally be made of solid propellant, but Lucite and other materials are frequently substituted. Penetrameter thicknesses are usually made 0.5 to 1.0 per cent of the equivalent grain thickness. The equivalent thickness of penetrameter material (Lucite, for example) is determined from the following:

$$\text{Equivalent thickness of Lucite} = \text{propellant thickness} \times \left(\frac{\mu_{\text{Lucite}}}{\mu_{\text{propellant}}}\right)$$

where μ is the linear absorption coefficient of material at the effective X-ray energy of the source, in^{-1}.

The slit block and wire types of penetrameters are used in the tangential exposures. The thickness of the slit block is often made 1 or 2 per cent of the equivalent thickness of the peripheral portion of the motor, and slit widths of 0.01 and 0.02 in. have been used. The wire penetrameters, which are similar to the DIN[5] standard, are also used mainly for tangential exposures. Wire diameters are made 0.25, 0.5, 1.0, or more per cent of the equivalent thickness in the area of the motor periphery of interest—for example, at the liner-propellant interface. Stainless steel is shown in the figure, but other materials may serve equally well as quality indicators.

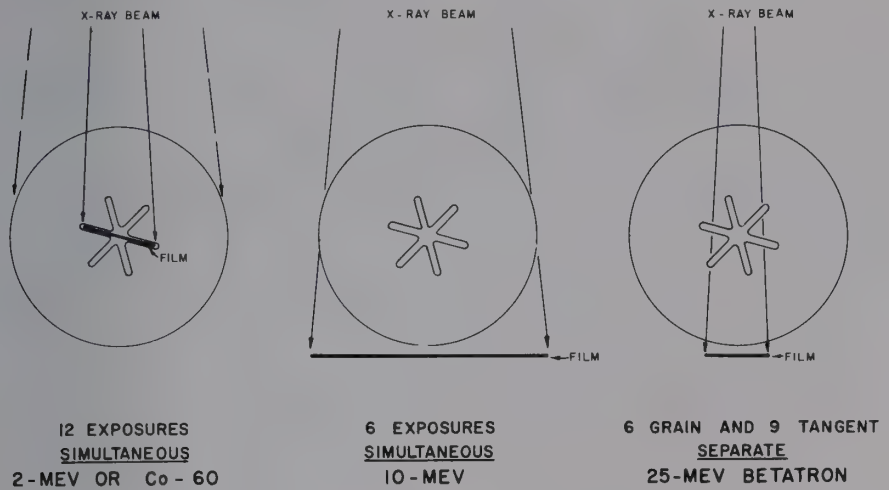

FIG. 13.—Grain and Tangential Radiographic Exposure Techniques.

Solid Propellant Grain Radiography:

Practical radiographic procedures have been established by many facilities and sensitive determinations of the soundness of grains have been made with penetrating radiation. Defects that radiography

[5] German Standards Agency.

can reveal are cracks, voids, and porosity. As stated above, there is a practical limit to the thickness of solid propellant that can be radiographed with a given source. In motors whose total diametrical thickness exceeds that limit, the film may be placed in the bore perforation if it is open and accessible and exposures made of half of the total thickness. Alternatively, some motor manufacturers place a small cobalt-60 source inside the bore and the film outside the motor for exposure. Figure 13 shows the arrangements for grain radiography of a large-diameter motor with the different sources. The plan for 2-Mev and cobalt-60 (placed externally) requires placement of the film in the bore, and about twelve exposures around the motor to obtain complete coverage. As Fig. 13 shows, the peripheral areas may be exposed simultaneously because of sufficient intensity of the beam at that angle off the central ray. Areas of multiple exposure occur in this plan, including the regions near the ends of the "fingers" where the propellant shrinkage stresses during curing produce the greatest strains.

High-Energy Techniques.—Completely assembled motors may not have the bore accessible, and grains with a complex perforation may not permit the insertion of film in the bore. Radiography of motors over 36 in. in diameter in these conditions requires the use of X-ray generators with energies of 8 Mev and higher. Recently developed linear accelerators and the older 25-Mev betatron have satisfactorily filled this need. Fewer exposures are required for complete coverage of the motor for radiography through the motor diameter. Figure 13 shows the plan for simultaneous grain and tangential radiography with the 10-Mev linear accelerator, which makes six exposures around the motor for complete coverage and good assurance of finding small defects. Areas exposed near the periphery require either a shorter exposure or slower speed film. Both techniques are used in some cases. The plan shown for the 25-Mev betatron indicates smaller coverage because of the beaming effect. Simultaneous tangential exposures may not be made with this generator for the same reason. In practice, six exposures are made around the motor with the betatron which may completely cover the grain, but which may not produce multiple coverage in any area.

Grain Radiography Results.—Defective areas in the grain such as voids, cracks, and conditions of porosity will produce a detectable increase in film density if the difference between the photon transmission through the defective area and sound area is equal to or greater than the sensitivity of the system. Tests with the 10-Mev linear accelerator have shown sensitivities of 0.2 per cent through propellant thicknesses of 60 in. or more when the potentially bad scattering conditions inherent in the propellant are controlled. Thus voids are readily demonstrated, depending only on the contrast sensitivity.

Porosity and conditions of innumerable small discrete gas pockets in large thicknesses of propellant are difficult to detect and cannot be adequately demonstrated except by a method which indicates their cumulative effect. If the propellant thickness is sufficiently great, void diameters fairly uniform, and void numbers sufficiently large, the effective mass will be radiographically homogeneous. The effect is the same as radiographing a large thickness of sponge rubber. A penetrameter with such conditions will be demonstrated fairly clearly because it effects a greater than average thickness. A number of voids may be demonstrated if they happen to be somewhat larger than average or if two or more slightly larger than average are

aligned. Thus, test results in which "numerous small voids" are found, and others in which "small peripheral gas voids" are observed must be considered in the light of the above concepts to determine their significance. In the radiography of peripheral areas, the propellant thickness is not sufficient to "acquire" homogeneity, and innumerable small voids can be demonstrated at the tangent points in such concentrations as to give the appearance of a liner-propellant gap.

Crack detection in the propellant depends on contrast sensitivity and the number of angles from which the crack is radiographed. In a single exposure, a crack at an angle to the beam will produce an image on film if the differential absorption exceeds the system sensitivity, therefore small cracks approaching a 90-deg angle to the beam may not be shown. To increase the probability of finding such cracks, additional exposures at other angles are needed. Figure 14 shows the relationship between the probability of detecting cracks and the number of exposures taken around the motor for cracks of varying size, at a particular sensitivity level. For example, at a 0.5 per cent contrast sensitivity level, it takes twelve exposures around a motor to be assured of finding cracks 30 mils wide or more. With twelve exposures, the probability of finding 10-mil cracks is about 30 per cent.

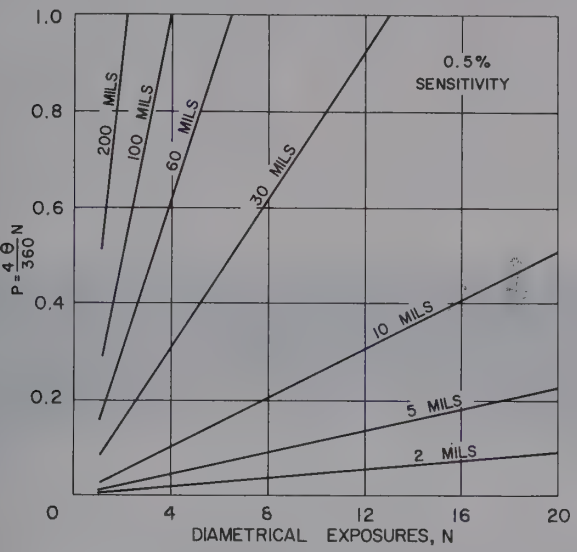

FIG. 14.—Probability of Demonstrating Longitudinal Cracks in a 54-in. Diameter Solid Propellant Motor at 0.5 Per Cent Sensitivity; Probability Decreases in Direct Ratio with Sensitivity.

Sensitivity, $S = \frac{\Delta X}{X}$, $\Delta X = \frac{W}{\sin \theta}$, W = crack width.

θ, crack angle to X-ray beam = arc sin $\frac{W}{SX}$.

X = function of diameter.

Tangential Radiography:

Peripheral or tangential radiography is used to demonstrate separations be-

tween the liner and propellant, and to check on the integrity of the thermal insulation. In this technique the beam is directed toward the motor periphery with the film placed a distance behind the motor. The cylindrical portion of the motor is easily set up for tangential exposures. Exposures of the forward and aft hemispherical head are a little more complex. Figure 15 shows a composite 10-Mev tangential radiograph of the forward head of a large motor. The clarity with which the separations are shown indicates the usefulness of this technique.

FIG. 15.—Composite of Tangential Radiographs of Forward Head of a Solid Propellant Missile Motor Showing Liner-Propellant Separation; Single Exposure, 10-Mev Linear Accelerator.

Interpretation of Radiographs.—The shape and the complex structure of the peripheral portions of a solid motor, particularly at the forward and aft heads, frequently lead to interpretation difficulties. Most often, these difficulties concern the analysis of the liner-propellant interface in the head ends of a motor. Due to processing and manufacturing variations, almost all motors exhibit differences in the tangential radiographs in these areas. A very thin liner causes the liner-propellant interface to be less apparent. Very thick liners produce radiographic densities at the interface which may approach that of small separations. The use of a small X-ray source size can provide sufficient definition, when adequate contrast is obtained, to distinguish between these two conditions and is generally desirable for tangential radiography. Asbestos insulation material is cut, overlapped, and formed to the internal contour of the head ends of the motor. The overlapped areas are sometimes projected over the liner-propellant interface, tending to confuse the radiograph. Variations in the thickness of the interlayer bonding agent further tend to obscure the true interface in these areas. To assist the film reader, and to serve as the basis in the establishment of the tangential procedures, it was found necessary to make a complete analysis of the tangential radiography problem.

Basis for Analysis.—The total absorption path lengths are computed from simple geometric relations. Concentric circles are assumed. Figure 16(*a*) shows the geometric configurations used in the calculations. Where the chord representing the path of X-rays penetrates liner and propellant in addition to the steel case, the relative linear absorption coefficients were used to calculate the total equivalent steel thickness. Figure 16(*b*) shows the values plotted against the radial depth below the periphery. This curve illustrates the general absorption pattern and over-all attenuation charac-

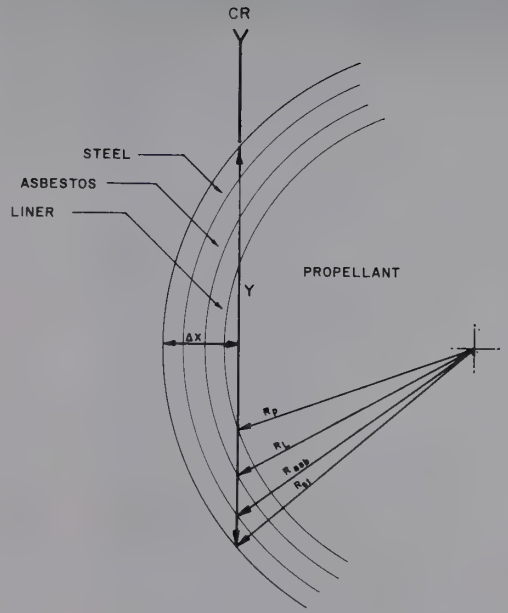

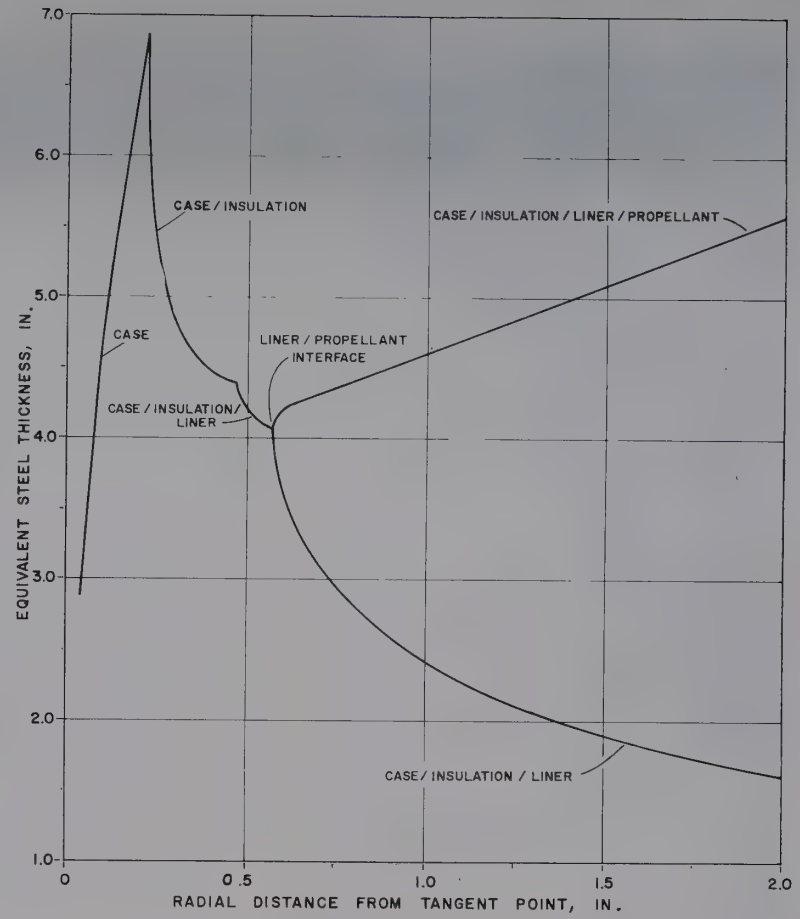

(*a*) Geometric relationship for determining path lengths.
(*b*) Absorption path lengths as a function of the radial distance from the tangent point.

FIG. 16.—Absorption Path Lengths in Tangential Radiography of a 54-in. Diameter Solid Propellant Missile Motor.

teristics experienced in tangential radiography of the motor. It is this relationship that allows the film reader to visualize film density variations in terms of the

TABLE 3.—SENSITIVITY, $\Delta X/X$, REQUIRED TO DEMONSTRATE LINER-PROPELLANT SEPARATIONS.[a]

Separation, in.	Sensitivity, $\Delta X/X$, per cent
0.001	2.3
0.002	3.3
0.003	4.0
0.004	4.6
0.005	5.1
0.010	7.3
0.020	10.3
0.030	12.6

[a] Data are for a 54-in. diameter motor with a steel case ¼ in. thick, and approximately ¼ in. insulation.

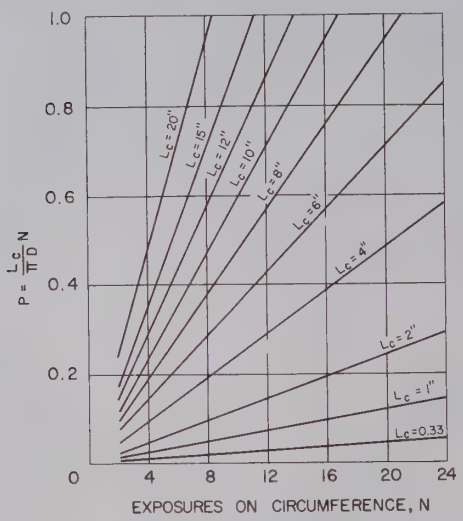

FIG. 17.—Probability of Demonstrating Liner-Propellant Separations in Tangential Radiography of 54-in. Diameter Motor.

L_c = Circumferential length of separation; D = diameter.

motor design and makeup. Film density is a reciprocal function of the equivalent steel curve.

Depending on the case thickness, a liner-propellant separation with about a 0.001 in. wide gap between the surfaces will affect an equivalent thickness differential of approximately 2 per cent in a 54-in. diameter motor. Therefore a contrast sensitivity of 2 per cent is adequate to detect this 0.001-in. separation if the inherent scattering conditions are properly controlled. Sensitivities in this section are determined by the ratio of the difference in total path length, due to the separation, to the total path length determined at the liner-propellant interface.

Table 3 lists the sensitivities required to demonstrate liner-propellant separations of various widths. It can be seen that the sensitivity required reaches a value of about 10 per cent for a 20-mil separation. Of course, demonstration of a narrow separation on film depends on adequate resolution in addition to contrast sensitivity. In high-energy radiography, however, with film-screen unsharpnesses of over 0.020 in., a 1-mil separation will produce an image on film that is much wider than 1 mil, and the problem of demonstration reverts to the presence of sufficient contrast.

Assuming, therefore, that controlled radiography results in better than 1.0 per cent sensitivity, it is probable that any liner-propellant separation occurring at the tangent point in a tangential radiograph will be seen. Thus the probability of detecting a liner-propellant separation is a function of the presence or absence of the separation at the tangent point, and this depends on the circumferential length of the separation and on the circumferential distance between tangential radiographs. Figure 17 shows the probability of demonstrating a separation in tangential radiography plotted as a function of the circumferential length of the separation and the number of exposures around a 54-in. diameter motor. This shows, for example, that an exposure plan with twelve circumferential exposures (evenly spaced) will detect all separations with a circum-

Upper, Radiograph of forward head section of motor, vertical (forward head up) showing large liner-propellant separation.

Lower, Radiograph of same area on motor, vertical (forward head down) showing apparent decreases in liner-propellant separation.

FIG. 18.—Illustrating Technique for Verifying the Presence of a Separation.

ferential length of 14 in. or more, and slightly less than 60 per cent probability of detecting a separation with an 8-in. circumferential length.

Special Technique for Verifying the Presence of a Separation.—When tangential radiographs taken with the regular exposure plan indicate a liner-propellant separation, a special technique to verify its presence has proved invaluable. This technique depends on propellant movement resulting from a change of motor attitude, from forward head up to forward head down, for example, to cause the opening and closing of a separation. Figure 18 illustrates this technique. The upper radiograph is of an area of the forward head of a motor made by the regular technique, with the forward head up, and shows that there is a possible liner-propellant separation. The lower radiograph is of the same area with the motor inverted. The weight of the propellant in this case was sufficient to close the separation. A similar technique is used in the cylindrical section.

Filmless Radiation Inspection Techniques:

The usefulness of penetrating radiation to assess the internal soundness of solid propellant motors has prompted the development of several radiation detector systems in which gas filled ion chambers and scintillators are used as the detectors. Complete grain integrity systems have been applied by motor fabricators, and large savings in the inspection times have been possible.

In spite of their useful characteristics, these detectors have several drawbacks. Their comparatively large size necessitates the use of small collimators over the sensitive area in order to achieve defect resolution. Also there are definite limits to the counting rates of both scintillators and ion chambers. This precludes their use with the high-energy pulsed X-ray generators. New developments in semiconductor radiation detectors indicate a potential answer to the limitations and drawbacks of scintillators and ion chambers.

Leak Test of Fully Assembled Motors:

Fully assembled solid propellant missile motors are given a leak test to ensure good tightness of the seals in closures, inserts, and nozzles. The procedure consists of internally pressurizing the motor with nitrogen gas containing a small percentage of Freon. Specifications require that there be no pressure drop in excess of about 0.1 per cent per hr when pressurized. If leakage is detected in the system in excess of that permitted, a probe type halogen leak detector is used to scan the motor to locate the leaks. There is no need in this test for the highly sensitive and quantitative types of leak tests, and the pressure drop and halogen leak tests have sufficient sensitivity and adequate response to make them effective and useful.

SUMMARY

The search for new improved materials and better test methods is continuing. Considerable work is being done on correlating test results and establishing standards for testing and acceptance. Among the techniques in which development work is progressing are vibration and mechanical impedance analysis, low-frequency ultrasonics, infrared radiation detection, and automatic film interpretation.

Vibration and Mechanical Impedance Analysis:

Large and abrupt differences of the mechanical impedance and phase angles of the force and acceleration in the bonded and unbonded conditions exist in the vibration test, and these differences in response may be used in bond detection. In this test, a small variable

frequency force generator is attached to the impedance head and the assembly used to scan the surface of the motor as in the ultrasonic test. For each application, the effects of geometry, standing waves, specific test frequencies, and data acquisition and evaluation require control and standardization.

Low-Frequency Ultrasonic Testing:

One problem in the application of pulse-echo ultrasonics to the problem of bonding has been the poor transmission of the ultrasound in the fiber glass, insulation, and propellant. This limitation has all but eliminated the technique for use other than that described earlier. A technique using the lower ranges of ultrasonic frequencies to improve penetration is under development. Problem areas in this technique have been the need for high-powered generators, transducers of a radical design, and improved methods of read-out.

Infrared Radiation Scanning:

Scanning with infrared detectors appears promising as an inspection technique for fiber glass cased motors. The recent emphasis in the development of this nondestructive testing method has been on the detection of liner to propellant unbonding, although the technique is capable of sensitive detection of case defects, case to liner unbonding, and near-peripheral propellant defects. Infrared detectors have reached a high state of development in other scientific and engineering applications; for nondestructive testing of missile motors, however, the method requires further development of the data acquisition, handling, and evaluation techniques.

Automatic Film Interpretation:

Interpretation difficulties in tangential radiography usually concern the detection of the liner-propellant interface. True separations are characterized by a fairly high film density depending on the width of the separation, and two distinctly sharp and rapid film density changes, one at the surface of the propellant and one at the surface of the liner. This characteristic permits the use of a densitometric scanning technique that graphically represents the rate of film density change at the interface to support the visual interpretation.

APPENDIX

GLOSSARY OF TERMS USED IN NONDESTRUCTIVE TESTING OF SOLID PROPELLANT MISSILE MOTORS

Bond, the adhesion at the interfaces of case, insulation, layers of insulation and the propellant.

Case-insulation separation, a separation between the metal case and thermal insulation caused by the failure of the bond and a movement of the insulation away from the case.

Crack, any separation within the cross-section of a solid propellant grain. This separation may be void or may contain foreign material.

Density (H&D), the degree of opacity of an exposed film after development. By definition, photographic density is the logarithm of the reciprocal of the (light) transmission.

Density ratio, the technique of evaluating a separation by measuring the density of a radiograph in the area of a separation and a sound area and obtaining a ratio. The ratio is used to compute the extent of separation through the use of established tables.

Effective (X-ray) energy, the average of the energies of the photons making up the X-ray beam spectrum (higher for the compensated beam).

Half-value layer (HVL), that thickness of a given material which attenuates the beam to 50 per cent of the intensity of the primary beam.

Insulation separation, a laminar separation between layers of asbestos insulation caused by the failure of the bond and movement of the insulation.

Liner-propellant separation, a separation between the thermal insulation and the propellant caused by the failure of the bond and propellant movement (may include laminar cracking of the propellant near the interface).

Penetrameter, drilled hole plaque, wires, or slit block made of material radiographically equivalent to the material being radiographed, usually tests for 1 or 2 per cent of the thickness of the object being radiographed. The penetrameter casts an image on the film and indicates the level of sensitivity achieved.

Peripheral (tangential) radiography, radiography of the peripheral portion of the motor to include case, insulation or liner, or both, and some distance into the propellant.

Polyurethane-rich area, volumes of polyurethane washcoat may occur between cast batches of propellant and in motor areas that have been repaired. These areas are of considerably less density and may appear to be voids or cracks.

Porosity, numerous small voids that are interconnected.

Radiographic sensitivity, the ability of the radiographic technique to demonstrate a given difference in thickness or the presence of a given type defect. The sensitivity may be established by a penetrameter. Per cent sensitivity of the penetrameter is related to that of the material being radiographed.

Star point, point in the propellant bordering the star-shaped perforation and nearest to the motor axis.

Star valley, point in the propellant bordering the star-shaped perforation and farthest from the motor axis.

Thick liner, refers to liner-washcoat bonding agent between the propellant and insulation occurring in thicknesses exceeding design specifications.

Void, a cavity within or on the surface of the propellant.

Web, that portion of the propellant located between the end of perforation fingers and the case.

GAMMA SCINTILLATION SCANNING FOR INSPECTING SOLID ROCKET MOTORS

By Paul E. Underhill[1]

At the request of Commander Smiley, Chairman of the POLARIS/MINUTEMAN/PERSHING Nondestructive Test Committee, we have cooperated with ASTM Committee E-7 on Nondestructive Testing in preparing a report on the development of the scanning technique now used at the Aerojet-General Corp. Sacramento plant to inspect the Polaris missile. The title of the device is GIGI, which stands for Gamma Inspection of the Grain Integrity. This paper presents a brief review of the research and development that went into designing the gamma inspection cubicle now in operation at the Sacramento plant. The parameters involved in the development of this grain inspection system, the analytical approach (see Appendix[2]), and the physical variables encountered will be considered.

Our objective was to develop an automated, gamma scintillation, nondestructive test instrument having good crack sensitivity and capable of supplying numerical information unencumbered by the operator's subjective response (Fig. 1).

The components of this radiographic inspection system: the source, the object under surveillance, the detector, the metering device, and the recorder and data reduction equipment, and the parameters associated with each, are discussed below.

[1] Manager, Instruments and Controls Department, Aerojet-General Nucleonics, San Ramon, Calif.

[2] See p. 90.

Components of System

Source:

The type of source selected to inspect a given motor depends upon many parameters. The first requirement is that the source provide sufficiently energetic electromagnetic radiation to penetrate the material to be examined without damaging it. To calculate the source strength, the number of photons to be counted must be established. Gamma photons pass through the motor under surveillance in a straight line, down the 6 in. of length of lead collimator to interact with the scintillation crystal of the detector. Only these gamma photons give rise to sufficiently energetic pulses to be counted in the metering device.

Let us further examine the source itself. Either cobalt-60 isotopic sources or the more energetic betatron and linear accelerator sources have been used almost exclusively for the inspection of large-diameter rockets. It is important to understand the nature of the radiation originating with each of these types of source. Cobalt-60 decays with two nearly identical gamma photon energies; therefore discrimination against lower energy photons can select accurately only those photons that have traveled through the material and void in a direct source-to-detector line. Both the betatron and linear accelerators bombard a target material with a stream of high-energy electrons. This bombard-

ment creates a radiation spectrum of gamma photons ranging from low energies up to that value equal to the most energetic electron that strikes the target.

cracks were initially limited to film, ion chambers, and scintillation crystals. The detectors for the gamma scintillation inspection device at Sacramento use thallium-activated sodium iodide

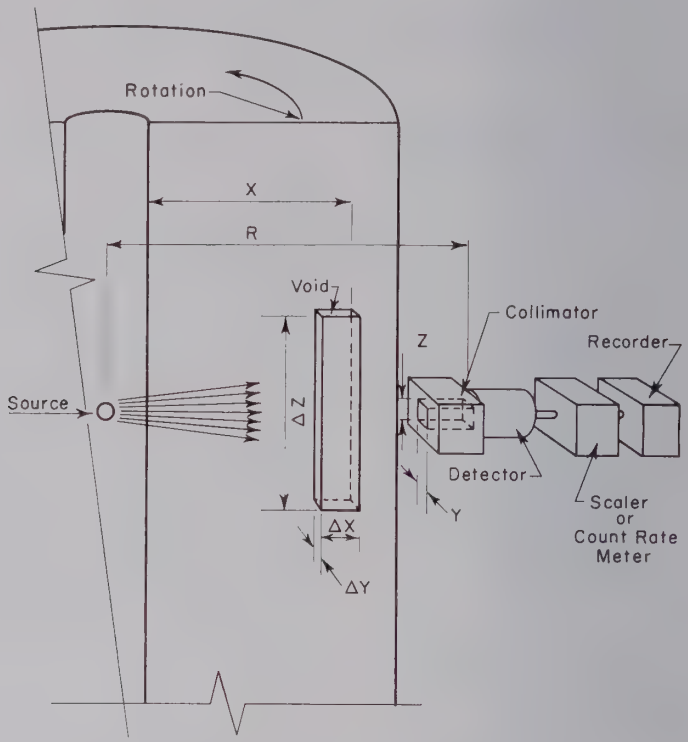

FIG. 1.—Scintillation System.

Object Under Surveillance:

For effective inspection, many physical parameters must be established for each object to be surveyed. The attenuation coefficient for the radiation quality of the source to be used must be determined. The production tolerances of diameter, shell thickness, liner thickness, core configuration, and material composition must all be known.

Detector:

The detection media associated with inspecting solid rocket propellant for

crystals optically coupled to photomultiplier tubes. The volume of sodium iodide crystals exposed in a direct line relationship to the radioactive source is determined by the cross-sectional area and length of the detector collimator. The shape and length of the collimator determine the volume of propellant under surveillance and, in effect, the shape of the beam between the source and crystal.

At this point it would be well to examine the reactions of the gamma photons within the sodium iodide

crystal. These reactions are not precisely defined by any of the theoretical quantum mechanics hypotheses. However, it is known that the wavelength of each energy level of gamma photon can be calculated from the relationship, $E = h\nu$, where ν, the frequency, is equal to the energy of the photon divided by Planck's constant. Keep in mind that in speaking of photons we are speaking of gamma photons. The indiscriminate use of the word "photon," to refer to light, X-rays, and gamma radiation, has often caused confusion. The number of light photons emitted by the crystal is proportional to the energy of the gamma photon that enters the crystal. The wavelength of the light photons emitted from the interaction of the gamma photon with the molecules of the sodium iodide crystal is characteristic of the vibrational mode set up within the crystal lattice, and is independent of the energy of the incident gamma photon. Therefore total light, per absorbed gamma ray photon, is a function of gamma ray wavelength or frequency.

Metering Device:

The instrument used to accumulate the pulses can be either analog (rateameter) or digital (scaler). The Sacramento system uses an amplifier-discriminator circuit ahead of a scaler to provide a mechanism for eliminating pulses from the photomultiplier tube which have originated from multiscattered (low-energy) gamma photons.

Recorder and Data Reduction Equipment:

There are many ways of recording and screening raw data to establish the flaw information. At Sacramento, the digital information is punched onto IBM cards and printed onto IBM printout sheets. Each number recorded represents the total number of gamma photons that have passed through a radial thickness of propellant in $4\frac{1}{2}$ sec. Since the stepped motion is in the direction of the motor axis, the radial thickness remains constant. Therefore, for equal time intervals, changes in the total gamma photons counted for each vertical position are indicative of voids in the propellant. The operator can then examine the columns of numbers to isolate any areas where a 5 per cent change in count exists between adjacent vertical numbers. This is equivalent to a void equal to 1 per cent of the length of material being examined. When first checked out, this equipment exhibited a 0.2 per cent sensitivity. Experience has shown that the tighter specifications are not necessary and allowed a total inspection time for a first-stage Polaris of 4 hr.

PARAMETERS

Aerojet's work with very early rockets showed that a radially oriented crack is the most detrimental type of flaw that can occur within a solid propellant system. These radial cracks can cause uncontrollable large burning surfaces which result in the malfunction of the missile. Spherical voids within the solid propellant do not generally impair the effectiveness of the burning operation until they reach a volume larger than a few cubic inches.

The inspection equipment has been designed to be maximally sensitive to cracks through attention to the following parameters: (1) the stepped axial motion; (2) the scaler-discriminator, pulse-counting technique; (3) the elongated, rectangular shape of the collimator, its long axis parallel to the expected direction of the crack; and (4) confidence in reporting small flaws in the areas inspected. Any compromise of these approaches decreases the sensitivity,

and thus the effectiveness, of the crack inspection technique.

Stepped Axial Motion:

Maximum efficiency in determining a given count rate by any method depends upon accumulating sufficient events to establish statistically the integrity of the section under investigation as compared with a section known to be sound. This, in turn, necessitates being at the specific investigation point long enough to accumulate a statistically significant number of events. Aerojet currently uses the stepped axial motion method in which discrete time interval stops are made to accumulate the amount of data required to achieve statistically a 95% detection confidence level for all voids in the volumes inspected.

The direction of motion becomes of paramount importance with a system designed specifically to detect cracks. From past experience, cracks originating in solid propellant right cylindrical sections have emanated in radial planes oriented nearly parallel to the central axis. Therefore the minimum dimension of the crack is measured perpendicular to its plane in the circumferential direction. To maintain these axially oriented cracks under optimum surveillance, the motion of the detector should be parallel to the central axis of the solid rocket motor as it is at Aerojet's Sacramento inspection facility.

The direction of the motion also affects the ability to interpret the count data accumulated by the detector pickup system. If an inspection scan is made axially along the motor, the plotting of the data obtained will result in a straight, or nearly straight line since, except for flaws, the propellant thickness is essentially constant.

If a circumferential scan is made, the data plot would show a cyclic variation caused by the core shape or by the varying thickness of propellant between the source and detector. It is much easier for an operator or a computer to detect deviations from a straight line than deviations from a relatively complex geometrical function.

The circumferential system designed by another company introduces a seven-harmonic bucking current to compensate for the propellant geometric discontinuity caused by the star points during circumferential inspection. It has been Aerojet's experience that, in practice, the accuracy of this type of bucking current is greatly influenced by very minute deviations in production standards. Slight misalignment of the casting core mandrel, although still within production tolerances, caused deviations in count rate greater than the minimum detectable void which must be observed. Another system attempts to compensate for this by using a dual detector and plotting only the ratio of the current out of the two adjacent ion chambers.

Scaler - Discriminator, Pulse - Counting Technique:

To attain the best void detection sensitivity in solid propellant, an inspection system must be able to count only those gamma photons which have emanated from the source and passed in a straight line through the propellant and collimator opening to the detector. These photons will have maximum energy. By using a scintillation pulse-counting technique with energy discrimination, only these more energetic photons are recorded. The electronic noise and third and fourth scattered radiation (which are degraded gamma photons) are discriminated against in the pulse-counting technique. The desired statistical accuracy is easily obtained by counting the total number of events required for that accuracy. By using a pure current measuring system

the amount of meaningful information is diluted because it is impossible to eliminate completely the degraded undesired spectrum of energy. By using either the pure current or the combined pulse-current system of a count rate-meter, the total numbers are averaged, or rounded out, to yield an integrated, or analog, readout. The averaged readout from a continually moving inspection system is difficult to analyze statistically. The count rate reading taken at any given point on the motor is not due to that point alone, since the integrating systems retain information from the points which the detector has already passed. This effect obscures the dimensions of any void by not indicating that void immediately. The average counting rate is obtained after void intersection, and is retained after passing the void to give a location displacement effect.

Collimator Shape:

Again it should be kept in mind that the maximum sensitivity to cracks is affected by the specific shape and orientation of the collimator. Most effective is an elongated, rectangularly shaped collimator having its long aperture axis along the axial length of the crack. In this way the maximum volume of the flaw and the minimum volume of the non-flaw are included in the inspection volume. Therefore maximum sensitivity is achieved by moving a long, narrow collimator in the most probable direction of the crack.

Confidence of Reporting Small Flaws in Inspected Areas:

A system which has the highest detection confidence for the smallest flaw will be the most effective for establishing the existence of cracks within inspected areas. The system now used by Aerojet has a proven confidence level of 95 per cent. The best sensitivity is not now being required; therefore the inspection time has decreased proportionately to the change in sensitivity.

FUTURE SCANNING SYSTEMS

The trend in scanning systems is toward television presentation of inspected areas coupled with a simplified computer analysis. These methods are closely allied to cineradiographic techniques. The contrast and line resolution are being perfected to make these methods competitive with radiographic techniques.

APPENDIX

ANALYSIS OF CONTINUOUS MOTION INSPECTION

Moving Void (Count Ratemeter for High Count Rate):

One advantage in using a count ratemeter is that a continuously moving mechanical system can be employed. To be practical in this type of system, a high count rate must be used. When the count rate of a NaI(Tl) crystal scintillation detector is above $\sim 5 \times 10^4$ per sec, or an ionization chamber detector is used, the individual pulses overlap each other to a large extent and individual gamma photons cannot be resolved. Thus a pulse integrating circuit, frequently referred to in this field as a count ratemeter circuit, must be used instead of a scaler. This overlap also makes it impossible to use pulse height discrimination as a means of eliminating scattered photons.

It is necessary, therefore, to calculate the adverse effects caused by (1) the count ratemeter, (2) the lack of discrimination, and (3) the loss resulting from the movement of the void during counting.

Some of the important considerations for the calculations are:

Count Ratemeter Circuit.—The standard deviation for a count ratemeter is:[3]

$$\sigma = \sqrt{\frac{I}{2\tau}}$$

Lack of Discrimination Factor B_f.—For a discrimination system counting at I to have the same minimum detectable void as a nondiscriminating system counting at $I_1' + I_1'$ = count rate from unscattered photons (meaningful), I_2' = count rate from scattered photons (containing no void information), and the fraction of meaningful count rate to the standard deviations of the two systems must be equal:

$$\frac{\sigma}{I} = \frac{\sigma'}{I'} \quad \text{or} \quad \frac{\sqrt{\frac{I}{2\tau}}}{I} = \frac{\sqrt{\frac{I_1' + I_2'}{2\tau}}}{I_1'} \quad \ldots (1)$$

During the preliminary evaluation of the Aerojet Gamma Inspection Facility in 1958, experiments roughly analogous to present systems showed $I_2' = 4I_1'$. Solution of Eq 1 gives

$$\frac{I_1'}{I} = 5,$$

or five times as much unscattered information is needed in the nondiscriminating system to overcome the loss of statistical accuracy caused by dilution of the meaningful data by unwanted lower energy photons.

Movement of Void Relative to Detector.—This is illustrated in the diagram below:

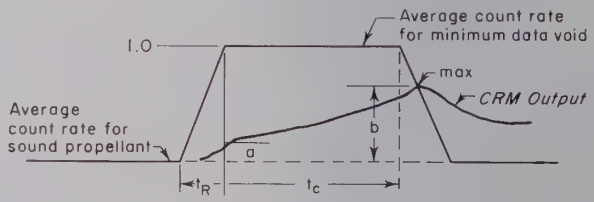

where:

t_R = time required for void to begin entering detector beam until all of the void is within detector beam;

[3] G. Friedlander and J. W. Kennedy, *Nuclear and Radiochemistry*, John Wiley & Sons, Inc. New York, N. Y., 1955, p. 267.

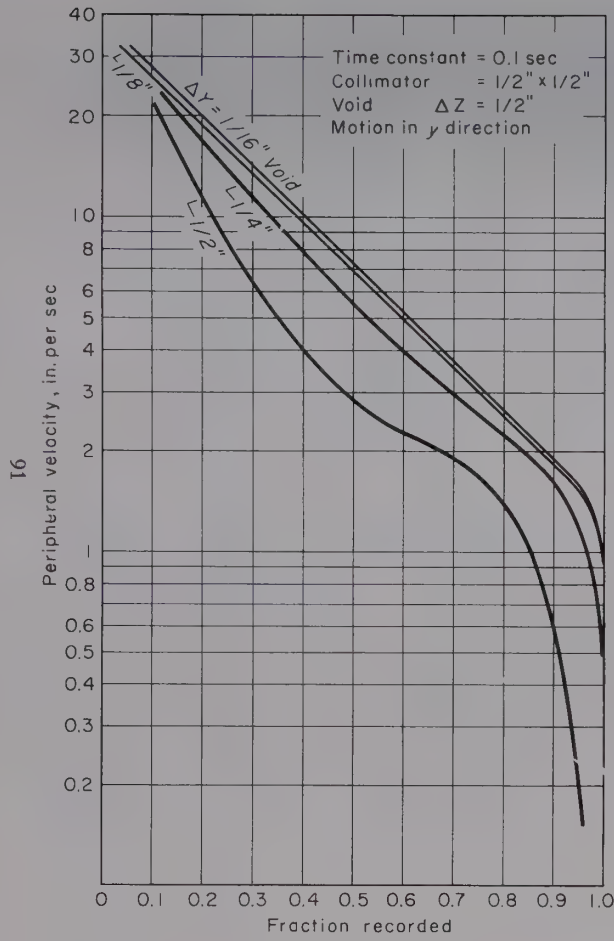

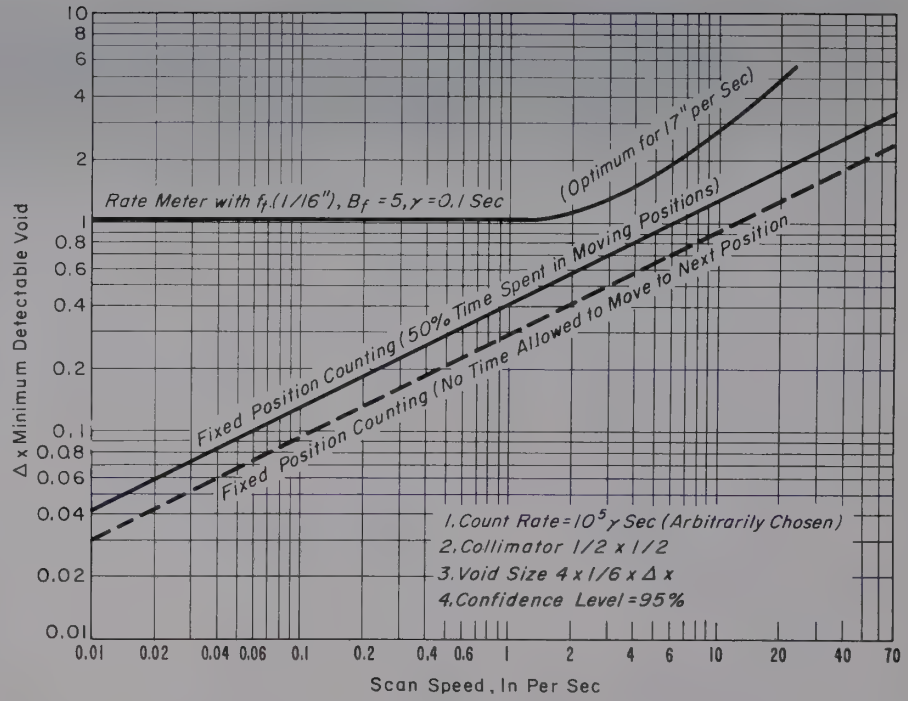
Rate Meter with f_f(1/16"), B_f = 5, γ = 0.1 Sec
(Optimum for 17" per Sec)
Fixed Position Counting (50% Time Spent in Moving Positions)
Fixed Position Counting (No Time Allowed to Move to Next Position)
1. Count Rate = 10^5 γ Sec (Arbitrarily Chosen)
2. Collimator 1/2 x 1/2
3. Void Size 4 x 1/6 x Δ x
4. Confidence Level = 95%
Δ x Minimum Detectable Void
Scan Speed, In Per Sec

FIG. 3.—Comparison of Minimum Detectable Void Versus Scan Speed for Stepped and Continuous Movement.

FIG. 2.—Fractional Change in Count Rate Due to Relative Motion of Detector and Void During Continuous Motion Counting Process.

t_c = time all of void remains in detector beam;
a = value of output from count ratemeter at end of ramp input; and
b = output from count ratemeter at maximum value.

Let $f_R = a/1$, $f_c = (b - a)/(1 - a)$, and $f_t = b/1$, so $f_t = f_R + f_c(1 - f_R)$; then the differential equations are:

$$f_R = \frac{\tau}{t_r}(e^{-t_R/\tau} - 1) + 1, \quad \text{and}$$

$$f_c = 1 - e^{-t_c/\tau}.$$

Note that t_R and t_c are functions of scan velocity, collimator size (in the direction of motion), void size (in direction of motion), and ratemeter time constant. The function f_t is therefore soluble. Typical solutions can be seen on Fig. 2.

Derivation of Ramp Formula.—To establish the transient response of a count ratemeter to a ramp input, consider first the ratemeter circuit:

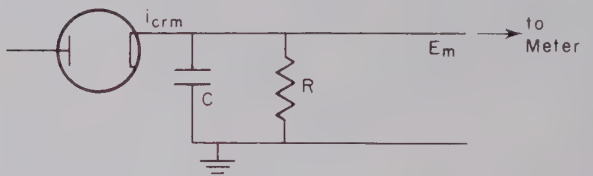

where $\tau = RC$. As an electron current proportional to the number of photons detected passes through the vacuum diode, the capacitor, C, is charged. The electrical potential that appears at the ratemeter is E. From Ohm's law, the voltage, E, equals the resistance, R, times the current from the vacuum diode minus the current to charge the capacitor, so

$$E = R\left[i_{crm} - c\frac{dE}{dt_R}\right]$$

In the case of a ramp count rate the current, i_{crm}, into the vacuum diode is equal to a constant times the time; so, by substitution,

$$E = R\left[Kt_R - c\frac{dE}{dt_R}\right]$$

This differential equation represents the response of the count ratemeter, and therefore is proportional to the indicated count rate.

The solution to this differential equation is

$$E = RK(RC\,e^{-t_R/RC} + t_R - RC)$$

To verify this solution for the differential equation, this solution can be differentiated and substituted back into the original equation by rearranging the solution,

$$E = R^2KC\,e^{-t_R/RC} + t_RRK = R^2KC$$

The differential is:

$$\frac{dE}{dt_R} = \frac{R^2KC\,e^{-t_R/RC}}{RC} + RK$$

so, by substituting into the original differential equation,

$$E = RKt_R - RC\left(-\frac{R^2KC\,e^{-t_R/RC}}{RC} + RK\right)$$

And since

$$E = R^2KC\,e^{-t_R/RC} + RKt_R - R^2KC,$$

then

$$R^2KC\,e^{-t_R/RC} + RKt_R - R^2KC = RKt_R + R^2KC\,e^{-t_R/RC} + R^2KC;\ 0 = 0$$

thus this solution is correct.

The ideal response (that is, without a count rate circuit) to a ramp input, Kt, would be $E_0 = RKt$. Therefore, to find f_R, which is the fraction of the ideal that is indicated by the count ratemeter,

$$f_R = \frac{E(\text{ratemeter})}{E(\text{ideal})} = \frac{R^2CK\,e^{-t_R/RC} + RKt_R - R^2KC}{RKt_R},$$

$$f_R = \frac{RC\,e^{-t_R/RC}}{t_R} + 1 = \frac{RC}{t_R}$$

Now, since $\tau = RC$, then

$$f_R = \frac{\tau}{t_R}\left(e^{-t_R/\tau} - 1\right) + 1$$

The differential equation for the response of the count ratemeter circuit during the constant input portion is as follows (the same circuit diagram is used as in the ramp equation derivation, except that here the current, i_{crm}, is a constant, k):

$$E = R\left(i - C\frac{dE}{dt_c}\right.$$

Let i_{crm} equal k. The solution to this differential equation is

$$E = Rk\left(i - e^{-t_c/Rc}\right)$$

Rearranging $E = Ek - Rk\ e^{-t_c/Rc}$ and differentiating $\frac{dE}{dt_c} = \frac{Rk}{Rc}\ e^{-t_c/Rc}$

and substituting in the original differential equation

$$E = R(k - c)\left(\frac{Rk}{Rc}e^{-t_c/Rc}\right) = Rk - Rk\ e^{-t_c/Rc}$$

from the original assumed solution or

$$Rk = Rk\ e^{-t_c/Rc} = Rk - Rk\ e^{-t_c/Rc},$$

Thus, the above solution, E, is correct.

In the ideal case (that is, where there is no ratemeter circuit),

$$E = Rk, \text{ so } (f_c) = \frac{E \text{ (from count rate circuit)}}{E \text{ (from ideal)}}$$

$$= \frac{Rk - Rk\ e^{-t_c/Rc}}{Rk} = 1 - e^{-t_c/Rc}$$

and

$$Rc = (f_c) = 1 - e^{-t_c/\tau}$$

So now a complete equation can be written for the moving void, since

$$\Delta x = \frac{\Delta I}{I}\left(\frac{Y}{\Delta y}\right)\left(\frac{1}{\mu}\right).$$

The moving void function is such that to maintain the same Δx, the observed ΔI at the count ratemeter must be increased by multiplying by

$$\frac{1}{f_t} \text{ (since } f_t \leqq 1),$$

so

$$\Delta x = \frac{1}{f_t}\left(\frac{\Delta I}{I}\right)\left(\frac{Y}{\Delta y}\right)\left(\frac{I}{\mu}\right) \ldots\ldots (2)$$

The count ratemeter standard deviation $\sigma = \sqrt{\frac{I}{2\tau}}$, and the minimum detectable void is 2σ. So substituting in Eq 2, $2\sqrt{\frac{I}{2\tau}}$ for ΔI,

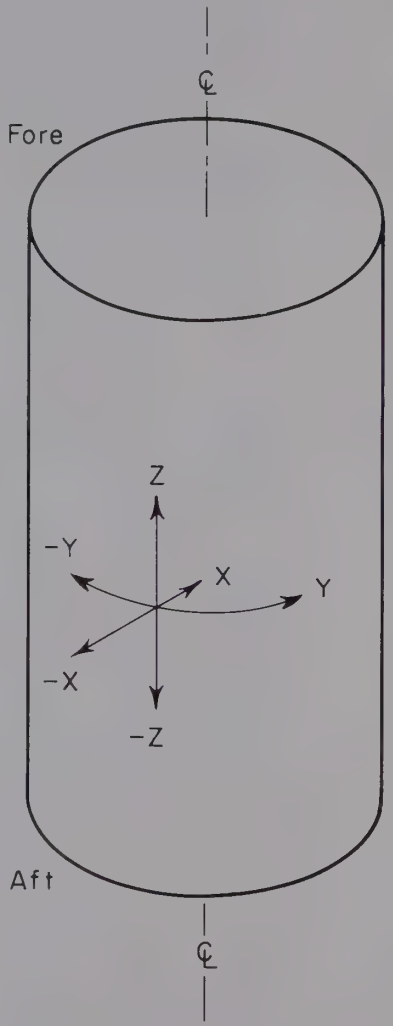

FIG. 4.—Titles for Rocket Motor Coordinate System.

Radial axis, X-X; circumferential axis, Y-Y; axial axis, Z-Z.

$$\Delta x = \frac{1}{f_t}\left(\frac{2\sqrt{\frac{I}{2\tau}}}{I}\right)\left(\frac{Y}{\Delta y}\right)\left(\frac{1}{\mu}\right)$$

$$\Delta x = \frac{1}{f_t}\sqrt{\frac{2}{\tau I}}\left(\frac{Y}{\Delta y}\right)\left(\frac{1}{\mu}\right)$$

and from the nondiscriminator factor, B_f, for the same Δx, the observed count rate must be reduced by dividing I by B_f, giving

$$\Delta x = \frac{1}{f_t}\sqrt{\frac{2B_f}{\tau I}}\left(\frac{Y}{\Delta y}\right)\left(\frac{1}{\mu}\right) \quad \ldots\ldots (3)$$

With the equation of static inspection conditions and Eq 3 a comparison between ultimate theoretical minimum detectable voids at 95 per cent confidence can be made.

A plot of typical values of the static condition combined with Eq 3 at the appropriate counting rates can be seen in Fig. 2 (the count ratemeter time constant, τ, is optimized for a 17 in. per sec scan speed).

It can be seen at any given count rate that, as the scanning speed is reduced, the moving void (count ratemeter) quickly levels off to a minimum detectable void, and any further reduction has only limited value. This limitation does not hold for the fixed counting systems, although the fixed counting system is limited to counting rates below approximately 5×10^4 per sec, if NaI(Tl) crystals are used.

A cross plot showing minimum detectable void versus scanning speed is given in Fig. 3 for the two types of detection systems. Figure 4 supplies titles for the rocket motor coordinate system discussed in this paper.

NONDESTRUCTIVE TESTING OF HIGH-STRENGTH STEEL ROCKET MOTOR CASES*

By J. A. Hendron[1]

Proportionately, the wall thickness of a hen's egg, compared to its outside diameter, is six times as great as the same comparative dimensions on one of the solid rocket motors currently in production. This fact proves nothing in terms of material strength, but it does serve to illustrate the degree of structural perfection demanded in high-strength steel rocket motor cases.

A crack $\frac{1}{32}$ in. long in an eggshell is of no consequence. A crack of the same length in a rocket motor case can cause disastrous failure for a million dollar missile. Because of this, nondestructive testing has had to meet exacting demands in rocket case manufacturing.

Established nondestructive test methods can meet these demands for motors of current design. The main challenge to be met is improvement of existing techniques and the quality of effort from inspection personnel. The role of the inspector assumes new importance when the involuntary blinking of his eyelids can result in a million dollar failure or a military disaster. And this could happen. Consider how easily a distracted inspector could miss the momentary flash of a small defect indication on the oscilloscope screen of an A-scan ultrasonic unit. Or think how easily a tired inspector's eyes can pass over a faint X-ray image of a $\frac{1}{32}$ in. crack without seeing it.

Perfection in manufacturing is the obvious goal, but since this cannot be achieved absolutely, nondestructive testing must exercise the highest degree of reliability that can be obtained from personnel, equipment, and techniques.

Few high-strength steel rocket motor cases fail in firing because of defects in chamber fabrication. Functional chamber failures are generally due to defective internal insulation or to abnormal pressures created by accidentally increased burning surfaces of propellant. Few cases fail in firing because of structural defects since prooftesting is done at hydrostatic pressures higher than firing pressures. In this sometimes destructive test, a serious defect reveals itself promptly, generally with total loss of the chamber.

Nondestructive testing must find such defects before the hydrotest does. It is not uncommon for costs to exceed $25,000 for large rocket cases by the time they reach hydrotest.

Examples of defects that have caused hydrotest failure illustrate the need for vigilant nondestructive testing.

A prior crack $\frac{1}{32}$ in. long initiated a fracture in a brittle manner during hydrotest in the heat-affected zone of the girth weld of a chamber with a 0.180-in. wall (Fig. 1). The crack propagated in full shear at the speed of sound, resulting in typical total destruction of the chamber. This destruction could have been prevented by closer attention to the X-ray in which the image of the crack was visible.

Another failure due to inadequate

---

* See also "Nondestructive Testing of Solid Propellant Missile Motors" by Frank C. Hund, p. 62.

[1] Aerojet-General Corp., Sacramento, Calif.

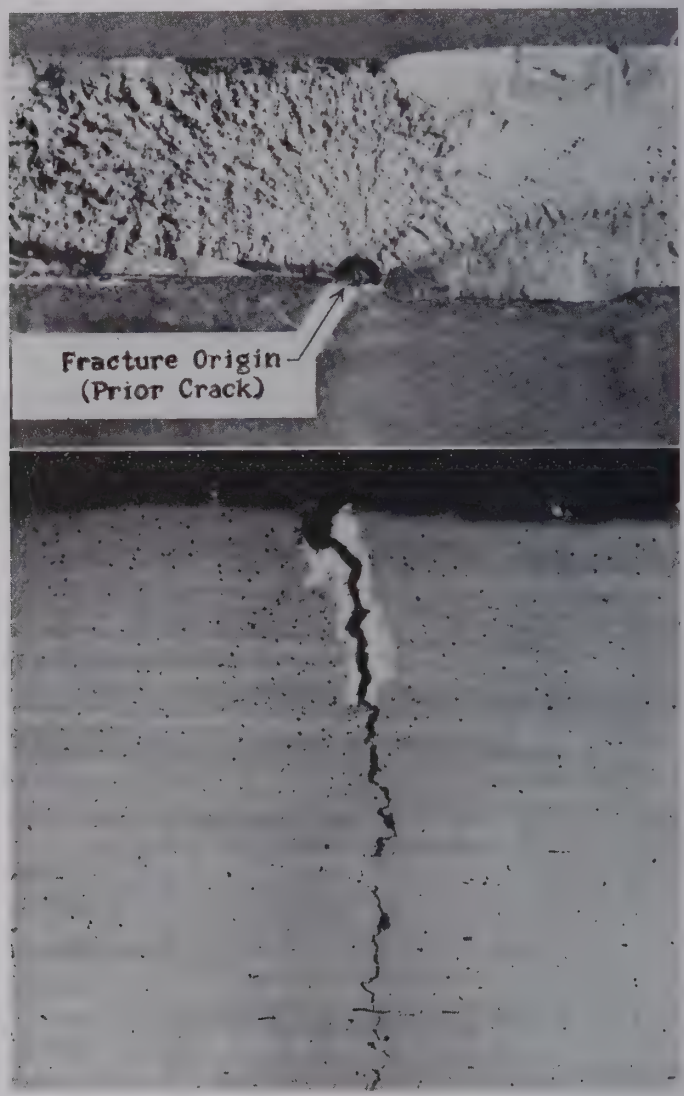

(*a*) Fracture origin.
(*b*) Cross-section of fracture origin showing oxidation which establishes that the crack existed prior to heat treatment. M255 material, alkaline chromate etch (×100).

FIG. 1.—A Prior Crack $\frac{1}{32}$ in. Long That Caused Chamber Failure.

nondestructive testing is illustrated in Fig. 2. A hot crack $\frac{1}{16}$ by $\frac{3}{32}$ in. in size was generated during welding. There are two basic reasons for this crack not being detected: (1) the X-rays were made with excessively high kilovoltage in order to reduce exposure time, resulting in a gray film with low contrast; and (2) the magnetic particle inspection was done with prods and dry magnetic powder. The latter method, which is adequate for many industrial inspections, does not provide sufficient sensitivity for rocket chamber inspection. The crack

(*a*) Fracture origin $\frac{1}{16}$ by $\frac{3}{32}$ in.; arrow shows location of the origin at the center girth weld.
(*b*) Chamber following failure resulting from prior crack; arrow shows point of origin.

FIG. 2.—Failure Caused by an Undetected Hot Crack Generated During Welding.

would have been detected by fluorescent magnetic particles suspended in oil and the use of currently available magnetic particle inspection equipment specifically designed for rocket chambers. Investment in either the proper X-ray unit or magnetic particle inspection unit would not have exceeded the cost of this one failure.

A failure that could have been prevented by the use of a microcaliper is shown in Fig. 3. Ultrasonic thickness measurement could prevent such failure if the underthickness condition which initiated failure had occurred in a part of the chamber where calipers could not be used. The cause of failure was simply that available inspection techniques were

not applied. The part had been overmachined, and the needed thickness check was not done.

Lack of penetration on long seam welds, illustrated in Fig. 4, presented a temporary nondestructive testing problem. Heat and shrinkage pressure caused semi-fusion of the unpenetrated weld faces. This fusion was so nearly complete that its line could not be detected by X-ray, magnetic particle inspection, eddy current, or penetrant. Because there was no evidence of the lack of penetration, the chamber was hydrotested and failed. The manufacturer solved the problem by etching the back of the weld with ammonium persulfate. The etch showed the weld outline where penetration was complete. Where the weld outline did not show, the lack of penetration was indicated.

An accidental arc strike (Fig. 5) caused failure in another case. The inspector assumed that the defect was purely a surface condition. He was not aware that this spot on the chamber wall had been melted halfway through, and that the mass quench resulting from the adjacent cold material had caused a minute, but disastrous, change in microstructure.

The foregoing few examples are past history. We now have the benefit of the lessons learned from them. In order to prevent repetition of such oversights in nondestructive testing, a master plan of nondestructive testing as shown in Fig. 6 is needed for each design of rocket motor. As these lessons are learned, the cure must be immediately incorporated into the master plan. This prevents repetition as memory fades or when personnel changes.

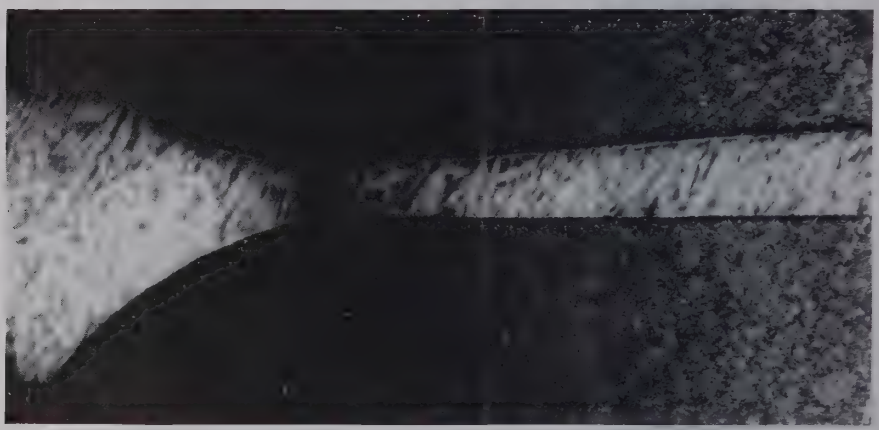

FIG. 3.—Fracture in Boss-Weld Area Because of Underthickness Resulting from Overmachining.

NONDESTRUCTIVE TESTING INSPECTION PLAN FOR STEEL ROCKET MOTOR CASES

Steel Billets:

Although it is not always possible for the purchaser of steel sheet and plate to specify in-process inspection of steel billets, there is an advantage in having nondestructive testing performed on the billets. Magnetic particle inspection can detect cracks and pipes so that billets can be adequately cropped prior to rolling. This will prevent laps and string-

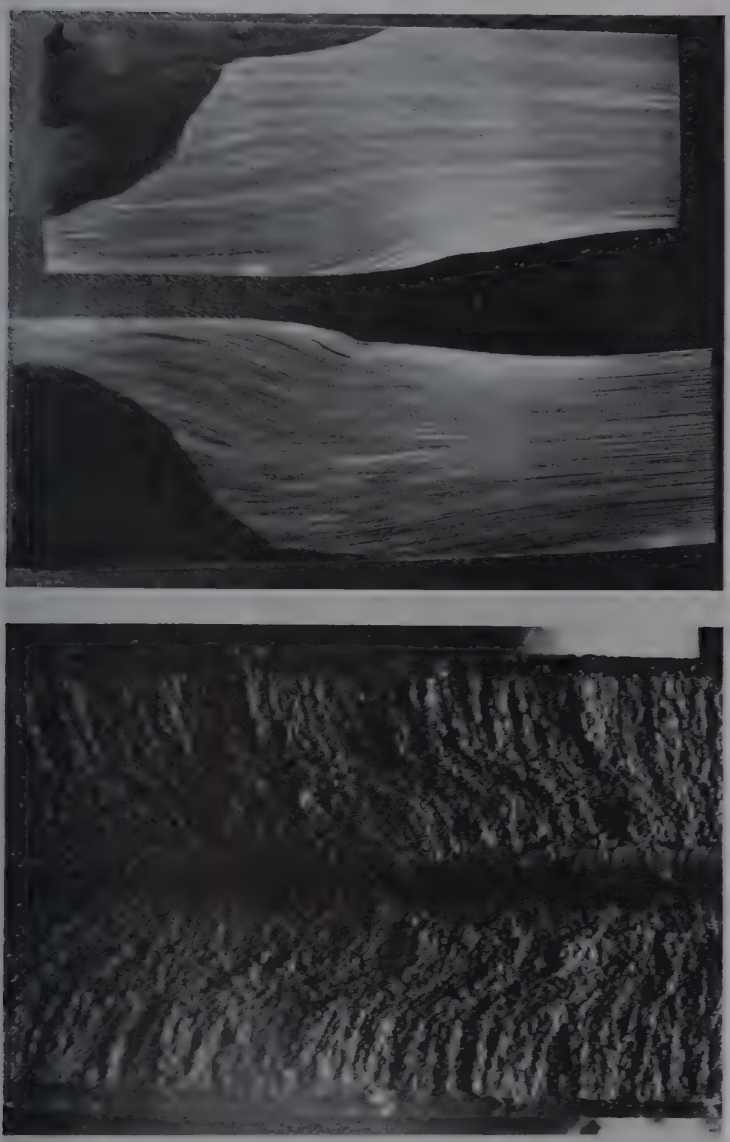

(*a*) Etched cross-section.
(*b*) Fracture faces showing lack-of-penetration areas along center line. Note semi-fused surfaces where weld had not penetrated.

FIG. 4.—Weld Which Failed in Hydrotest Because of Lack of Penetration.

(*a*) Photograph of arc strike on chamber wall surface. The arc strike was the point of origin of chamber failure in hydrotest.

(*b*) Etched cross-section through arc strike at point of fracture origin. Dark semicircle indicates depth to which the material was melted.

FIG. 5.—Failure Caused by Accidental Arc Strike.

ers from being rolled into the plate. Ultrasonic inspection of billets can ensure that internal voids and inclusions have been cropped from the billet. This will prevent laminar type defects.

Rolled Plate or Sheet:

Experience has established that magnetic particle inspection of plate for rocket chambers is economically advisable. As the tensile strength of steel

plate is increased, there appears to be a greater tendency for cracking. This inspection can be readily accomplished by the use of clamps on the ends and sides of the plate to create a magnetic field by passing a current through the plate. Two forms of ultrasonics should be used on the plate prior to further processing: thickness measurements should be taken at the intersections of a square grid pattern to establish thickness requirements throughout the plate, while shear wave ultrasonic contact scanning can detect laminations and inclusions as well as surface cracks. This inspection can be done quickly and inexpensively by scanning with an oscillating motion of the shear wave crystal along lines approximately 2 ft apart. These parallel lines should run in both directions of the plate in order to ensure coverage for defects oriented in all directions.

Formed Heads:

Following the forming of dome-shaped heads for chambers, magnetic particle inspection of the entire inside and outside surfaces should be performed. Thickness measurement using resonant ultrasonics is also imperative.

Forgings:

After cleanup of forgings, magnetic particle inspection is necessary in order to locate all surface defects. Immersion ultrasonic inspection is required in a minimum of two directions in order to ensure the absence of internal defects. Some activities have required X-ray inspection of forgings. In general, X-ray of forgings is an unnecessary expenditure and an unfruitful inspection. Defects within forgings are generally oriented in such a manner that they cannot be detected by X-ray. In such cases reliance on X-ray may be misleading and can result in failure if the inspection is not supported by ultrasonics.

Machined Forgings:

Because ultrasonic inspection has been performed on the cleaned forgings,

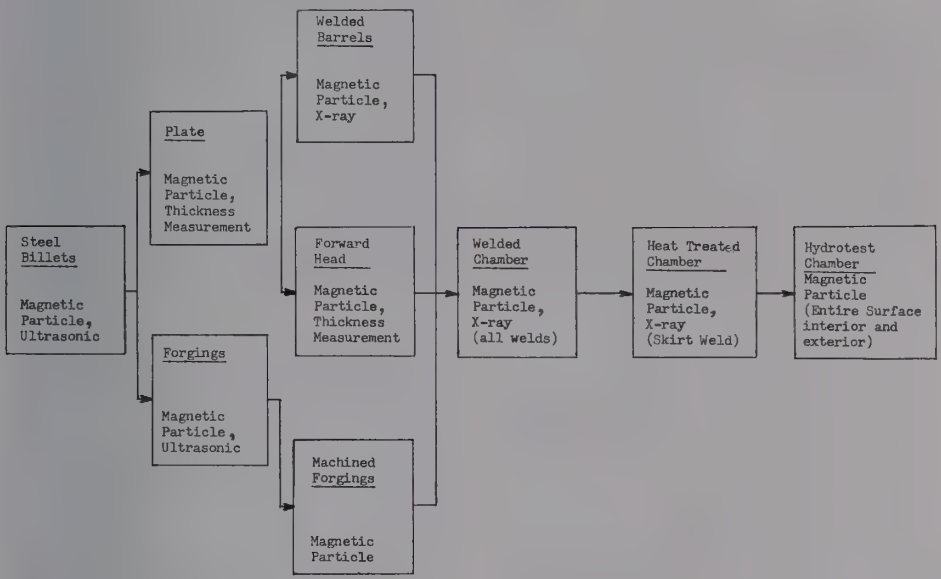

FIG. 6.—Nondestructive Testing Master Plan Flow Chart for High-Strength Steel Rocket Motor Cases.

the absence of significant internal defects is ensured. Machining will not induce internal defects and no further internal inspection is needed. Magnetic particle inspection should be performed on the machined surfaces of the forging to detect defects which may have occurred as a result of relief of forging stresses during machining, or overstressing of points on the surface as a result of machining.

Chambers and Closures After Welding (Before Heat Treatment):

As barrel sections are welded, the longitudinal weld should be both magnetically inspected and X-rayed. Gross defects which would cause absolute rejection of components are then detected early in processing so that defective material is discarded before being included in a more expensive assembly. Defects in the welds, which can be repaired, can be taken care of much more easily in the barrel stages than after the barrel has been welded into a chamber. This rule of checking welds as the size of the assembly increases should be followed.

X-ray with fine-grain film, such as Eastman M, Ansco B, or DuPont 510, is essential for the definition needed for interpretation of rocket motor case weldments. Because most thicknesses involved do not call for kilovoltage as high as 200 kv, the use of screens does not improve the X-ray. The lowest possible kilovoltage which will provide the required density should be used, otherwise the resulting loss of contrast may cause defects to be missed. Many problems of X-ray interpretation in the rocket industry could have been prevented if this rule had been observed.

Magnetic particle inspection of the entire surface of the rocket chamber, both inside and out, has been found to be essential. This inspection cannot be done adequately with the magnetic prod method. Also, magnetic prods have resulted in failure of chambers due to small arc strikes. Equipment is now available which can magnetize an entire chamber in both circumferential and longitudinal directions. Coverage of the entire surfaces with magnetization in both these directions is necessary in order to ensure absence of all surface defects. The use of large equipment which can provide over-all chamber magnetization is highly recommended to eliminate the possibility of human error which results from the use of small magnetic fields manually applied. The larger equipment, provided with motor drive and automatic spraying of magnetic particle fluids, also ensures even distribution of fluids with controlled particle concentrations, and considerable reduction in man-hours expended on inspection.

Fluorescent magnetic particles suspended in water-white, odor-free kerosene give the greatest sensitivity for detection of minute defects. Very small cracks are more easily detected as fluorescent indications in a dark field than they would be if nonfluorescent material were used on a lighted field. Care should be taken to provide good darkening of the area and absence of light reflections during visual scanning for defects. Magnetic particle suspension should be carefully maintained just above the minimum concentration level for adequate indication of defects. If the concentration becomes too high, the background retains too much fluorescence and inhibits detection of small defects. Degreasing of chamber surfaces is necessary prior to the magnetic inspection because oil will fluoresce and could mask indications.

The area in which magnetic particle inspection is done should be kept clean and free of airborne lint and dust. Small

particles of foreign materials on the surface of chambers cause collection of fluorescent particles and decrease contrast between indications and background. Use of steel handling fixtures on the chambers should be avoided because of the magnetic writing they cause. Time spent in ensuring that magnetic writing indications are not defect indications is one cause of unnecessarily slow inspection. When many fine magnetic writing lines occur on a chamber surface, an inspector could assume that a defect indication is one of these lines; this could result in an undetected defect.

The combination of X-ray and magnetic particle inspection has been sufficient for detection of the typical flaws that cause hydrotest failure of chambers. Highly refined ultrasonic equipment has been developed for the inspection of rocket chamber welds, but it is not currently in use. It was found that X-ray and magnetic particle inspection together were capable of finding more than ultrasonics could show. It was also found that ultrasonics gave spurious indications as a result of the differences in grain structure within welds. No defects should be undetectable with X-ray and magnetic particle inspection, with the exception of underbead cracks parallel to the surface of the weld. The existence of this unusual type of defect in careful chamber welding has never been apparent.

Chambers and Closures After Heat Treatment:

Magnetic particle inspection of chambers and closures following heat treatment is imperative. It has been shown that it is necessary to inspect the entire chamber surface with magnetic particle inspection. X-ray of welds is required after heat treatment on some projects, usually at the request of the customer. Results to date have shown that this additional X-ray is not necessary. Defects detected after heat treatment have been defects connected to the surface so that they can be detected by magnetic particle inspection. The requirement sometimes imposed by the customer for X-ray is based on the assumption that internal defects could propagate during heat treatment without connection to the surface.

Chamber with Skirts Welded:

As a rule, stub-skirts are welded to a chamber prior to heat treatment. After heat treatment, skirts are then welded to the stub-skirt so that the stub-skirt-to-chamber weld is heat treated, but the skirt is not. Dimensional control on skirts makes this necessary. The skirt-to-stub-skirt weld is generally thin, and a certain amount of lack of penetration has often been permitted. If it is possible to obtain full penetration of this weld, it should be done in order to improve inspection. This weld is necessarily X-rayed, and if a line of lack of penetration remains, it results in an X-ray which is difficult to interpret. The lack of penetration is a stress-riser for the propagation of cracks, and such cracks may not be observed over the lack-of-penetration image on the film. Porosity and inclusions in this weld should be interpreted with greater tolerance than on the pressure welds of the chamber. Magnetic particle inspection is necessary on this weld also.

Chambers and Closures Following Hydrostatic Pressure Test:

Most activities require that rocket motor cases receive more than one cycle of hydrotest. Because some chambers have failed in the second cycle of hydrotest as a result of cracks initiated during the first cycle, it is economically advised that magnetic particle inspection be

done following each hydrotest cycle. X-rays have been made at this time as a customer requirement in some projects, but their value has not yet been established. Magnetic particle inspection should be sufficient. Following the final hydrotest, magnetic particle inspection is imperative over all surfaces of the chamber, its welds, and its attachments. This inspection must be done with the most critical care. Since some cracks have been found to initiate, but not propagate, during the last intended hydrotest, it would be possible for a chamber to fail during firing if these cracks are not detected.

Closure Bolts:

The destructive tests required on materials used in the manufacture of high-strength bolts give good assurance of the absence of all defects other than those that can be detected by careful magnetic particle inspection. It is common for bolt manufacturers to repeat this inspection several times during the processing of bolts. This repetition is for the manufacturer's benefit. The reliability requirement for closure bolts can be satisfied with one magnetic particle test using magnetic fields in both circumferential and longitudinal directions. This test should be done following the last process in the manufacture of the bolts, but before plating. Although magnetic particle inspection over thin plating surfaces is effective, it is considered more sensitive to minute defects on the unplated surface. The plating process has not induced defects of a nature which cannot be detected by magnetic particle inspection. The only serious degradation in such bolts, as a result of plating, has been hydrogen embrittlement for which an adequate nondestructive test has not yet been developed.

SUMMARY

Adherence to the nondestructive tests described will result in detection of the types of prior defects which have resulted in rocket case failure.

There remains an area of nondestructive testing which needs further development. A test is needed to indicate incipient failure in chambers free of structural defects. There have been a number of hydrotest failures in some projects which are known to have initiated in steel with no detectable defect, even at a microscopic level.

Experiments have indicated some degree of difference in the electrical conductivity between these failed chambers and those that were successful. To date, no manufacturer of eddy current equipment has fully exploited the potential for positive eddy current inspection on rocket motor cases of high tensile strength. Refinement of the eddy current technique for this purpose is one of the opportunities of the future.

Audiosonic inspection, another infant science being explored on a small scale, may also contribute to greater rocket case reliability. As better methods for material quality assurance are developed, the inert weight of rockets can be reduced. Development of new tests is strongly urged.

INFRARED NONDESTRUCTIVE TESTING OF GLASS FILAMENT-WOUND ROCKET MOTOR CASES*

By Frederick E. Alzofon,[1] Lester E. Florant,[1] Richard K. Ronald,[1] Marvin J. Vann,[1] and Julian E. Fitzgerald[1]

Synopsis

A description of experimental and theoretical studies leading to the demonstration of the feasibility of flaw detection in glass filament-wound rocket motor cases, using infrared scanning, is presented. The importance of selecting the best method of heating the specimen in order better to improve the information derived from observation is emphasized. Sources of error are reviewed. The apparatus, measurement techniques, and experimental results are described.

The high cost of modern weapon and satellite systems and the consequent exacting demands for reliability have led to increased use of nondestructive testing. The development of many kinds of structural materials and techniques has made it imperative that new nondestructive testing methods be devised.

One method of nondestructive testing which has recently appeared promising, especially to fill a need for which X-rays and ultrasonic testing do not appear adequate, is infrared nondestructive testing.

The penetrating power of X-rays makes this radiation a reasonable choice for testing the integrity of structural materials. On the other hand, the use of a highly penetrating radiation may cause some kinds of flaws (such as two substances that are in optical contact, but which are not bonded) to escape detection.

Ultrasonic techniques offer a means of flaw detection which is not as energetic as X-rays (and can detect unbonds), but there is difficulty in coupling an ultrasonic transducer to some substances. Moreover an ultrasonic disturbance may be strongly damped in organic materials, as in the epoxy resins used in glass filament-wound pressure vessels.

On the other hand, heat can penetrate any substance, even organic materials. Any lack of integrity in a specimen should generate a variation in the heat current conducted through the specimen; this variation in heat current conceivably could be detected by sensing a variation in the infrared radiation emitted at the surface of the structure. This is the principle on which infrared nondestructive testing is based.

Although in conception this method of testing is straightforward enough, several difficulties arise in attempting a practical realization of the principle. Any variation in the emissivity of the specimen surface obscures the information de-

* This work was supported by Navy Contract NOw 63-0050-c.

[1] Lockheed Missiles and Space Co., Sunnyvale, Calif.

livered to that surface from its interior. If the specimen should be a composite structure, the interfaces between materials composing the structure may give rise to spurious signals. Complex surface configurations may complicate interpretation of the data. In transient specimen heating, the attenuation of the signal is very great, with corresponding loss of information.

Theoretical evaluation of the factors influencing infrared detection of flaws is of doubtful value since so little is known of these factors. It is far more desirable to conduct an experimental feasibility study; the results of such a study are described in the present paper.

The consequences of the choice of various methods of heating the specimen will be discussed first. The magnitude of the effects expected on the basis of the heating method will be estimated and applied to determining the causes of error in the observations. The infrared scanning system will be briefly described, followed by a discussion of some of the experimental results.

METHODS OF SPECIMEN HEATING

The method selected for specimen heating is of paramount importance in infrared nondestructive testing since it determines the kind of information that can be derived from heat current signals.

Heating methods can be classified into two broad divisions characterized by the behavior of the temperature as a function of time at the point of observation: *transient* and *steady state* methods of heating (or cooling). As implied by the terms, in the first the temperature varies with time, while in the second, temperature does not vary with time. Further subdivision of these methods of heating (cooling) may be made on the basis of the spatial distribution of the heating (cooling) pattern.

At present, simple spatial distributions are commonly used. For example, in transient heating the heat may be injected over a small circular area at the surface of the specimen which is then allowed to cool into ambient conditions. In the heat soak method of heating (which is, by our classification, a transient kind of heating) the specimen is simply placed in an environment at a constant temperature until equilibrium is reached and then allowed to cool into the ambient conditions. In steady state heating, the spatial distribution is often chosen to provide a uniform heat current over the region of observation; flat plates, for example, may be heated to a constant temperature on one side while the other side is allowed to cool by radiation.

It is important to note that the spatial distribution may be allowed to vary, even in the latter case described, provided the rate of variation is not so large as that expected from the presence of flaws in the interior of the specimen.

The relative merits of the two methods of heating will be considered in the next section.

TRANSIENT VERSUS STEADY STATE HEATING

In view of the complex configurations which specimens may assume, as well as the nonlinear boundary conditions that may exist, it is not advisable to attempt a general evaluation of the transient and steady state heating conditions. For a description of a general method of analysis suited to the purpose at hand, the reader is referred to a recent paper by one of the authors.[2]

For the purpose of obtaining insight into some of the simpler aspects of the two methods of heating, which have bearing on the practicability of their

[2] Frederick E. Alzofon, "Retardation and Diffraction Aspects of the Conduction of Heat in Solids," *American Journal of Physics*, Vol. 30, 1962, p. 285.

use, we now consider two point scoures in an infinite medium and enquire as to the attenuation of the difference signal from these sources.

Superposition of two transient pulses at locations not far removed from one another is represented by

$$\delta_t = \left| \frac{e^{-r_1^2/4\kappa t}}{(\pi\kappa t)^{3/2}} - \frac{e^{-r_2^2/4\kappa t}}{(\pi\kappa t)^{3/2}} \right| \quad \ldots\ldots (1)$$

In Eq 1, r_1 and r_2 represent the separation of the sources from the point of observation, t the time interval, and κ the diffusivity of the specimen. A difference is used in Eq 1 since the testing method detects gradients. Now letting R denote the distance of a point midway between the sources, from the point of observation, and located a distance a from each source, and θ the angle between the direction of the segment R and the line joining the sources, one finds:

$$\delta_t \cong \frac{2 \exp\left[- \frac{R^2 + a^2 \cos^2\theta}{4\kappa t} \right]}{(\pi\kappa t)^{3/2}} \left| \sinh\left(\frac{aR\cos\theta}{2\kappa t} \right) \right| \quad \ldots (2)$$

The quantity δ_t attains a maximum value at a fixed point of observation approximately at the time $t_m \sim R^2/6\kappa$, while for a fixed time the magnitude of δ_t is rapidly damped with increase of R. That is, there appears to be an optimum time for information retrieval from a thermal gradient pulse, and the magnitude of the signal attenuates rapidly with increasing distance from the sources.

The latter conclusions are essentially in agreement with experimental results found by organizations engaged in the development of infrared nondestructive testing.[3,4]

On the other hand, superposition of two static point sources

$$\delta = \left| \frac{1}{r_1} - \frac{1}{r_2} \right| \quad \ldots\ldots (3)$$

$$\delta_s \cong \left| \frac{2a\cos\theta}{R^2} \right| \quad \ldots\ldots (4)$$

leads to the conclusion that the attenuation of the signal is much less rapid than for the transient case, and there is no restriction on the time of observation.

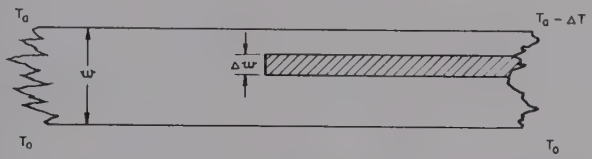

FIG. 1.—Semi-Infinite Slab Embedded in an Infinite Slab.

With the latter result in mind, the steady state heating method will be the only one considered in this study. Several other features recommend this method for the use of industry:

1. The scanning speed is not limited by the speed of response of the solid to a thermal pulse.

2. Data obtained from repeated observations should be repetitive and hence can be compared with one another easily; this would serve to isolate variability of test conditions.

---

[3] Maxwell A. Kerr, "Non-Destructive Bonding Flaw Detection Using Pulsed Infrared Energy," Perkin-Elmer Corp., Electro-Optical Division, *Technical Report 5746*, Quarterly Report for June 1960 to August 1960.

[4] "Feasibility Study of a Non-Destructive Testing Infrared Inspection System for Bonding Flaw Detection," Perkin-Elmer Corp., Electro-Optical Division, *Technical Report 5959, Interim Report No. 2*, November 1960 to April 1961.

3. The analysis of expected temperature variations is greatly simplified.

In the following section some of the simpler aspects of steady state heating analysis will be explored.

DETECTION OF A SEMI-INFINITE THIN INCLUSION

The magnitude of the temperature difference to be expected in the detection of flaws due to solid inclusions may be estimated by consideration of a semi-infinite slab embedded in an infinite slab (Fig. 1). The information indicating the presence of a flaw in this case is taken to be the difference of surface temperatures T_a and $T_a - \Delta T$ at infinity, that is, ΔT. The gradient of the temperature over the edge of the flaw is not under consideration here.

Assuming Newton's law of cooling to hold, it is possible to show that the temperature T_a is given by

$$1 - \frac{T_a}{T_0} = \frac{Aw/K}{1 + Aw/K}\left(1 - \frac{T_\infty}{T_0}\right) \quad \ldots (5)$$

where:

T_a = temperature of the radiating surface of the infinite slab in the absence of a flaw, in degrees Kelvin,
T_0 = temperature of the heated surface of the infinite slab,
T_∞ = ambient temperature,

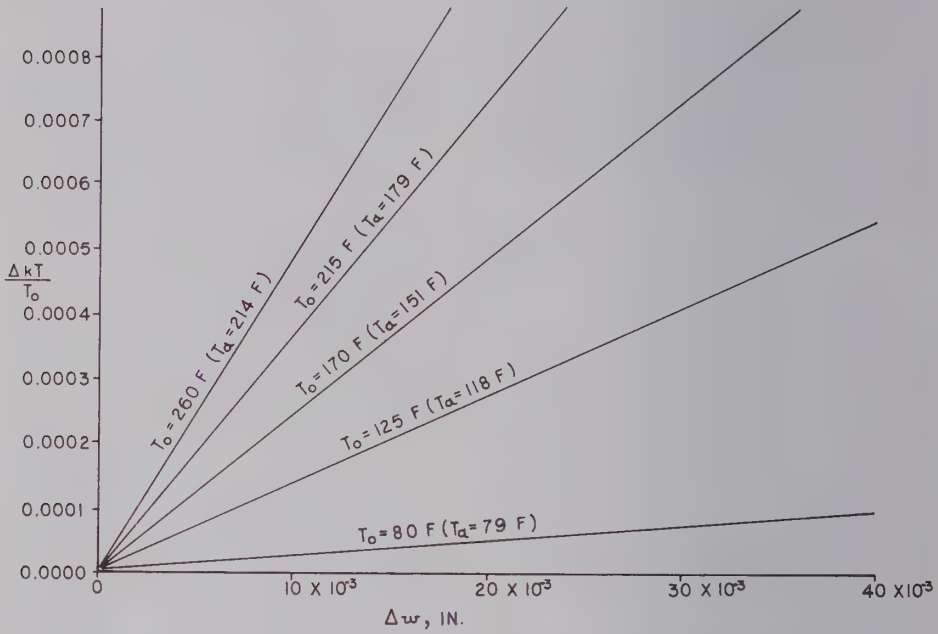

FIG. 2.—Curves Derived from Resin Flaw in $\frac{1}{4}$-in. Spiralloy; Ambient Temperature 72 F.

Assuming Newton's law of cooling to hold, it is possible to show that the temperature T_a is given by

$$1 - \frac{T_a}{T_0} = \frac{Aw/K}{1 + Aw/K}\left(1 - \frac{T_\infty}{T_0}\right) \quad \ldots (5)$$

where:

T_a = temperature of the radiating surface of the infinite slab in the absence of a flaw, in degrees Kelvin,
T_0 = temperature of the heated surface of the infinite slab,
T_∞ = ambient temperature,
A = $4e\sigma\bar{T}^3$,
e = emissivity of the radiating surface,
σ = Stefan-Boltzmann constant = 5.67×10^{-12} w-cm^{-2} (deg K)$^{-4}$,
$\bar{T}$ = $(T_a + T_\infty)/2$,
w = thickness of the infinite slab, and
K = thermal conductivity of the infinite slab.

Now, if the conductivity of the semi-infinite insert be denoted by K' and its thickness by Δw, then the temperature

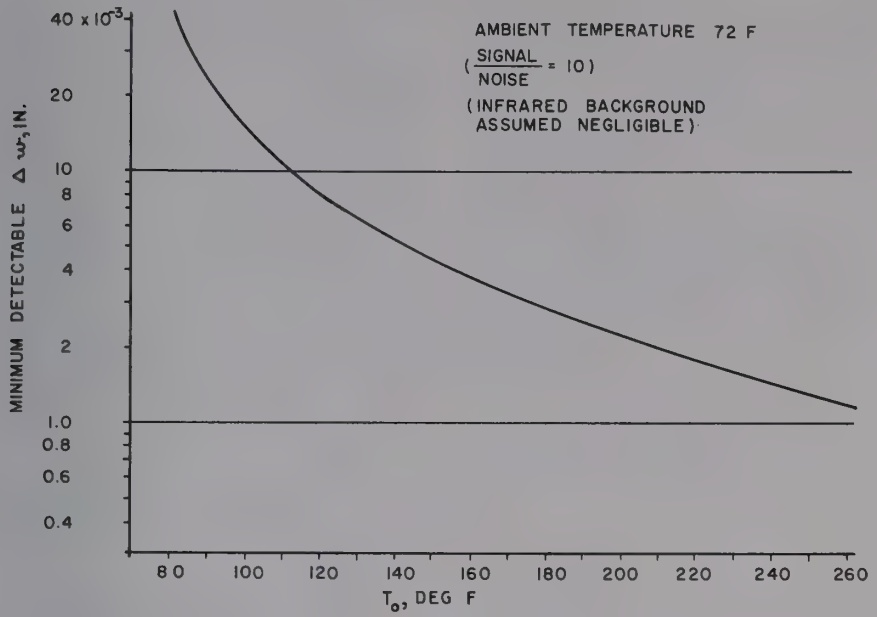

FIG. 3.—Curve Derived from Resin Flaw in $\frac{1}{4}$-in. Spiralloy with a Signal to Noise Ratio of 10:1.

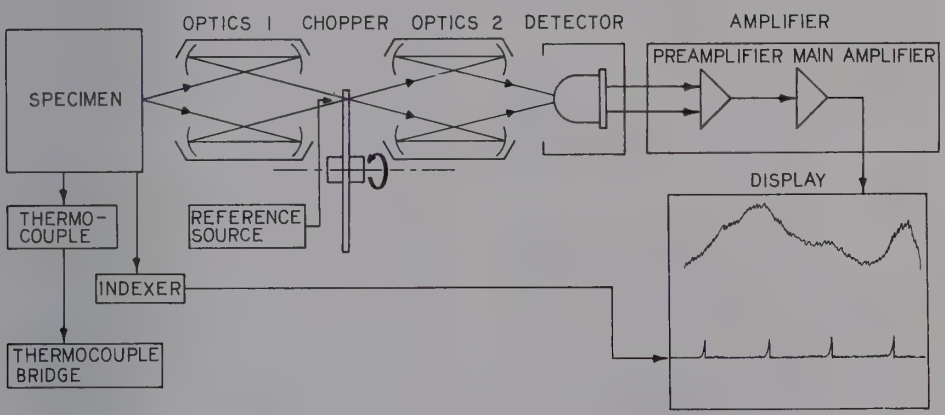

FIG. 4.—Schematic Diagram of Functional Units for Infrared Nondestructive Testing.

at infinity is altered from the value T_a to the temperature $T_a - \Delta_K T$, where

$$\frac{\Delta_K T}{T_0} = \left(1 - \frac{T_\infty}{T_0}\right) \frac{Aw/K}{(1 + Aw/K)^2}$$

$$\left(\frac{K}{K'} - 1\right) \frac{\Delta w}{w} \quad . . (6)$$

To obtain some typical magnitudes, suppose one has a resin inclusion in a glass filament-wound rocket motor casing; then the curves shown in Fig. 2 may be derived.

Moreover, if one demands a signal to noise ratio of about 10:1 as a criterion for detection of a minimum thickness of

flaw, one obtains the curve shown in Fig. 3. The latter curve is valid only in the absence of noise.

The influence of some factors contributing to noise are considered in the next section.

FACTORS OTHER THAN CONDUCTIVITY INFLUENCING FLAW DETECTION

Inasmuch as the value of $\Delta_K T$ in Eq 6 depends only on the ratio w/K, it is not possible to separate the influence of the w and K variations under the conditions of measurement proposed. Indeed, if a variation of thickness alone is responsible for the difference in temperature, then

$$\left| \frac{\Delta_w T}{T_0} \right| = \left(1 - \frac{T_\infty}{T_0}\right) \frac{Aw/K}{(1 + Aw/K)^2} \frac{\Delta w}{w} \quad (7)$$

It is easily shown that, for equal values of Δ_w, the magnitude of $\Delta_w T$ is about three times greater than the value of $\Delta_K T$, for a resin flaw inclusion in a glass filament-wound motor case.

Variation in the emissivity of the surface of the specimen may also influence the data. A variation of magnitude Δe in the emissivity will cause a variation $\Delta_e T$:

$$\frac{\Delta_e T}{T_0} = \left(1 - \frac{T_\infty}{T_0}\right) \frac{Aw/K}{(1 + Aw/K)^2} \frac{\Delta e}{e} \quad (8)$$

in the temperature observed. And since a fourth power of the temperature provides a more accurate estimate of the rate of radiation than Newton's law, it follows that the rate of radiation will be very sensitive to emissivity variation. For example, if it is desired to discriminate temperature differences of 0.01 F at a reference temperature of about 100 F, a variation of 0.1 per cent in emissivity is enough to cause a variation in the rate of radiation more than ten times greater than the variation due to the temperature difference. Unfortunately there appear to be few data available on the magnitude of emissivity variation to be expected over prepared surfaces, and predictions are correspondingly difficult. As pointed out above, it is necessary to make an experimental study to determine the feasibility of infrared nondestructive testing.

INSTRUMENTATION FOR INFRARED NONDESTRUCTIVE TESTING

The functional units required for infrared nondestructive testing are illustrated in Fig. 4. The role of each unit and the instruments used are as follows:

1. *Optics (1).* A 1:1 reflective optical system with pierced mirrors is used to collect, focus, and transmit radiation from the specimen. The entrance angle is 20 deg and the specimen is placed at a distance of 0.5 in. from the entrance aperture.

2. *Chopper and Reference Source.*—The chopper interrupts the radiation from the first optics stage at a rate of 90 cps. It also serves as a reference source of radiation; the blades of the chopper are heated and maintained at a constant temperature. Thus the chopper alternately transmits radiation from the optics and its own radiation; the signal is the difference in the radiation rates of chopper and specimen.

3. *Optics (2).*—A 1:1 reflective system, similar to Optics (1), is used to collect, focus, and transmit radiation from the plane of the chopper to the detector.

4. *Detector.*—A thermistor bolometer with a germanium window is used to detect the incident radiation. This type of detector is sensitive to wavelengths from the near to the far infrared, approximately from 1 to 15 μ. The energy received is converted to heat which alters the resistance of a detector flake. The flake is one arm of a bridge circuit which is balanced in the absence of a signal; a compensating flake is used to ensure balance as temperature variations in the surroundings occur. In the presence of a signal, the bridge is unbalanced and an output voltage is obtained proportional to the change of resistance. The alternating levels of radiation received result in approximately a square wave with fundamental frequency of

90 cps and amplitude proportional to the difference in radiation levels of chopper and specimen.

5. *Amplifiers.*—A specially designed preamplifier with a fixed gain of 1000 is used to amplify the signal from the detector. The output of the preamplifier is then further amplified by a fixed frequency (90 cps) main amplifier. The main amplifier gain ranges from 0.067 to 6667 in eleven fixed steps. The band width of the amplifier can be selected to be 0.1, 1.0, or 10 cps by means of a front panel switch.

6. *Display and Indexing.*—The output of the system is displayed in two ways. The metered output and gain selection switch of the main amplifier are calibrated to read microvolts input to the preamplifier. In addition, an output jack is provided and the output voltage is recorded on a Sanborn Model 650 optical recorder.

An indexing device which generates five pulses per degree of rotation is used with circular specimens. The pulses are recorded simultaneously with the signal, on a separate channel, in order that the location of all signals is established. The index consists of a disk mounted to the drive shaft of the specimen and contains equally spaced holes around its perimeter. Light from a lamp mounted on one side of the disk passes through the holes and strikes a photocell of the photoconductive type. The photocell is in series with a battery and resistor and the output voltage across the resistor is used to drive the indexing channel of the recorder.

7. *Thermocouple Bridge.*—The temperatures at the surface and interior of the specimen are measured by using copper-constantan thermocouples and a Leeds and Northrup Model 8667 thermocouple bridge. These measurements provide information to establish temperature gradients in the specimen and the radiation level from the specimen surface.

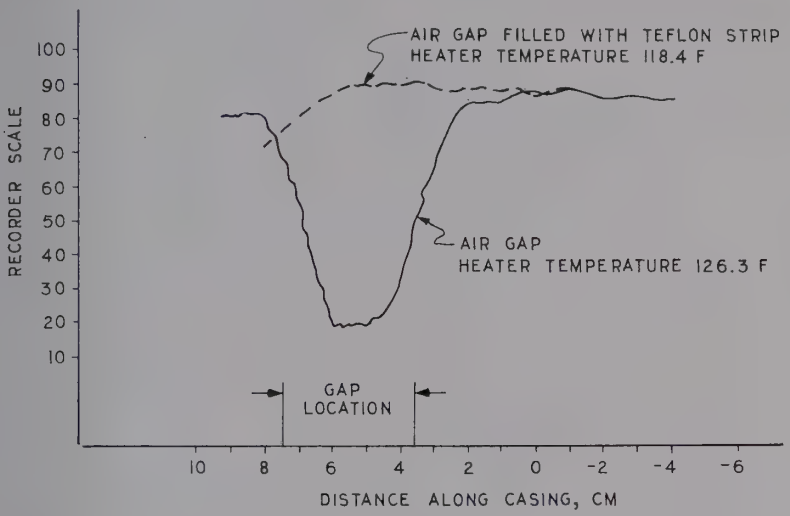

FIG. 5.—Effect of 0.031-in. Air Gap in 0.250-in. Specimen.

In order to determine the magnitude of the flaws in the specimen in an absolute manner, it is necessary to know the temperature change which causes a given change of output voltage from the system. Knowing the gain of the system, it is only necessary to determine the change in specimen temperature that causes a given change in input voltage. It is found that a change of 1 F in a black body used as reference source is sufficient to cause a change of 23 μv at the input to the preamplifier, with an accuracy of about 20 per cent, in the temperature range of interest.

The noise contributed internally by the infrared scanning system is largely

due to the noise generated in the thermistor bolometer; this is about 0.5 μv at room temperature at the input to the preamplifier. It follows that the scanning system can detect a temperature difference of 0.1 F or better at a specimen temperature of about 120 F, corresponding to a signal to noise ratio of about 4:1.

For the feasibility phase of the program it was unnecessary to establish the absolute level of radiation from the specimen, but only to verify that signals could be correlated with the location of known flaws in the presence of background noise.

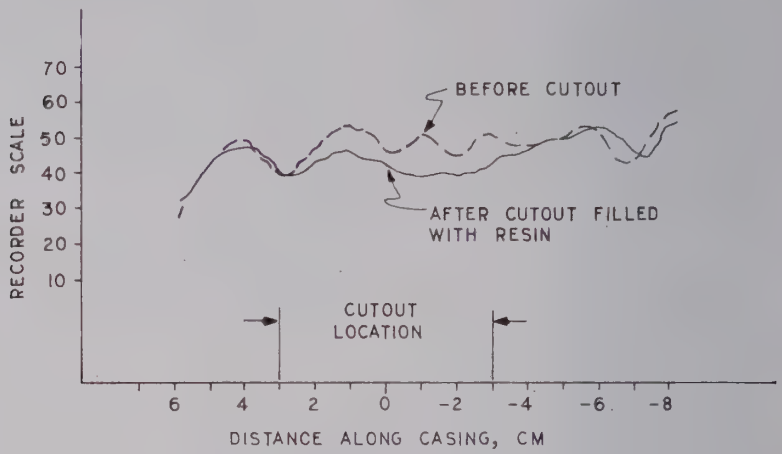

FIG. 6.—Effect of 0.017-in. Cutout Filled with Resin in 0.210-in. Specimen; Heater Temperature 122 F.

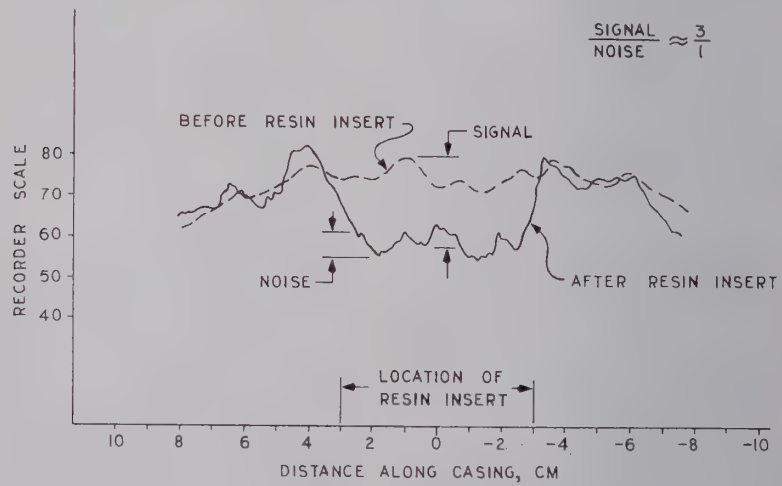

FIG. 7.—Effect of $\frac{1}{32}$-in. Resin Insert in $\frac{1}{4}$-in. Thick Casing; Heater Temperature 107 F.

FEASIBILITY STUDY IN INFRARED NONDESTRUCTIVE TESTING

Glass filament-wound rocket motor cases both with and without liner were

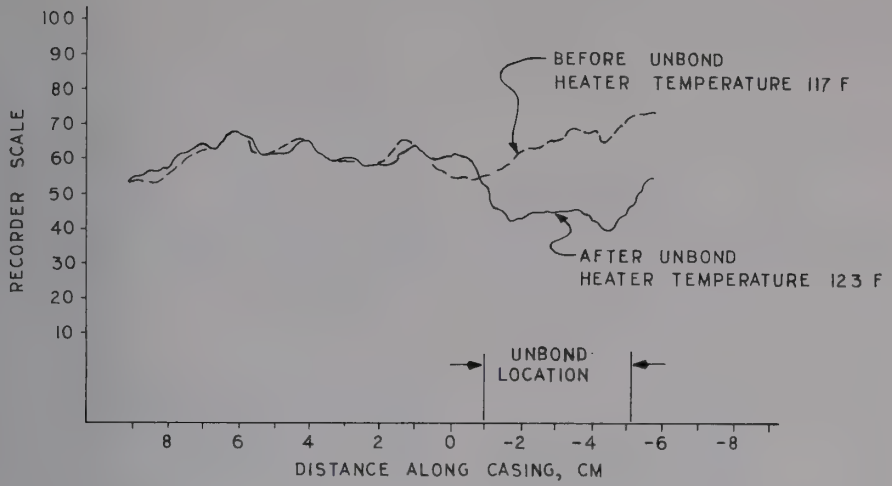

FIG. 8.—Effect of Unbond Between Casing and Liner in 0.265-in. Specimen.

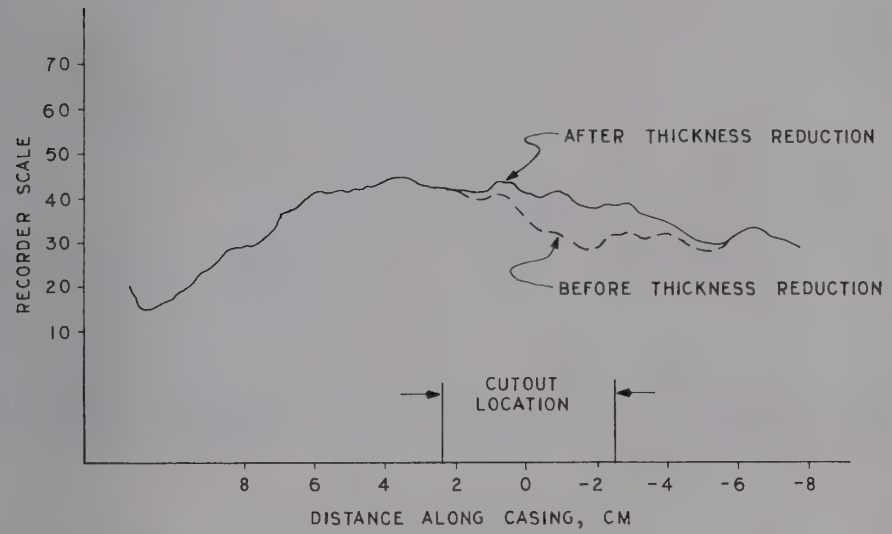

FIG. 9.—Effect of 0.007-in. Cutout in 0.210-in. Specimen; Heater Temperature 128 F.

the subject of investigation. The effect of surface background had to be evaluated first for casings without liner. Because of the existence of a rubber liner bonded to the fiber glass there was a possibility that inclusions in the rubber or variations in bonding quality might interfere with the detection of flaws.

In order to be certain of the nature of the flaws under observation, the flaws to be observed were simulated. These included voids, resin inclusions, and unbonded areas between liner and casing. Wherever possible the flaws were located on the side of the casing opposite the detector so that the most unfavorable conditions for observation were generated, and detection of a signal could not be at-

tributed to variation in surface emissivity owing to the presence of a flaw on the surface.

The following results of the experiments were noted:

1. Background noise presents no serious problem in detecting signals received from flaws. The noise appears to be associated with variation in emissivity from the surface of the specimens.

2. The background noise observed for casings with liner of various thicknesses is essentially the same as that observed for casings without liner.

3. Voids $\frac{1}{32}$ in. thick in a casing $\frac{1}{4}$ in. thick, without liner, are observed with a signal to noise ratio of about 25 to 1 at a heater temperature of about 115 F. Since signal to noise ratio is approximately proportional to void thickness, a signal to noise level of about unity, representing a threshhold, would be obtained with an air gap of about 0.0015 in. at the heater temperature given. A higher heating temperature leads to greater flaw resolution. An example of this type of signal is presented in Fig. 5; the apparatus was somewhat different from that described.

4. Resin-rich areas $\frac{1}{32}$ in. thick in a casing $\frac{1}{4}$ in. thick, without liner, are observed with a signal to noise ratio of 3 to 1 for a heater temperature of 115 F. Hence threshold would correspond to about 0.01 in. thickness of resin at the temperature given. Figures 6 and 7 illustrate some typical curves derived from this kind of flaw.

5. Unbonded areas between liner and casing have been observed with a signal to noise ratio of about 5 to 1 for a heater temperature of about 112 F. The liner was pressed tightly against the casing by the pressure of the heating fluid (about 90 lb per sq ft) during the observation (Fig. 8).

6. Variation of thickness of the casing gives rise to the kind of signal shown in Fig. 9.

In cases where it was possible, the order of magnitude of the signal was estimated and found to be of the order predicted by the simple theory presented above.

SUMMARY

It is now clear that a variety of flaws in glass filament-wound rocket motor cases can be detected by infrared scanning. Many questions remain to be answered, but the technique appears to be feasible.

Acknowledgments:

The authors wish to acknowledge the aid of R. C. Redden, who suggested the optical design; J. G. Holbrook, who designed and built the amplifiers; and R. J. Salmon, who was responsible for mechanical engineering design. T. B. Paulson and L. K. Loomer aided in the measurements and preparation of the report.

THIS PUBLICATION is one of many issued by the American Society for Testing and Materials in connection with its work of promoting knowledge of the properties of materials and developing standard specifications and tests for materials. Much of the data result from the voluntary contributions of many of the country's leading technical authorities from industry, scientific agencies, and government.

Over the years the Society has published many technical symposiums, reports, and special books. These may consist of a series of technical papers, reports by the ASTM technical committees, or compilations of data developed in special Society groups with many organizations cooperating. A list of ASTM publications and information on the work of the Society will be furnished on request.

Duke University Libraries
D00805819V

Engineering Library

OCT 25 1965

DUKE LSC
D00805819V